Simultaneous tissue extraction and quantification of reproductive neuropeptides and sex steroids in zebrafish and mouse

Chunyu Lu

Thesis submitted to the University of Ottawa in partial
Fulfillment of the requirements for the
Ph.D.

Department of Biology
Faculty of Science
University of Ottawa

Abstract

The detection and quantification of hormones are important to assess the reproductive and stress status of experimental models and for the diagnosis of diseases in human and veterinary clinics. The peptide secretoneurin (SN) has been proposed as a new sex hormone, but effective quantification methods are challenging. Traditional methods require the use of antibodies with either radioactive or non-radioactive tracers. There are difficulties with these methods in terms of sensitivity, specificity, and inter-laboratory repeatability. Liquid chromatography-tandem mass spectrometry (LC-MS/MS) can circumvent many of these challenges. Another source of variation is the extraction of lipophilic steroidal compounds, which is incompatible with the extraction of hydrophilic peptide hormones. I have developed efficient extraction and sensitive detection methods of SN with numerous other peptide and steroid hormones in the same tissue sample in mice and zebrafish. The extraction efficiency for both peptide and steroid analytes is over 85%. The standard deviation for extraction and LC-MS/MS analysis for each compound varies between 5-10%. The steroid hormones can be quantified in the low to medium fmol/µL range. We quantified peptide hormones in the high fmol/µL to low pmol/µL range. Mouse SN levels were measured and compared against the levels of GnRH 1, oxytocin, vasopressin, E2, and P4 in multiple tissues at 3 important periods through the estrous cycle. In addition, SN levels were found to be moderately related to GnRH 1 levels in the hypothalamus in the estrous cycle. This is important because it is GnRH 1 that stimulates the luteinizing hormone surge in the pituitary that regulates ovulation in all vertebrate species. I also determined that SNa and SNb were both within the 2-8 pmol/µL range in the brain or pituitary harvested from a single female zebrafish. This makes it feasible for the first time to study the correlation between the SNs and other peptides and steroid hormones by quantifying them simultaneously in very small tissue samples. Untargeted peptidomics determined that the SN peptides in zebrafish can be further processed into smaller discrete fragments. This implies not only active synthesis and selective peptide processing but suggests that the are unknown functions of the SN peptide fragments that await discovery. This cost-effective package was used for the detailed assessment of hypothalamic-pituitary-gonadal function in mice and zebrafish and may be adaptable to many other hormones across species.

Resumé

La détection et la quantification des hormones sont importantes pour évaluer l'état de reproduction et de stress des modèles animaux expérimentaux et pour le diagnostic des maladies dans les cliniques humaines et vétérinaires. Le peptide secretoneurine (SN) a été proposé comme une nouvelle hormone sexuelle, mais les méthodes de quantification efficaces y sont difficilement applicables. Les méthodes traditionnelles nécessitent l'utilisation d'anticorps avec des traceurs radioactifs ou non radioactifs. Ces méthodes présentent des difficultés en termes de sensibilité, de spécificité et de répétabilité inter-laboratoires. La chromatographie en phase liquide et la spectrométrie de masse en tandem (LC-MS/MS) permettent de contourner bon nombre de ces difficultés. Une autre source de variation est l'extraction des composés stéroïdiens lipophiles, qui est incompatible avec l'extraction des hormones peptidiques hydrophiles. J'ai mis au point des méthodes efficaces d'extraction et de détection de la SN avec de nombreuses autres hormones peptidiques et stéroïdiennes dans un même échantillon de tissu chez la souris et le poisson zèbre. L'efficacité de l'extraction pour les analytes peptidiques et stéroïdiens est supérieure à 85 %. L'écart-type pour l'extraction et l'analyse LC-MS/MS pour chaque composé varie entre 5 et 10 %. Les hormones stéroïdiennes peuvent être quantifiées dans la gamme basse à moyenne de l'ordre de la fmol/µL. Nous avons quantifié les hormones peptidiques dans la gamme haute de la fmol/µL à faible du pmol/µL. Les niveaux de SN de souris ont été mesurés et comparés aux niveaux de GnRH 1 (*Gonadotropin-Releasing Hormone 1* ou gonadolibérine 1), d'ocytocine, de vasopressine, d'estradiol et de progestérone dans de multiples tissus à 3 périodes importantes du cycle œstral. En outre, on a constaté que les niveaux de SN étaient modérément liés au niveau de GnRH 1 dans l'hypothalamus au cours de l'œstrus. Ceci est important car c'est la GnRH 1 qui stimule le pic de l'hormone lutéinisante hypophysaire, qui régule l'ovulation chez toutes les espèces vertébrées. J'ai également déterminé que les niveaux de SNa et le SNb étaient tous deux compris entre 2 et 8 pmol/µL dans le cerveau ou l'hypophyse prélevés d'un seul poisson zèbre femelle. Cela permet pour la première fois d'étudier la corrélation entre les SN et d'autres peptides et hormones stéroïdes en les quantifiant simultanément dans de très petits échantillons de tissus. Une analyse peptidomique non ciblée a permis de déterminer que les peptides SN chez le poisson zèbre peuvent être transformés en fragments distincts plus petits. Cela implique non seulement une synthèse active et un traitement sélectif des peptides, mais suggère que ces fragments de peptides SN ont des fonctions inconnues qui restent à découvrir. Cette méthode rentable a été utilisée pour l'étude détaillée de la fonction hypothalamo-hypophyso-gonadique chez la souris et le poisson zèbre et peut être adaptée à de nombreuses autres hormones, chez différentes espèces.

Acknowledgments

Thank you to my supervisor, Vance L. Trudeau, for the opportunity to do this work, and my advisory committee, Professors Kyle Biggar, Jeffrey W. Keillor, and Cory Harris for their time and insight, which helped shape this thesis.

I gratefully acknowledge the individuals who have directly contributed to the data presented in this thesis. Di Peng provided the zebrafish tissues in Chapters 2, 3, and 4, and did all sample processing work using the extraction methods I developed for this thesis research. Professor Nafissa Ismail (Dept. of Psychology) provided the mice and, Di Peng and Kevin Smith helped with mouse dissections for Chapter 5. Dr. Zhibin Ning (Ottawa Health Research Institute) helped with the database searches for the peptidomics part in Chapter 4.

I acknowledge the financial support of NSERC.

Table of Content

List of Figures

list of abbreviations

N_t	Number of theoretical plates
11-KT	11-Ketotestosterone
5a-DHT	5alpha-dihydrotestosterone
Acm	acetamidomethyl
ACN	Acetonitrile
Boc	tert-butoxycarbonyl
BSA	bovine serum albumin
cAMP	adenosine 3',5'-cyclic monophosphate
CID	collision-induced dissociation
DAD	Diode-array detection
DCM	Dichloromethane
DMF	Dimethylformamide
DMSO	dimethylsulfoxide
EMPV	Electromagnetic proportional valve
ERK	Extracellular signal-regulated kinase
ESI	Electrospray ionization
ETD	electron-transfer dissociation
FA	Formic Acid
Fmoc	Fluorenylmethyloxycarbonyl
FTMS	fourier transform mass spectrometry
FWHM	Full width at half maximum
GnRH	Gonadotropin-releasing hormone
HBTU	Hexafluorophosphate Benzotriazole Tetramethyl Uronium (2-(1H-benzotriazol-1-yl)-1,1,3,3-tetramethyluronium hexafluorophosphate)
HETP	Height equivalent to a theoretical plate
HLOQ	higher limit of quantification
HPG	Hypothalamic-pituitary-gonadal
HPLC	High Performance Liquid Chromatography
HV	High voltage
ID	interior diameter
ID	Internal diameter
LC-MS/MS	Liquid chromatography-tandem mass spectrometry
LH	luteinizing hormone
LLOQ	lower limit of quantification
m/z	mass over charge ratio
MRM	Multiple reaction monitoring
MS	Mass spectrometry
mSN	mouse secretoneurin
N	Newton
nL	nanoliter

NL	normalization level
NMM	N-Methylmorpholine
NMP	N-Methyl-2-pyrrolidone
OD	Outside diameter
OEM	Original equipment manufacturer
PEEK	polyetheretherketone
ppm	Parts per million
PSI	pound per square inch
RP-HPLC	Reverse Phase High Performance Liquid Chromatography
S/N	Signal-to-noise ratio
SGII	secretogranin 2
SN	Secretoneurin
SOP	Standard operation procedure
SPE	Solid phase extraction
SPPS	Solid Phase Peptide Synthesis
SRM	Selected reaction monitoring
tBu	tert-Butyl
TFA	Trifluoroacetic acid
Trt	trityl
UHPLC	Ultra-High Performance Liquid Chromatography

Chapter I General introduction

1.1 Background on secretoneurin

Secretoneurin (SN) is a 31- to 43-amino acid length neuropeptide derived from specific proteolytic cleavage of secretogranin-II (SCG2), a large ~600-amino acid long secretory protein synthesized by endocrine, neuroendocrine, and neural tissues [1]. There has been considerable research from our group to suggest that SN can stimulate luteinizing hormone (LH) [2-4]. It is LH that is produced and released from the pituitary gland to regulate ovulation in females, sperm release in males, and gonadal steroid production in both sexes. Other research groups discovered the role of SN in neurogenic inflammation, angiogenesis, and other functions [1, 5-7]. Our research group has recently reviewed some aspects of this [8] and has established that SN is a new reproductive hormone [9].

1.1.1 Detection of SN

The detection and measurements of SN by immunoassays are dependent on an intact epitope in the SN peptide, and without cumbersome separation, larger fragments of the precursor will be also detected [10]. With the development of peptidomics techniques and LC-MS/MS equipment, it is possible to measure the level of SN while also confirming the actual structure

With improvements in LC-MS/MS equipment, the intact SN peptide (33 amino acids) has been characterized from human, mouse, and bovine samples [8, 11, 12]. In these studies, human SN was measured by targeted peptidomics, while mouse and bovine were untargeted. These results indicate evidence of the existence of mammalian SN peptides. In zebrafish, there are two SN peptides predicted from the distinct SCG2a and SCG2b precursor proteins respectively called SNa, and SNb. The existence of these two peptides has been suspected for decades, however, definite evidence on the integrity of these SN peptides is still missing [13]. There have been no definitive LC-MS/MS identifications of any non-mammalian SNs, even though numerous SCG2 and SCG2b fragments have been detected by untargeted LC-MS/MS in zebrafish brain [14]. Therefore, it is important to confirm that SN exists in zebrafish as an intact peptide using targeted peptidomics. More details about untargeted and targeted peptidomics are reviewed in Appendix II

1.1.2 SN as a neuroendocrine and paracrine factor

Various early immunolocalization studies reported on SN-immunoreactivity in different cell types in the anterior pituitary [5, 15]. Over the past decade, our group has shown that SN plays a role in pituitary neuroendocrine and paracrine functions. In goldfish pituitary, SN was first shown to increase the release of pituitary luteinizing hormone (LH) *in vivo*, and from dispersed pituitary cells *in vitro* [2, 3]. We also discovered that SN regulates LH release from gonadotrophs in the pituitary via neuroendocrine and paracrine pathways [13]. In addition to the classic gonadotropin-releasing hormone (GnRH) neuropeptide, goldfish gonadotrophs can be stimulated to release LH by SN. There is evidence showing that SN-immunopositive neurons of unknown origin project to the area close to gonadotrophs in the proximal pars distalis of the pituitary. Neuroanatomical evidence indicates that SN is also in pituitary lactotrophs. The current model suggests that GnRH stimulates lactotrophs to release both prolactin and SN, and SN in turn stimulates LH release by paracrine action [13]. Other *in vitro* experiments indicate that SN also stimulates LH release from the mouse LβT2 gonadotroph cell line [4]. When the cells were exposed to nM concentrations of SN, both LHβ mRNA level and the LH released to the medium were increased in 6-12 hrs. Additionally, it was shown that SN increases LH release via activation of cyclic adenosine monophosphate (cAMP)/protein kinase A (PKA) signaling in LβT2 cells, independent of the GnRH receptor [4]. Pharmacological data from our lab has shown that SN rapidly activates the mitogen-activated protein kinase MAPK kinase (MEK) and extracellular signal-regulated kinases (ERK) signaling pathway [4].

1.1.3 SN Function in Neurogenic Inflammation

Neurogenic inflammation can be induced by stimulation of the somatic nervous system following chemical, mechanical, or immunological injuries. The action potentials in nociceptors can be transmitted to the periphery, in parallel to orthodromic inputs to the spinal cord and brain. In response to these modes of neuro-activation, neuropeptides (such as substance P and calcitonin gene-related peptides) are rapidly released from sensory nerve endings into the periphery. After neuropeptide-receptor recognition, inflammatory cells migrate to injury sites. Secretoneurin is believed to be a novel neuropeptide important for these neuro-immune interactions and has been shown to affect several types of cells in the inflammatory response [6, 16]. When inflammation occurs, monocytes migrate from the bloodstream to injured peripheral tissues guided by local

factors including neuropeptides. They usually differentiate into macrophages or dendritic cells to effectively control and eliminate viral, bacterial, fungal, and protozoal infections [17]. SN was found to trigger human monocyte-selective migration both *in vitro* and *in vivo* [18]. SN was also shown to time- and concentration-dependently increase human monocyte (MonoMac 6 and U937) adhesion to arterial and venous endothelial cells. This SN-facilitated monocyte adhesion was not tissue-specific and could be blocked by a specific SN antibody [19]. These studies indicate that SN should play an important role in recruiting monocytes to inflamed tissues during the inflammation process.

1.1.4 Secretoneurin related clinical discoveries

In the past decade, several clinical researchers have discovered important relationships between SN and diseases as a biomarker. For example, Røsjø et.al. studied the relationship between SN and multiple cardiovascular issues [20, 21]. In a separate study, Kolosov et.al. discovered that SN can induce airway mucus hypersecretion in a dose- and time-dependent manner [22]. Additionally, SN is shown to be a potential early biomarker for hypoxic brain injury after cardiopulmonary resuscitation [23].

1.2 Variations in secretoneurin production during the mouse estrous cycle

The estrous cycle is the period between one ovulation to the next ovulation. It consists of a cyclical pattern of ovarian activity and reproductive receptivity behaviors (e.g., estrus) [24]. It is controlled by the hypothalamic-pituitary-gonadal (HPG) axis and various reproductive hormones, including GnRH, LH, follicle-stimulating hormone (FSH), and estradiol (E2) as presented in Figure 1.8 [25]. In recent years, evidence shows that the neuropeptide SN can have an important role in fish reproduction and is thus proposed as a new hormone [8, 13, 26]. However, there have been no attempts to determine the role of SN in the estrous cycle of mammals. In this project, I propose to measure SN in relation to well-known reproductive regulators in the mouse estrous cycle. Below I will review key hormonal regulators of the mouse HPG axis as well as recent studies of the reproductive functions of SN in fish and cell line models.

1.2.1 Female mouse HPG axis and related major reproductive hormones

The hypothalamus, pituitary, and ovaries are individual endocrine glands commonly referred to as the hypothalamic-pituitary-gonadal axis of female vertebrates. When studying reproductive questions, these glands must be regarded as a network because they work together accordingly to generate gonadotropins (LH and FSH) and steroid hormones. The GnRH neurons are located in the hypothalamus and septal area. They send their axons to the median eminence to release GnRH. This GnRH hormone diffuses out of capillaries and stimulates the gonadotropes in the anterior pituitary, which release LH and FSH into the peripheral blood circulation in response. The LH and FSH circulate to ovaries and trigger ovulation and control the production of E2. Estradiol is produced by ovarian follicles and released to blood circulation to control numerous aspects of female reproductive physiology, including regulation of ovulation, and sexual receptivity and through both positive and negative feedback loops at the hypothalamus and pituitary, also the production and release of LH and FSH (Figure 1.8) [27, 28]. These hormones are generated in a repeated pattern through the estrous cycle [29]. The mouse estrous cycle lasts approximately 4-5 days. It contains 4 major stages, metestrus, diestrus, proestrus, and estrus [28]. The main hormonal profiles of these stages are briefly summarized below.

Metestrus (day 1): Progesterone and estradiol circulate at a low level. GnRH 1 pulse frequency and levels are low, which maintains LH and FSH at the basal level [30]

Diestrus (day 2): Diestrus starts with the increase of progesterone levels in blood circulation. It then quickly drops at the end of the day [31]. The blood level of E2 is increased at this stage, which leads to enhanced GnRH pulse frequency and level [32].

Proestrus (day 3): The level of E2 increases quickly, which drives the pulses of GnRH more frequently. The condensed GnRH pulses lead to LH surge in the early evening of day 3. The level of E2 quickly drops when LH surges, which also leads to a progesterone peak. The frequency of GnRH also decreases to the basal level with induction of negative feedback from progesterone and E2 [33].

Estrus (day 4): Ovulation occurs and all hormones return to baseline [34].

Besides these hormones, there are many other important pathways and related messenger compounds that play important role in the mouse reproductive system. For example, hypothalamic kisspeptin is also critical to the generation of GnRH pulses, and ultimately successful ovulation in female mammals [32]. This information is not closely related to the purpose of this project and my discovery. Therefore they are not being reviewed in detail in this chapter.

1.2.2 SN and LH in goldfish

The possible function of SN in the reproduction system was initially studied in goldfish. The first cDNA for a non-mammalian SCG2 precursor was sequenced from goldfish and it was shown that SNa could stimulate LH release in vivo [35]. Zhao et al. later expanded on this discovery showing that SNa can stimulate the production and release of LH from the goldfish pituitary [2, 3]. In these experiments, dispersed goldfish pituitary was incubated with SNa *in vitro*. Both cellular expression of LHβ mRNA and LH released into the culture medium was increased. A significant LH release from the pituitary was also measured following *in vivo* injection of SNa. In a separate study, SNa exhibited dose-dependent regulatory impact on goldfish radial glial cells proteome and transcriptome, which is the only cell type expressing aromatase B in the teleost brain regulating estrogen synthesis from androgen precursors [36, 37].

1.2.3 SN and LH in Zebrafish

Mitchell et al. conducted an extensive analysis of reproduction in zebrafish in which both SCG2a and SCG2b genes were mutated using the TALENs approach [9]. In both single and double

frameshift mutant fish, many aspects of reproductive physiology were dramatically reduced. For example, in fish with both SCG2 genes mutated, sexual behaviors, ovulation, egg-laying, and embryo survival were all reduced. Part of the mechanism behind reduced fertility was a reducting in GnRH3 mRNA level in the brain and reduced expression of the genes encoding for LH production in the pituitary [9]. Moreover, injection of synthetic SNa but not SNb partially rescued reproductive defects in the SCG2a/b double mutant fish. These observations set the foundation for the development of methods to quantify the SN peptides in the zebrafish model.

1.2.4 SN, GnRH 1, and LH in mouse LβT2 cells

Using mouse pituitary LβT2 tumor cell line LβT2, Zhao et al. reported that SN can stimulate gonadotrophs to produce and release LH, which is similar to the response to GnRH agonists. In addition, this stimulation was indicated to be through protein kinase A and cAMP-induced ERK signaling pathways [4]. The study also indicated that SN did activate GnRH receptors to cause the release of LH [4]. Moreover, it was GnRH 1 that decreased the cellular level of SN-containing proteins (SCG2), while promoting the release of SN. This led the authors to propose that SN was part of an autocrine feedback loop controlling LH release [13].

1.2.5 Importance of current study

Using goldfish and zebrafish as experimental models, SN has been shown to be critical to the reproductive endocrine system. It could play an important role in the HPG axis by controlling other well-known reproductive hormones. The study on the LβT2 cell line established the function of SN in mouse gonadotrophs. However, an *in vivo* study is still missing. Therefore, the goal was to develop methods to provide the first measurements of SN in the HPG axis during the ovulatory cycle and to compare this to well-known peptide and steroid hormones to regulate vertebrate reproduction.

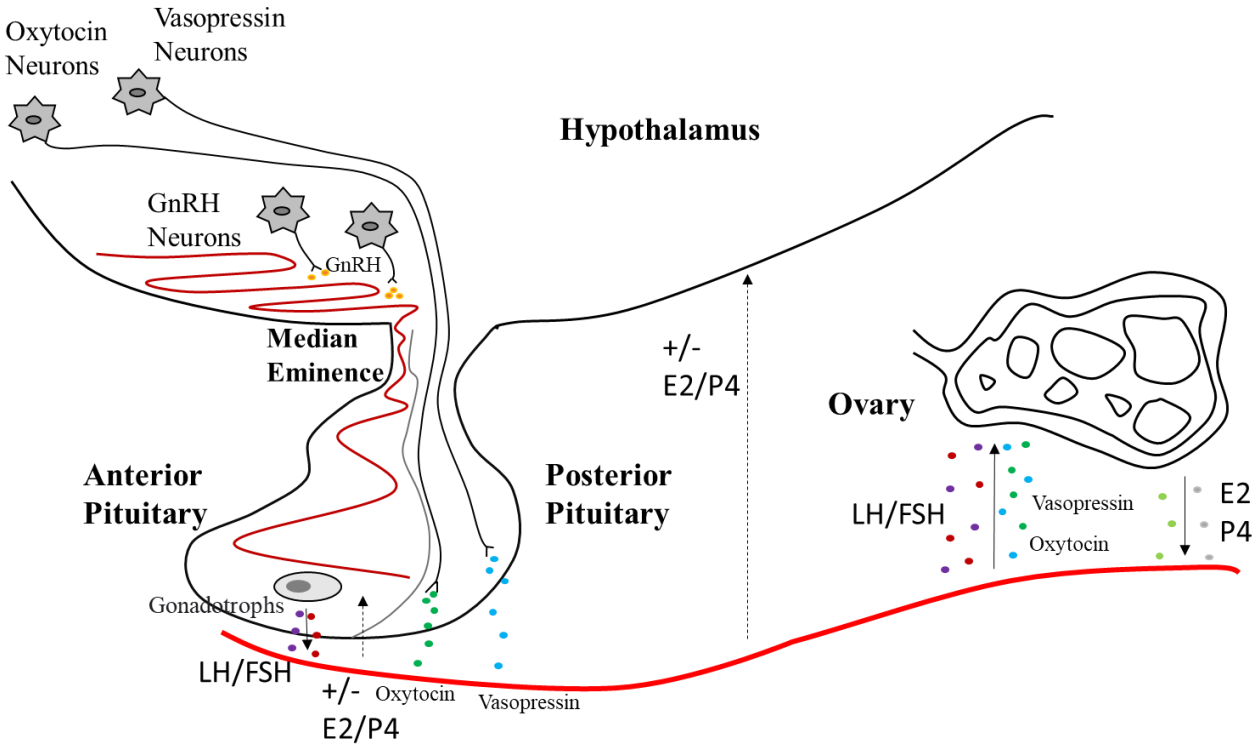

Figure 1-1 Hypothalamic-pituitary-gonadal (HPG) axis and major reproductive hormones during the estrus cycle. The hypothalamus releases GnRH to stimulate the pituitary to release luteinizing hormone (LH) and follicle-stimulating hormone (FSH) to control ovarian development, steroidogenesis, and ovulation. In turn, ovarian cells produce and release estradiol (E2) and progesterone (P4) to control sexual development, and sexual behavior and to exert feedback control on the hypothalamus and pituitary.

1.3 The demand for a new set of methods

Measuring the level of reproductive hormones in tissue extracts is a critical way to study physiological processes under healthy conditions or in numerous pathological states. Traditionally, immunological assays have been widely employed and proved to be successful for hormone measurements. These assays rely on presumably specific antibodies and cannot measure many analytes of different classes at the same time. Moreover, there is ample evidence that they are qualitative, relative measurements, and absolute hormone concentrations can vary considerably between assay formats and the clinics and labs that generate the data [38-40]. Therefore, with the development of analytical chemistry, liquid chromatography-tandem mass spectrometry (LC-MS/MS) has become more popular in hormone quantifications. The currently published LC-MS/MS methods and their corresponding extraction methods are suitable for either peptide hormones or steroid hormones, and to my knowledge, never together. This presents a challenge for data interpretation, since different subjects, or subsamples must be analyzed separately.

In the following introduction, I will review extraction and LC-MS/MS techniques to reveal a possible strategy to simultaneous measure peptide and steroid homes from small tissue sample.

1.4 Isolating steroids and peptides at the same time from tissue samples for LC-MS/MS analysis

Generally, tissue sample processing methods are comprised of two major steps: homogenization and extraction. In LC-MS/MS experiments, the solvent used to dissolve a sample should be similar to the starting mobile phase. To guarantee the reliability and the throughput of the LC-MS/MS analysis, this sample processing procedure has to be highly reproducible and convenient. It is also important that the entire process is cost-efficient. Therefore, developing a reliable sample processing method was the first technical difficulty of the entire project. There are publications on the sample processing methods for either peptides or steroids [41-43], however, there are no such methods published that can cover both of these types of analytes. Therefore, I set out to establish a reliable sample processing method to ensure the success of simultaneous quantification of peptide and steroid hormones.

1.4.1 Homogenization

Tissue samples have complex structural, cellular, and chemical elements. Soluble analytes can be either inside the cells or in the interstitial fluids between different cells in various organs comprising the brain-pituitary-gonadal axis. There are two common ways to acquire these analytes in solution. They are microdialysis and homogenization. Microdialysis can be applied in a living animal when the tissues need to be intact [44]. For the current research, it is not necessary to maintain the integrity of the tissue samples, so tissue homogenization will be used to gain an understanding of total hormone production.

In the homogenization step, there are two critical components the homogenization equipment (homogenizer) and the homogenization buffer. The homogenization equipment provides the mechanical force that breaks up the tissue and releases the analytes. The homogenization buffer provides a situation where the analytes can maintain their chemical structure and stay dissolved during and after the homogenization period. The composition of a homogenization buffer is directly related to the properties of analytes which should also be compatible with downstream analysis. For the method under development here, peptide and steroid compounds must remain dissolved in the tissue homogenate when full-length protein compounds are precipitated. In this way, the solution sample contains peptide and steroid analytes, and precipitated protein components can be preserved for future analysis. Other critical considerations for sample processing are the downstream steps that contribute to the success of analyte quantification in the biological sample. Before a sample can be loaded to HPLC it must be very clean and relatively devoid of interfering substances. In certain situations, the column can be easily plugged. The common origin of the plugging issues is fine suspended particles, lipid contamination, and on-column precipitation. Moreover, if the sample contains excess metal ions and is loaded into LC-MS/MS system, they may not only suppress the MS signal but also contaminate the mass spectrometer.

For the extraction of peptide compounds, Hamlin's group discovered an efficient method to extract antimicrobial peptides from *E. coli* lysates [45]. This study demonstrated that 66.7% ethanol can significantly increase the recovery rate of antimicrobial peptides. In another study, Fricker's group used water, acid, and heat treatment to isolate neuropeptides from mouse hypothalamus. In this

study, they successfully identified multiple neuropeptides (including SN) from 4 mice hypothalamus pooled samples [43]. This study indicated that long and short peptides (0.5-3.5 kDa) can be extracted into one solution by the right homogenization buffer composition. Homogenization buffers for steroids have been reported repeatedly [46-48]. They were slightly different but shared a similar concept, which is steroid analytes stay in low polarity solvents.

1.4.2 Solid Phase Extraction (SPE)

Solid Phase Extraction (SPE) is a technique to separate compounds of interest from a complex chemical mixture, such as a tissue homogenate. An SPE step before chromatographic analysis protects the chromatographic system and enhances the signal output for the analytes under investigation. For SPE, the samples are forced to flow through the SPE resin (also called sorbents) bed. A packed bed is a hollow tube, pipe, or another vessel that is filled with sorbent. The purpose of a packed bed is to improve contact between two phases in a chemical separation process for achieving rapid mass and heat transfer. Target compounds that have strong interaction with the bed stay on the bed while other chemicals with weaker interactions flow through the bed. After the bed is washed with enough washing buffer, an eluting buffer is used to reduce the interaction between target compounds and the SPE bed. Thus, the target compounds are eluted while leaving other chemicals with stronger interactions behind on the bed. SPE is often a crucial step for the success of the LC-MS/MS analysis that follows. It can minimize signal noise while optimizing the lifetime of the chromatographic column and mass analyzer [49]. For this project, it was important to select an appropriate sorbent and discover a suitable way to operate the sorbent as an SPE bed.

1.4.2.1 Sorbents

The potential uses of SPE are countless because there are many different kinds of sorbents generally classified as reversed-phase, normal phase, and ion exchange [50, 51]. My main objective was to extract short peptides, long peptides, and steroids from tissues while eliminating salt and lipid contaminants. Therefore, a reverse-phase packing material should be appropriate. In addition, numerous publications successfully used reverse phase HPLC columns to analyze steroid compounds or peptide compounds separately [42, 45, 52, 53]. The challenge here is to select the most suitable material in the reverse phase family. In reality, these packing materials would have direct contact with the supernatant of tissue homogenate. This requires that the packing material

not only extracts and elutes the target compounds efficiently but also must endure the contamination from the sample for at least one time.

1.4.2.2 Online SPE versus offline SPE

Another way to classify SPE experiments is on whether the SPE cartridge is disposable or reusable [54]. Most of the time, the SPE cartridge is one-time use only and disposable. These cartridges are made in different sizes. It can be as small as a 10 µL pipette tip for 1-5 µL of sample volume or as big as a 10 mL syringe for a large sample volume. The sorbent filled in these cartridges forms a loosely packed bed. These cartridges can be operated by gravitational force or accelerated by centrifuge or vacuum.

These offline cartridges can cost $1.5 to $10 each, depending on the brand, sorbent, and size. When purchasing these SPE cartridges, they usually come with a standard operation protocol, which is generally similar to each other. They usually consist of five steps: activating; equilibrium; loading; washing; and eluting [54, 55]. In reality, every research lab has a different project, which leads to a different working condition for the SPE cartridge. The binding-eluting limit and efficiency for each potential compound change with the working condition. Few studies optimize and/or validate the protocol according to specific experimental conditions, but most simply follow the standard protocol [45, 56].

The offline SPE cartridges are not made to be used repeatedly, even though some have the capacity to be regenerated. In contrast, there is another type of SPE cartridge which is called online SPE cartridges. These SPE cartridges work as a mini HPLC column. They can trap and release analytes repeatedly, but they need dedicated equipment [41].

1.4.2.3 Commercialized SPE kits

Currently, there are many kinds of SPE cartridges available on the market. These cartridges may contain a large selection of packing materials that target different groups of molecules from various types of samples. Both peptides and steroids are recommended to be extracted by reverse phase C18 or C8 packing materials. However, the actual materials appropriate for peptides and steroids are different. This difference is mainly related to the surface modification of the sorbent. The

sorbent that performs well on peptides is designed to favor moderate hydrophilic compounds. When using them to extract hydrophobic compounds, like steroids, a very large amount of elution buffer is required to recover the analytes. On the other hand, the ideal SPE packing materials for steroids cannot retain polar compounds like short peptides. Also, particle size, pore size, and bed dimensions are critical to the success of the SPE procedure. For the small samples that our lab is working with, we need the bed volume to be as small as possible. Therefore, to maintain sufficient surface area for mass transfer, I identified materials with smaller particles and smaller pore sizes. These particles in a packed bed will cause high bed pressure. When working with tissue extracts on a narrow bed, fatty nano-droplets in the sample can plug the packed bed and make the pressure unreachable for a regular SPE experiment.

Another issue with the SPE cartridge kits on today's market is the high price. For common small tissue extracts, an SPE cartridge containing 5-15 mg packing can range between $6 and $15 per sample. A 100-sample experiment can cost over $1000 for the SPE step only. This would be sufficient for only 2-4 days of LC-MS/MS equipment use. Such high consumable costs are a major barrier for many labs hoping to use LC-MS/MS systems for routine analysis. Therefore, cost-effectiveness was an important consideration in the design of my extraction methods.

1.5 Liquid chromatography-tandem mass spectrometry for peptide and steroid hormones quantification

Hormones are a group of compounds that regulate bodily functions, including growth, development, metabolism, electrolyte balance, and reproduction [57]. Determination of the levels of hormones is critically important to physiologists and endocrinologists to understand the physiological or pathophysiological status of an organism [58]. Traditionally, hormones are measured by radioimmunoassay or enzyme-linked immunoassay, which have proved to be efficient and successful [59, 60]. These immunoassays were designed based on the specific interactions between antigens and antibodies. Normally, immunoassays were designed to measure one hormone specifically. Complex multiplexing methods could only quantify very few hormone candidates simultaneously. In addition, regarding peptide and protein hormones, the immunoassays tend to only confirm the existence of binding site(s). They do not necessarily provide information on the integrity of the hormone molecule. To quantify multiple hormones at the same time with a limited amount of samples, HPLC tandem mass spectrometry LC-MS/MS

has to be employed [52]. Over years of development, these LC-MS/MS hormone quantification methods tended to focus on a single category of the hormone, for example, steroids versus peptides and proteins, rather than attempting to simultaneously detect and quantify them [56, 61-63]. In addition, following the discovery of a new emerging hormone, secretoneurin (SN), an accurate and effective quantification method for this neuropeptide is still required [13, 64].

An appropriate quantification method for the hormones under investigation in this project needs to have a low detection limit, low false-positive rate, high throughput, and high reproducibility. To develop an LC-MS/MS method to achieve these goals, I present below a review of some of the basic concepts involved. These are: theoretical plates, HPLC separation efficiency, chromatographic dilution, packing nanoscale HPLC columns, accessible HPLC systems, nano electrospray ionization (ESI), accessible MS systems, mass accuracy and mass tolerance, MS resolution, linear ion trap, and orbitrap analyzers, scanning and acquisition speeds, and data-dependent and independent acquisition, and time segment.

1.5.1 Evaluating HPLC performance and selecting an appropriate equipment

High-performance liquid chromatography (HPLC) is a technique in analytical chemistry to separate and analyze compounds dissolved in a solvent [65, 66]. A modern HPLC system usually consists of mobile phases (solvents), a mobile phase delivery system (pump), an autosampler (injector), a stationary phase (column), a detector (UV, DAD, MS, etc.), and a computer to control the system and collect data [66]. In general, the pump delivers the mobile phase through the column into the detector. The injector loads a certain amount of sample on the top of the column at the start of each analysis. The computer controls the entire process and collects data from the detector. Analytes in samples are separated in the column based on the compound-mobile phase and compound-stationary phase relative affinity [67].

1.5.1.1 Separation efficiency and theoretical plates

The column on an HPLC is critical to the separation, which is directly related to the success of an HPLC experiment [68]. It is important to select the right column with sufficient separation efficiency to ensure the success of the LC-MS/MS experiment. To evaluate the separation efficiency in an HPLC column, analytical chemists adopted a concept from industrial distillation columns, that is the number of theoretical plates, N_t [69].

Traditional distillation columns contain a series of actual plates [70]. These plates are made up of bubble caps and liquid trays. As shown in Figure 1.1, in an industrial distillation column, vapor flows from bottom to top of the column and liquid flows from top to bottom. A typical plate takes vapor from underneath and liquid from above. The bubble cap and weir maintain the continuous flow of fluid (both gas and liquid). Mass transfer and heat transfer are conducted on the tray of each plate. A perfectly operated distillation column has the mass transfer on each plate reaching equilibrium. These perfectly operated plates are called theoretical plates. The number of theoretical plates is represented by N_t. In modern distillation columns, to reach a higher mass and heat transfer efficiency, packing particles are used to fill the column which replaced the actual plates. These packing particles provide a surface for the heat and mass transfer between rising vapors and descending condensate. The more liquid-vapor contact, the better separation it provides. These particles are either loosely packed and work as a fluidic bed or densely packed and work as a packed bed. In these columns, traditional plates are not used anymore. However, the definition and number of theoretical plates are still used conceptually to represent the separation efficiency of the column. Due to technical and economical issues, the actual distillation factories always need to fit more theoretical plates in a shorter column to reach better separation at a lower expense. This demand requests the theoretical plates be made as thin as possible. Another concept was developed to describe the height of each theoretical plate, which is a height equivalent to a theoretical plate (HETP). The HETP has a relationship between the height (length) of a distillation column (H) and N_t (Equation 1) [71, 72]. A smaller HETP represents higher separation efficiency of packing material.

Equation 1 Height equivalent to a theoretical plate (HETP)

$$N_t = \frac{H}{\mathrm{HETP}}$$

Since HPLC columns are packed beds and are highly similar to the packed bed in industrial distillation, in 1941 Martin and Synge adopted the theoretical plate concept to characterize the efficiency of HPLC columns and packing materials. In Equation 1, H can represent the length of the column, N_t represents number of theoretical plates, and HETP represents the height equivalent to a theoretical plate. Therefore, higher N_t stands better separationin the entire column. A lower HETP can have a shorter column for the same separation in an HPLC column [73].

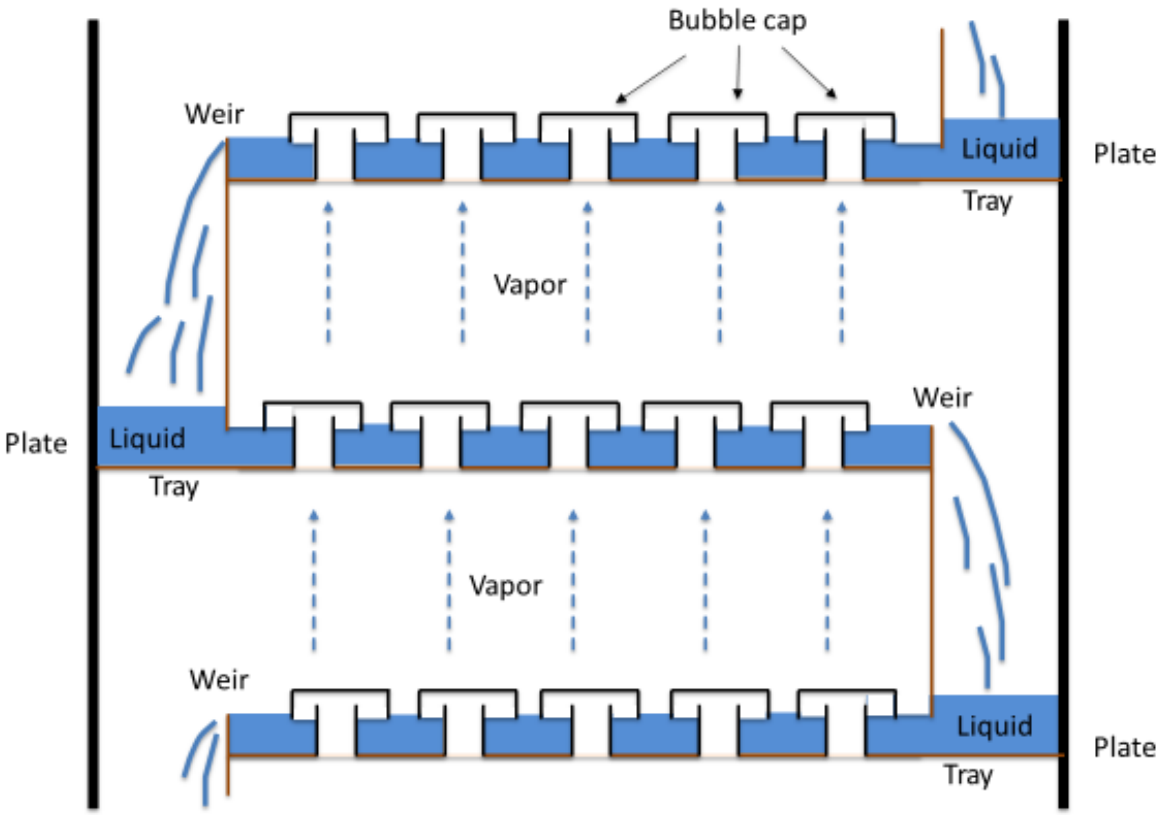

Figure 1-2 Typical plates made up of bubble caps and liquid trays in industrial distillation columns

To a given HPLC column and mobile phase, HETP can also be affected by the flow rate of the mobile phase. An inadequate flow rate can lead to insufficient solvent for mass transfer. A high flow rate can lead to the mobile phase refreshment exceeding the stationary phase-mobile phase mass transfer limit. This wastes mobile phase materials and decreases detector responses. Therefore, an optimized flow rate for the mobile phase is important to the success of an HPLC experiment.

The van Deemter equation (Equation 2) was developed to calculate the most appropriate linear velocity of the mobile phase to acquire the minimum HETP in a given HPLC system. In this equation, A is the eddy-diffusion parameter; B is the longitudinal diffusion coefficiency; C_s and C_m are the mass transfer coefficiency between the stationary phase and mobile phase. u is flow rate on linear velocity. In a given HPLC system, A, B, C_s, and C_m are fixed values. The eddy-

diffusion parameter A relates to the channeling-through generated by non-ideal packing. In another word, A is only related to the given packed column. B relates to the natural tendency of analytes to transfer from a higher concentration location to a lower concentration location. It follows Fick's laws of diffusion. Finally, C is determined by the correlation between the analyte, stationary phase, and mobile phase [73].

Equation 2. Van Deemter equation

$$\text{HETP} = A + \frac{B}{u} + (C_s + C_m) \times u$$

In Equation 2, the constants A, B, C_s, and C_m are bigger than zero. When plotting a figure of HETP against u , it falls into quadrant I. The derivative of HETP is:

$$\frac{dHETP}{du} = -Bu^{-2} + C_s + C_m$$

Let:

$$\frac{dHETP}{du} = 0$$

$$u = \sqrt{\frac{B}{C_s + C_m}}$$

Let:

$$u < \sqrt{\frac{B}{C_s + C_m}}$$

$$\frac{dHETP}{du} < 0$$

Let:

$$u > \sqrt{\frac{B}{C_s + C_m}}$$

$$\frac{dHETP}{du} > 0$$

Therefore, HETP has a theoretical minimum in the first quadrant. Both inadequate and excessive flow rates can increase HETP. When operating an analytical column, to reach the optimum separation efficiency, the flow rate shall be set around the most appropriate range. It should be close to:

$$u = \sqrt{\frac{B}{C_s + C_m}}$$

In a real experiment, the constants B, C_s, and C_m are unknown. The most appropriate flow rate is experimentally determined.

1.5.1.2 Chromatographic Dilution

During an HPLC experiment, the sample injected into the system is diluted by the mobile phase on the column. This dilution is called chromatographic dilution. It theoretically follows Equation 3 [74, 75].

Equation 3. Chromatographic Dilution

$$D = \frac{C_0}{C_{max}} = \frac{\pi d_c^2 \varepsilon (1 + k)\sqrt{2H \times \mathrm{HETP} \times \pi}}{4V_{inj}}$$

The chromatographic dilution factor (D) is defined by the initial concentration of the analyte (C_0) divided by the highest eluting concentration of the analyte during the chromatographic process (C_{max}). In the equation, d_c represents column ID, ε is total column porosity, k is retention factor, H is column length, HETP is plate height, and V_{inj} is injection volume [75].

1.5.1.3 Advantages of nano-HPLC

Traditional HPLC analysis usually employs a column with a 2.1-4.6 mm internal diameter (ID). The typical flow rate is usually set at 0.1-1 mL/min. The nano-HPLC approach, however, is performed on much narrower columns with 20-100 μm ID, and flow rates can range between 10-500 nL/min [76]. These narrow columns are made from capillary tubes and are called capillary columns.

Importantly, capillary columns are so narrow that the eddy diffusion phenomenon becomes negligible. Therefore, the eddy diffusion factor A in the van Deemter equation (Equation 2) approaches zero. It makes the capillary columns have dramatically lower HETP than regular HPLC columns. For the same column length, capillary columns can achieve a lot more theoretical plates than regular columns (Equation 1). In consequence, for the same kind of packing material, the capillary column can achieve much better chromatographic separation compared to regular HPLC columns [77].

According to Equation 3, D is and d_c^2 are positively correlated. Compared to conventional HPLC, nanoscale HPLC minimizes chromatographic dilution. When introducing a trapping column, the dilution factor becomes much lower than one. Therefore, the downscaling of an HPLC system to the nano range can dramatically decrease the chromatographic dilution factor, which significantly increases the downstream detection limit [78]. In theory, replacing the 4.6 mm ID column with a 50 μm ID column can lead to an over 8000 times improvement on the detection limit [79]. Details of packing nano-HPLC columns are described in Appendix I.

1.5.1.4 Agilent 1100 Capillary HPLC System and Thermo Easy nLC System

When I started this project, to achieve the nano-flow HPLC, I had access to two HPLC systems. They are a set of Agilent 1100 capillary HPLC stacks and a Thermo true nano HPLC system. In this section, I will demonstrate the mechanism and the advantages of each system.

The Agilent 1100 HPLC systems have been widely used by researchers for over two decades. They are easy to operate and modify which was important to the success of the approaches I have developed. Figure 1.2 depicts the general mechanism of the operation of an Agilent 1100 system in capillary flow mode. In this system, pumphead A and pumphead B deliver mobile phase A and mobile phase B independently according to the pre-set gradient. It is very similar to most binary pumps in Agilent HPLC systems. When operating in micro-mode, the flow rate of these two pumps together is set at 200 µL/min consistently. This is called primary flow. The electromagnetic proportional valve (EMPV) splits the primary flow into two portions. The major portion is released into waste and a smaller portion enters the flow sensor, which measures the flow rate between 1 µL/min and 20 µL/min. According to the flow rate setup in the HPLC method, the flow sensor feeds back to the system. The system controls the EMPV to actively adjust the splitting ratio to maintain the correct flow rate. The design of the autosampler in this system ensures the metering device (syringe), loop, needle, and all connections are either offline together when picking up the sample from sample plates or online together through the rest of the analysis. This design generates 15 µL of pre-column dead volume. When the system is set to operate on 20 µL/min from EMPV, this dead volume can cause less than one min delay on the gradient. However, this had a major impact on the ability to analyze the SNs which will be discussed in the following sections. The sampler can be set offline in the analysis period, but it was not necessary for this experiment.

Using the Agilent capillary HPLC to generate a nano-scale HPLC flow is not the ideal approach for nano-LCMS, but it is practical and cost-effective. This has been employed in various research publications [80-82]. The detailed setup of these systems is slightly different, but they are the same in general. To allow capillary HPLC to work as a nanoflow HPLC, the flow has to be split another time after the autosampler and a two-column (trap-elute) system has to be employed. The trap-elute setup is shown in Figure 1.3. It consists of an automatic external six-port valve (located on the mass spectrometer and controlled by the mass spectrometer method interface), a pre-column flow splitter, and a flow restrictor. The six-port valve has port #1 plugged and other ports connected

according to Figure 1.3. By switching the 6-port valve between the loading position and the analyzing position, the flow path of the mobile phase is alternated. When the system is in the loading position, shown in Figure 1.3a, the capillary pump delivers the mobile phase at the initial composition. The HPLC delivers the mobile phase on a low flow rate from EMPV (the actual flow rate will be discussed in the experiment section); the autosampler injects desired amount of sample (0.1-8 µL); and the mobile phase flow through the trapping column directly to the waste. The waste bottle is grounded to the frame of the mass spectrometer which in turn is grounded to the power supply. The system is set to maintain at the loading position for a few minutes to ensure the sample is captured by the trapping column and the majority of ionic compounds are flushed into the waste. The analytical column stays offline when the system is in the loading position to avoid salt contamination to a mass spectrometer from samples. When the system finishes loading, the six-port valve turns to the analyzing position and the flow rate of the capillary pump quickly ramps to 20 µL/min (Figure 1.4b). In this position, the majority of the mobile phase is split into the flow restrictor and eventually flows into the waste. Only 100-350 nL of the mobile phase flushes through the trapping column and the analytical column in each minute. The flow restrictor was made from fused silica capillary. Multiple lengths of fused silica restrictors have been tested. The testing result will be demonstrated in the result section (Chapter III). The function of the restrictor is to provide resistance to the mobile phase. This resistance changes with the gradient, but it produced a reproducible splitting ratio to the mobile phase going through the columns for the same gradient method. The 6 port valve on the autosampler is manufactured with M4 threads. This makes it very convenient and stable to connect 360 µm OD fused silica tubing directly to the system. The connection can be made of a standard M4 connector for 1/32" tubing with 0.015" ID 1/32" tubing as a sleeve. Part numbers will be demonstrated in the method section (Chapter III).

The Thermo Easy nLC system can operate either with one column similar to traditional HPLC or operate with two columns on the trap and elute mode as shown in Figure 1.4. All of the 6 port valves are using 10-32 thread, which is extremely difficult to connect with 360 µm OD fused silica tubing. Therefore, the OEM HPLC tubings, with connectors pre-installed, are inevitable when operating the Easy nLC system. It increases the operating expense dramatically. The sampler needle, one port, and one flow channel on the 6 port valve are permanently out of the flow path of the mobile phase. The sampling loop is only online for a very short period at the beginning of the

analysis. If the sample loop is kept online permanently, it introduces microliters of void volume before the column, which leads to a significant delay on the gradient. This design makes it possible to let the sampler needle pick up the sample while the system equilibrates the column. It can also wash the needle and the sample loop when the system runs gradient. This makes the overall operation much more efficient, especially for a nanoflow system. However, this design inevitably caused a major loss of SN peptides from the samples due to significant non-specific binding (see Chapter III, “Matrix effects for the SN family of peptides”).

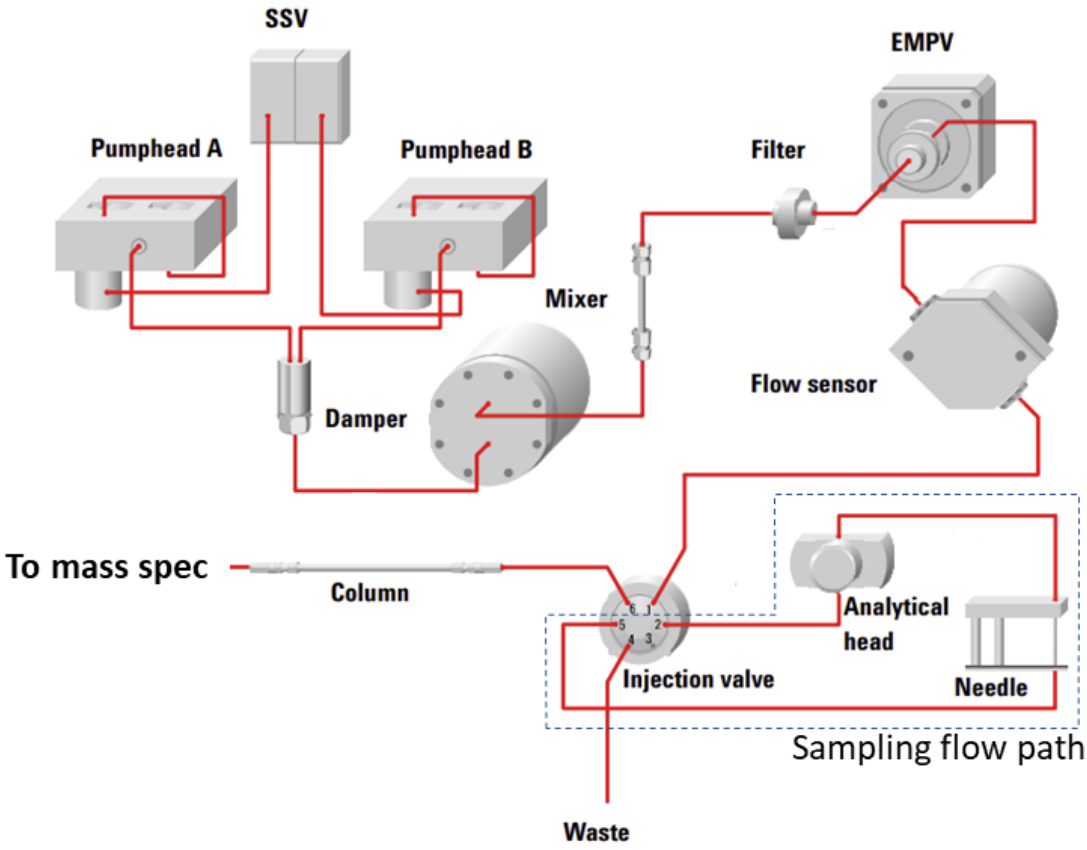

Figure 1-3 Mobile phase flow diagram of Agilent 1100 system capillary LC system. This diagram is modified from the Agilent manual edition 08/2002 Figure 2. The sampling flow path, within the dot line area, can be kept in the system for the entire elution time by connecting positions 1 to 2 and 5 to 6 of the injection valve.

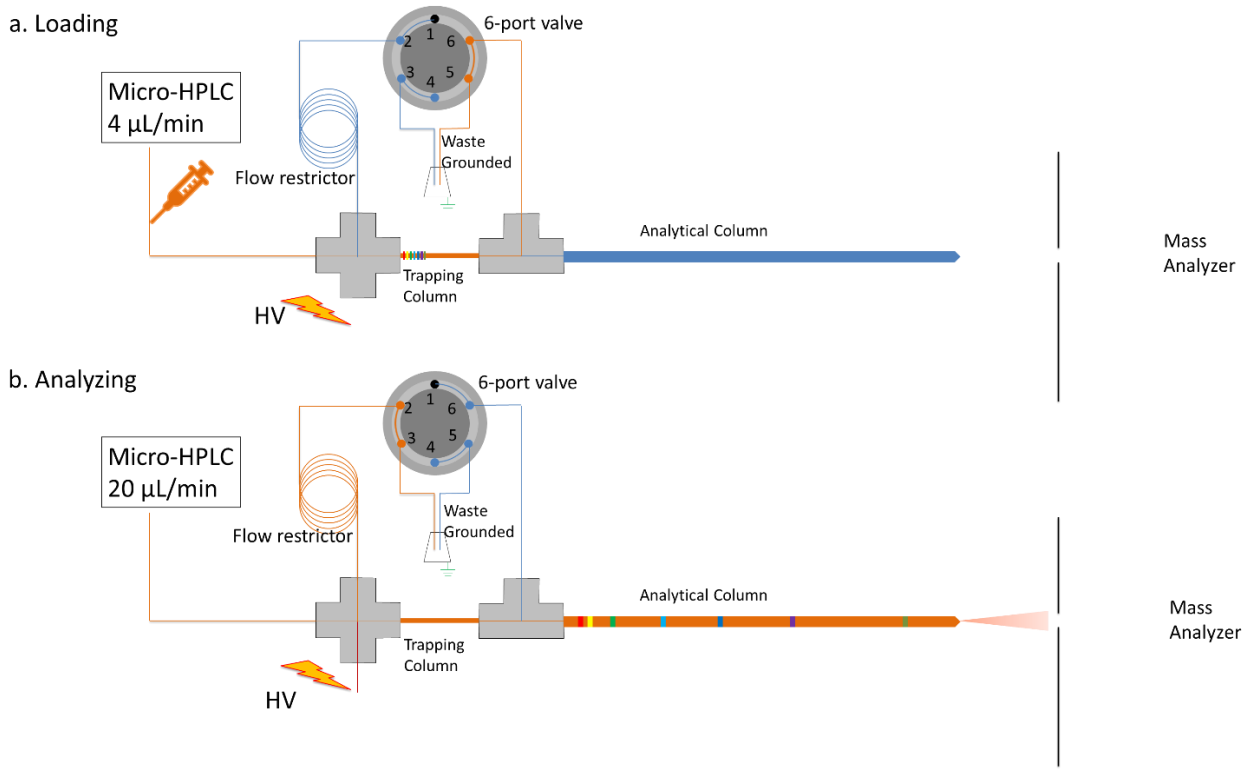

Figure 1-4 Fluidic connection diagram of Agilent 1100 capillary HPLC works as nanoscale HPLC in LCMS experiments. A represents the loading position. B represents analyzing position.

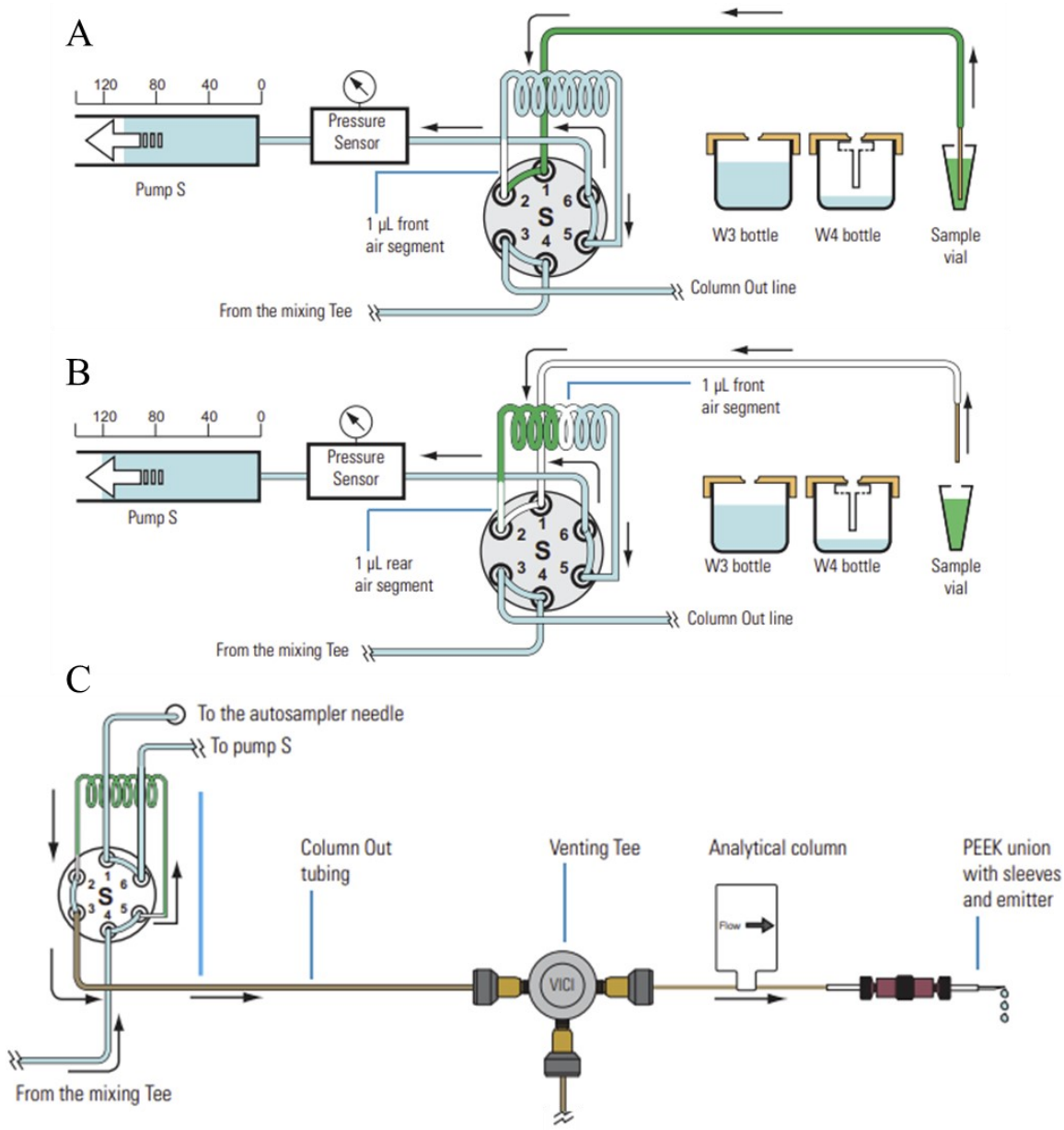

Figure 1-5 Physical layout and diagrams of the EASY-nLC 1000 sample pickup and loading steps. This diagram is modified from Thermo manual edition 'Touch-screen software Thermo EASY-nLC version 3.0'. A and B represent the sample pickup procedure with air segments before and after the sample solution. C represents the loading step on one column setup. The sampler loop is installed between 2 and 5 positions on the sampler 6-port valve. The loop is only included in the elution flow path when loading the sample. The injector needle and needle tube are connected on position 1 of the sampler valve. The needle, needle tube, valve port 1, and the flow channel between ports 1 and 2 are permanently out of the elution flow path.

Using the Agilent 1100 capillary HPLC systems as a nano-HPLC has been very successful in shotgun proteomics [83-85]. However, it has not been used routinely in other types of HPLC experiments. The LC elution in proteomic analysis has a very narrow and shallow gradient. In most cases, mobile phase B changes from 15% to 35% in 60 min [86, 87]. However, I wanted to analyze short peptides, long peptides, and steroids in one injection. This necessitates a wide, steep gradient slope in a limited time. The splitting ratio generated by the splitter is proportional to the difference in resistance generated by the column and by the flow restrictor. This resistance is directly decided by the flow rate and the viscosity of the fluid [88]. During a gradient elution, acetonitrile and water mix with each other in different ratios. This generates a continuous change in viscosity in the mobile phase. There is a dramatic difference in fluid dynamics between a capillary tube and a packed column bed [89]. When the viscosity of the mobile phase change with the gradient, the resistance generated by the restrictor and the column changes independently and differently. This causes splitting ratio inconsistencies through the HPLC gradient. When the gradient is narrow and shallow, the change in viscosity is slow and minor while the change in the splitting ratio is negligible. However, when the gradient becomes wide and steep, for example, a 70% change in 30 min in my experiment, the viscosity of the mobile phase changes rapidly. This causes a rapid change in the splitting ratio, leading to a dynamically changing flow rate and pressure in the column through the gradient. In regular HPLC experiments, the pump maintains the flow rate and tolerances the change in pressure. It is the key point to guarantee a reproducible chromatogram. If the flow rate and the pressure are both changing dynamically, a reproducible chromatogram becomes extremely difficult but very important.

1.5.2. Mass Spectrometry (MS)

Mass spectrometry was originally invented to measure the weight of a molecule. With modern technological advances, it can be used as a sensitive and accurate detector for HPLC in LC-MS/MS systems [90, 91]. In this section, I will review MS from ionization, resolution, accuracy, and data collection. In particular, understanding the concepts of mass resolution and data collection efficiency is important to utilize the analyzing power of a mass spectrometer for the hormone measurements outlined.

1.5.2.1 Nano-ESI

The mass spectrometer can only take gas-phase ions to analyze. When coupling with HPLC, ESI can be an ideal method to introduce the analytes into MS as gas-phase ions. In the ESI process, the less the solvent flows, the finer the spray is. It directly leads to significantly higher ionization efficiency, in another word, much higher sensitivity [92, 93].

1.5.2.2 Mass resolution

Mass resolution is one of the key factors to describe the analyzing power of a mass spectrometer. A mass spectrometer with sufficient resolution can significantly decrease the chance of false-positive results in LC-MS/MS experiments [94]. According to the International Union of Pure and Applied Chemistry (IUPAC), the resolution of a mass spectrometer can be characterized in 2 different ways [95]:

- 10 percent valley: Assuming two mass spectrum peaks with equal relative intensity, their m/z ratios are m_1 and m_2. These two peaks are separated by a valley with the lowest point equal to 10 percent of the height of either peak. The resolution R can be defined as Equation 4 or Equation 5. It is also represented in Figure 1.5A.
- Peak width: The peak width definition is made up of the single peak mass spectrum of a singly charged molecule. The resolution of a mass spectrometer can be expressed as Equation 6 where Δm represents the width of the peak at a certain peak height and m represents the mass of the molecule. This certain peak height is assigned as a fraction of the maximum peak height. There are three values commonly used as this fraction which are 0.5%, 5%, and 50%. When the fraction of 50% is employed, the peak width can also be called Full Width at Half Maximum (FWHM). Peak width using FWHM can be derived as Equation 7. It is also shown in Figure 1.5B.

Equation 4. 10 percent valley (a)

$$R = \frac{m_2}{m_2 - m_1}$$

Equation 5. 10 percent valley (b)

$$R = \frac{m}{d_m}$$

$$m = m_2$$

$$d_m = m_2 - m_1$$

Equation 6. Peak width

$$R = \frac{m}{\Delta m}$$

Equation 7. Peak width on Full Width at Half Maximum (FWHM)

$$R = \frac{m}{FWHM}$$

These three mass spectrometer resolution definitions are different in expression, but they demonstrate the same concept. In practical terms, this is how well a mass spectrometer can resolve a certain m/z ion from other very similar ones. Each of these definitions has its advantages in dealing with real issues.

FWHM-based peak width is more commonly used in LC-MS/MS articles and mass spectrometer operation interfaces. This will be the definition of mass resolution employed here.

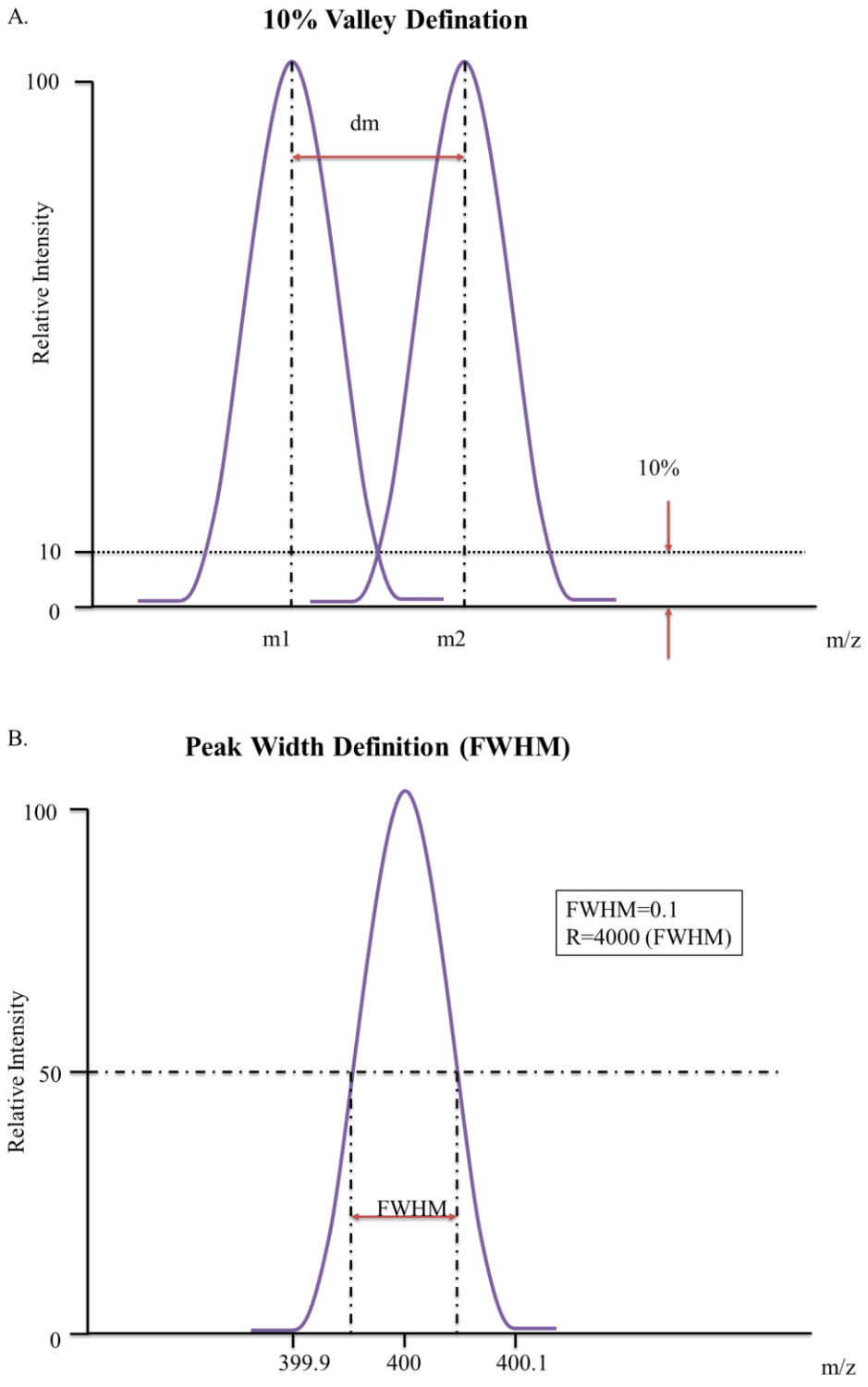

Figure 1-6 Mass spectrometer resolution is defined at A. 10 percent valley definition and B. peak width definition (FWHM). The peak width definition took 400 m/z ions with resolution 4000 as an example.

1.5.2.3 Mass Accuracy and Mass Tolerance

Acquiring the accurate mass of the molecule is important in a mass spectrometry measurement experiment. However, errors always exist, as with all the other measurements. Therefore, mass accuracy is another key factor to evaluate a mass spectrometer. Mass accuracy refers to the degree of conformity of a measured mass value to its actual true value [53, 94, 96]. Caused by equipment limitations, there will always be a difference between the experimental value and theoretical value in mass spectrometer measurements. Mass tolerance defines the maximum acceptable difference between these two values [97].

When processing data, mass tolerance can be manually set. It can be either an absolute difference in Daltons or a fractional difference in parts per million (ppm.). In most cases, the fractional difference form is employed because the measurement and calibration error is proportional to the mass [98]. It is important to set up an appropriate mass tolerance value. If the value is set too high, the false positive would be significant. If the value is set too low, some mass spec signals may be neglected and result in no MS response [99].

1.5.2.4 Scan Speed and Acquisition Speed

In the previous sections, I reviewed mass resolution and mass accuracy. These two concepts evaluate how much detail and how accurate a mass spectrometer can measure when studying the weight of a molecule. When using a mass spectrometer as a detector for a chromatography system, there is another crucial to evaluate the machine, which is how quickly the mass spectrometer can complete a measurement [100].

When running an HPLC experiment, the analyte elutes out of the column within a certain time. The concentration of the analyte fits into normal distribution during this period. When studying multiple compounds of interest in an HPLC run, these compounds can be overlapping in elution time. This requests the mass spectrometer to work quickly enough to collect sufficient mass information for qualification and quantification studies [101].

Scan speed and acquisition speed are critical parameters to evaluate how quickly a mass spectrometer can work. Scan speed refers to how many daltons a mass spectrometer can analyze in one second, expressed as $Da \cdot s^{-1}$. The different mass analyzers have different scan speeds. For

the same analyzer, the setting on resolution can also influence the scan speed. In general, the higher resolution, the slower a mass spectrometer can scan [102]. Acquisition speed represents how many spectra a mass spectrometer can generate in one second, expressed as $Spec \cdot s^{-1}$or Hz. To a given mass spectrometer, acquisition speed can be influenced not only by analyzing speed but also by mass range, acquisition mode, ion injection time, enrolment of collision cell, etc [103].

1.5.2.5 Data-Dependent and Data-Independent Acquisition, and Time Segment

Data-dependent and data-independent acquisition are two common methods to collect MS data from chromatographic elution. They are meant to optimize the analyzing power of a mass spectrometer [62, 101, 104]. Data-dependent acquisition starts with a master scan in each duty cycle. The onboard computer (located inside the mass spectrometer) analyzes the mass information collected from the master scan and decides on how to proceed with the following scans within the current duty cycle. The following scans perform MS^n on selected ions with a certain charge, m/z ratio, neutron loss, or isotopic distribution. The onboard computer can also monitor the mass spectrum intensity as a chromatogram from the master scan to decide the most appropriate timing to trigger the data-dependent scan [104]. Data independent acquisition runs on the pre-set method from the off-board computer regardless of what mass information it acquires during the LC-MS/MS analysis [104]. The time segment lets the mass spectrometer operator allocate the analyzing power by the time [63, 104]. In my work, all of the MS2 data were collected by data-dependent acquisition on mass list and charge state. More details will be described in the Materials and Methods section.

1.5.2.6 Linear ion trap analyzer and orbitrap analyzer

I was able to access two mass spectrometer systems. The Finigan LTQ mass spectrometer uses a linear ion trap as a mass analyzer. It can have a mass resolution (FWHM) of 1,000 on normal scan mode or mass resolution (FWHM) of 10,000 on ultra-zoom scan mode. The acquisition speed for a 1,000 Da range is 10 Hz in regular scan mode and 0.8 Hz in ultra zoom scan mode. Taking the monoisotopic ion of mSN (1217.9 m/z triply charged), into Equation 7, the theoretical FWHM is 1.2 in normal scan mode and 0.12 in ultra zoom scan mode. Because the isotopic peaks are 0.33 apart for the triply charged ions, the normal mode can not isolate the monoisotopic ion of mSN (and other SNs) for quantification purposes. The ultra zoom scan mode can isolate the

monoisotopic ion of mSN (and other SNs) for quantification purposes. However, the 0.8 Hz acquisition speed can only provide 8 mass spectrums within a 10 s chromatographic peak, which is not sufficient for MS2 structural confirmation [105].

The Thermo LTQ Velos Pro Orbitrap is a hybrid duo pressure linear ion-trap analyzer and orbitrap analyzer. The linear ion-trap analyzer has a mass resolution (FWHM) of 1,000 on normal scan mode or mass resolution (FWHM) 10,000 on ultra-zoom scan mode. The acquisition speed for the linear ion-trap analyzer for a 1,000 Da range is 10 Hz in regular scan mode and 0.8 Hz for ultra-zoom scan mode. The orbitrap analyzer, for a 1,000 Da scan, has an acquisition speed of 1 Hz on mass resolution (FWHM) 60,000 or an acquisition speed of 3 Hz on mass resolution (FWHM)30,000. The resolution of the orbitrap analyzer is enough to isolate the monoisotopic peaks for all analytes with 10 ppm mass tolerance. It can also provide enough data points to plot chromatograms for quantification purposes. When setting up a data-dependent acquisition for MS2 scans properly, the machine can commend the ion-trap analyzer to use the MS1 from the orbitrap analyzer as a master scan and collect the MS2 information of target analytes with no interference to the duty cycle of the orbitrap analyzer [106, 107].

Considering accessibility and the different costs and to run these two mass spectrometer systems, I used the Finigan LTQ mass spectrometer (in-house) to develop and validate the HPLC method. All experimental samples were run on the LTQ Orbitrap mass spectrometer (Figeys Lab, OHRI).

1.6 Preparing standard peptides by FMOC chemistry and HPLC purification as well as confirming zebrafish secretoneurin peptide sequences by targeted and untargeted peptidomics

The sensitivity and reliability of peptide LC-MS/MS analysis can be improved if there are synthetic standard peptides available. I prepared standard peptide samples by FMOC solid-phase chemistry followed by HPLC purification. In this section, I will review the FMOC chemistry including the basic mechanism, peptide synthesis resins, and building disulfide bonds.

Except for the intact SN peptides, all the sequences and modifications I needed had been previously characterized by LC-MS/MS. Therefore, I had to confirm the sequence of intact SN peptides ahead of synthesis. I will review this part from the background of secretoneurin, untargeted peptidomics, targeted peptidomics, and current progress in measuring SN by LC-MS/MS (see section 1.5 Background on secretoneurin).

1.6.1 The basic principles of FMOC chemistry

SPPS

In 1963 and the years after, a few publications contributed by Merrifield demonstrated the possibility of a revolutionary peptide synthesis concept [108-110]. This new route to prepare synthetic peptides is named solid-phase peptide synthesis (SPPS). After numerous successful practices, R.B. Merrifield was awarded the 1984 Nobel Prize in Chemistry for his outstanding achievements in chemical synthesis on a solid matrix. Since then, the solid matrix material and related reagents used in SPPS have evolved significantly, but the frame of the strategy has not changed significantly. Shown in Figure 1.6, peptide chains are constructed on a solid matrix (resin) with stepwise elongation. By repetitive proceed deprotecting, washing, coupling, and washing steps, desired peptides could be built on resin with all side-chain protected from C-terminus to N-terminus. The efficiency of each coupling or deprotection step can approach 100% by extending the reaction time and repeating the reaction multiple times. This, as a result, can optimize the overall yield and purity. The final peptide product can be obtained by cleaving the peptide from the resin and removing all sidechain protection simultaneously [111, 112].

Fmoc chemistry and coupling reagents

When Merrifield first introduced SPPS, he used Boc chemistry which requires harsh acidic deprotection (hydrogen fluoride) and basic labile synthesis resin. The restricted reaction conditions made it unreachable for most of the research laboratories [108]. The situation did not change much until, three decades later, Fmoc chemistry was developed and used in SPPS [112-114]. The milder alkylic deprotection and acidic cleavage conditions make the SPPS methods more applicable to most of the labs with a higher yield.

Fmoc chemistry SPPS has dominated the peptide synthesis industry for thirty years. Numerous coupling reagents have been developed to pursue higher kinetic and dynamic when maintaining accuracy. After HBTU proved its success, most of the newly invented coupling reagents are aminium salts. The efficiencies of these reagents are similar when their structures are similar as well. More details of these coupling reagents have been well-reviewed, and will not be covered here [115].

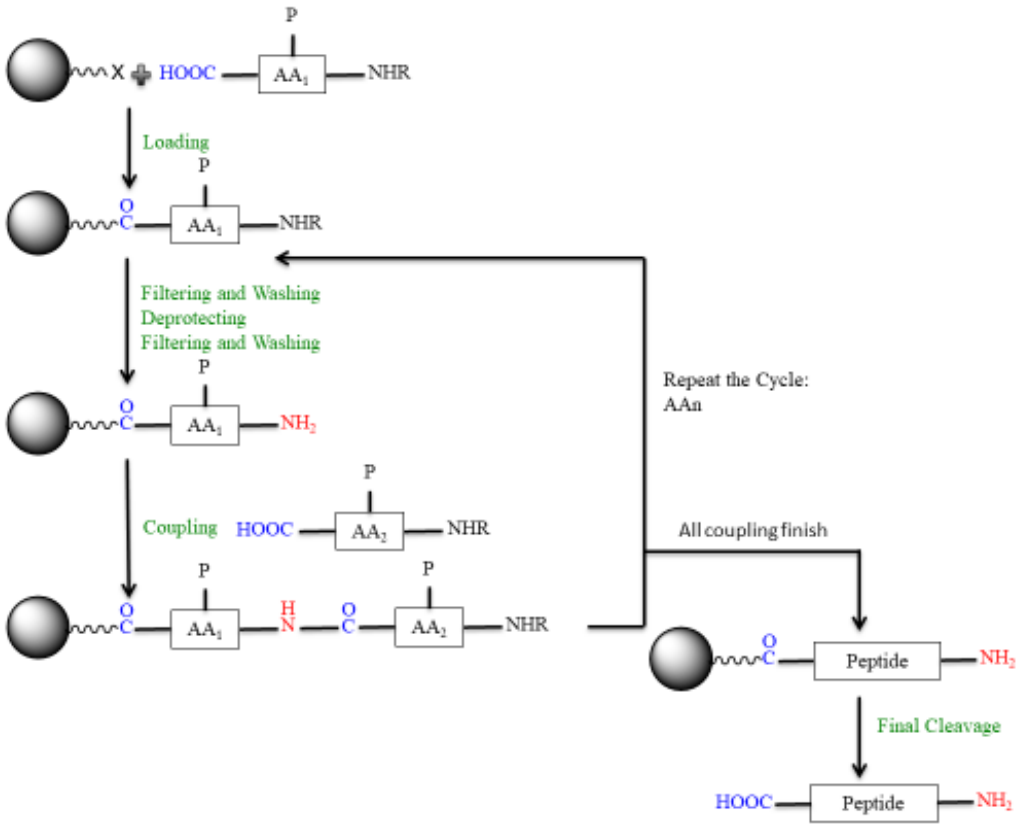

Figure 1-7 A schematic diagram represents the common procedure of SPPS. AA represents an amino acid. AAn represents the nth amino acid counted from the C-terminus of the peptide.

Peptide synthesis resins

Resin is very important to SPPS. It is made from crosslinked polymers with active reaction sites scattering on the polymer chains. As shown in Figure 1.7, reactants and washing solvents need to be absorbed into the crosslinking network so that they could access the reaction sites and let the reactions happen [116, 117]. Therefore, the swelling factor (usually between 1-15 times the original resin volume) is one of the key factors when choosing resin for SPPS. A higher swelling factor can provide better reaction kinetic but consumes more material and is harder to wash. A lower swelling factor resin is easier to work with but may not give enough access to the reactants, especially for larger peptides. The density of reaction sites loaded on the resin (usually between 0.1-1.0 mmol/g of resin) is also important to the success of SPPS. For a certain amount of resin,

more reaction sites can lead to a bigger amount of final product but decrease the purity of the final product. Contrarily, lower loading density can usually increase the final purity but consume more reagents. Today, after years of development, many grafted polystyrene-based solid phase synthesis resins with various particle sizes, swelling factors, and loading densities are commercially available for different research and industrial purposes.

Another key factor when choosing the most appropriate resin is the linker. The linkers provide the connections between the active reaction sites to the polymer resin. They are stable through the synthesis procedures and labile at the cleavage step. To prepare peptides with different modifications or structures, various linkers have been developed and combined with the previously introduced resins. The most popular linkers presently are Rink amide, Wang, and 2-chlorotrityl linkers. The Rink amide linker was purpose-developed for Fmoc chemistry to produce peptide amide. It is stable under alkalic conditions and moderate acidic conditions[118]. To provide better stability for long-time storage, Rink amide resins are usually produced as Fmoc coupled amide. The Wang linker is the most widely used acid-labile linker in SPPS to prepare peptide amide. They are 4-hydroxy benzyl alcohol moieties connected to the polystyrene backbone, which is easy to manufacture at a very low cost. However, it is hard to couple the first amino acid to the hydroxyl group, especially with a regular peptide synthesis coupling protocol. This makes it hard to finish the first amino acid coupling in automated machine synthesis. Therefore, Wang linker resins are usually sold with amino acid-loaded forms [119]. Resins with 2-chlorotrityl linkers are widely used to prepare peptide acids. 2-Chlorotrityl linker could be cleaved by 1% TFA in DCM while all side-chain protections are maintained. It is suitable to prepare peptides that need off-resin modifications [120].

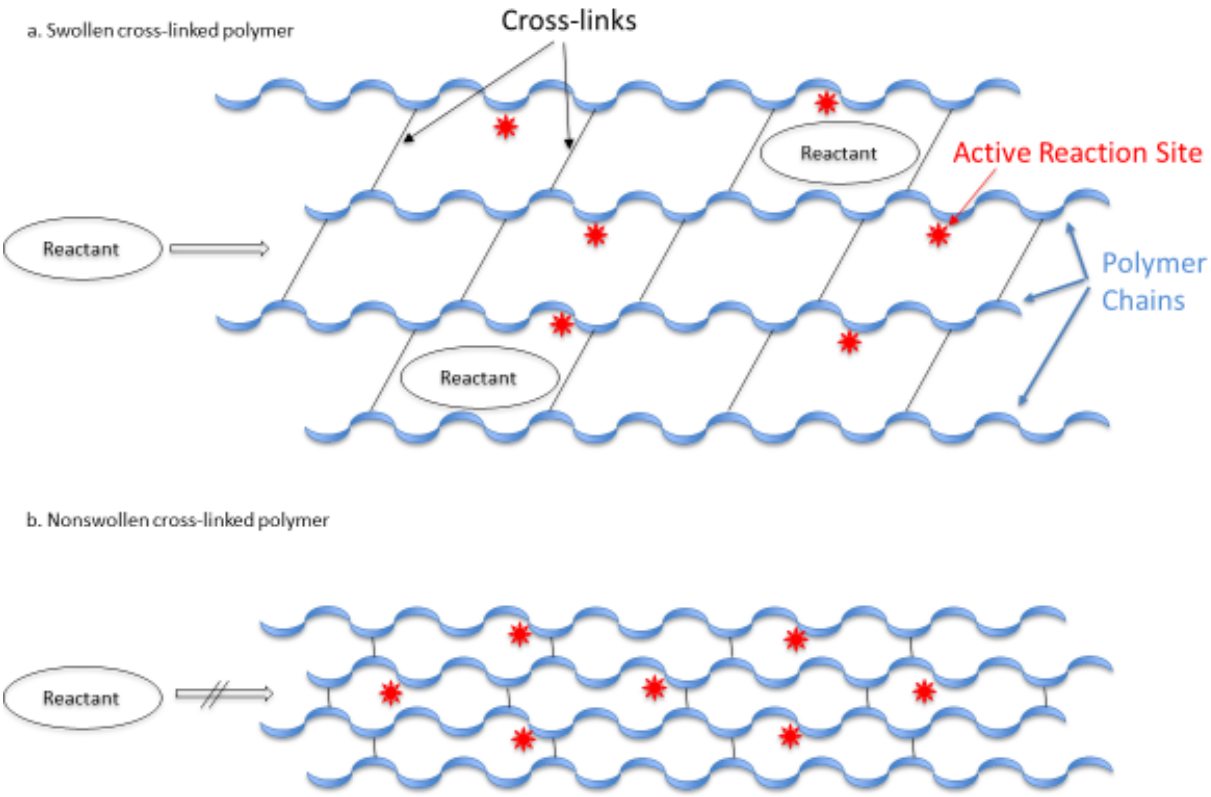

Figure 1-8 Schematic diagram of swollen effect on cross-linked polymer. a. reactant can access the active sites in the polymer network when swollen in. b. reactant can not access the reactant inside the polymer network without swollen

Building disulfide bonds

Mouse oxytocin, mouse vasopressin, zebrafish isotocin, and zebrafish vasotocin are cyclic peptides with disulfide bridges between C1 and C6. The intramolecular disulfide bound can be formed in solution after the peptide is cleaved from the solid support. With appropriate deprotection reagents and oxidants (oxygen or DMSO), the peptide can naturally fold in the correct conformation ensuring the correct disulfide bridge pattern [121, 122]. The in-solution oxidation may lead to self-aggregation. There is another strategy to build the disulfide bridges, which is to proceed with the oxidation reaction on resin with all the sidechains protected except the thiol groups. This can avoid self-aggregation because the intermolecular thiol groups are too far to establish a disulfide bond. In the meantime, because the other side chains remain protected, the

peptide chain is ridged and difficult to fold to form the bound. Hu et al. successfully built the disulfide bridge with 2.5 h on-resin treatment of iodine at room temperature using Fmoc chemistry. In that reaction, the iodine treatment showed the ability to remove the thiol-Acm protecting group and establish the intramolecular disulfide bridge at the same time [123]. In this experiment, both the in-solution oxidation and the on-resin oxidation strategies were tested on all of the cyclic peptides.

1.7 Hypothesis

In this thesis, I will test the hypothesis that sorbent composition and extraction strategy will determine the resolution of simultaneous detection and quantification of peptide, steroid (and protein) hormones from small tissue samples.

To test the hypothesis, I propose a novel approach to extract and quantify hydrophilic neuropeptides and lipophilic steroids from the same sample. The list of targeted hormones is shown in Table 2. Zebrafish and mouse are selected as biological models for method development and validation.

Chapter II Development of a robust sample processing method for peptide and steroid extraction in a single sample

2.1 Introduction

There are many kinds of commercialized homogenization buffers and disposable SPE cartridges on the market. Regarding steroid and peptide extraction, these buffers and cartridges target the steroid or peptide analytes separately. Table 1 lists a few commonly used SPE cartridge products. I tested the Agilent SampliQ SPE cartridge. It had a reproducible, high recovery rate on the steroid analytes, however, it did not retain hydrophilic peptides like GnRH peptides. Another extraction cartridge I tested was the Thermo Pierce spin columns. These spin columns were very reliable on peptide extractions and cleanups, however, their recovery rate on steroids was low and variable. I attempted to blend the sorbents from these cartridges. There were no successful results. There are research laboratories that published in-house prepared homogenization buffers, SPE cartridges, and corresponding protocols [41, 49]. These methods were also focusing on either steroids or

peptides, and never at the same time. However, these publications laid the foundation for me to develop a sample processing method and corresponding protocol for my project.

In this chapter, I will introduce the development of a novel sample processing method. It includes both the homogenizing and SPE methodologies. It is the first time that steroid and peptide hormones are extracted at the same time with very high reproducibility.

Table 1 Common disposable SPE cartridges for peptide or steroid sample processing

Distributor	Description	Catalog number	Price/ cartridge	Target analyte	Sorbent Amount
Agilent	SampliQ Solid Phase Extraction (SPE)	5982-3036	$4.80	Steroid	60 mg
Sigma	Discovery® DSC-Si SPE Tube	52652-U	$2.00	Steroid	50 mg
Thermo	Pierce™ C18 Spin Columns	89870	$6.34	Peptides	20 mg
Thermo	SOLA™ SPE Cartridges	60109-001	$3.45	Steroids	10 mg
Waters	Oasis MCX 1 cc Vac Cartridge	186000252	$3.75	Peptide	30 mg

2.2 Experiments

2.2.1 Materials and methods

The reverse-phase sorbent employed in this experiment was ReproSir-Pur 120 C18-AQ from Dr. Maisch HPLC GmbH (Cat# r10. aq). The filtered 96-well plate was from OROCHEM (Cat#. OF1100-7PE). Water was in-lab prepared using the Milli-Q water purification system and all other chemicals were purchased from Thermo Fisher Scientific.

All zebrafish tissues were dissected and placed directly into 1.5 mL centrifuge tubes with 200 µL homogenization buffer. Mouse tissues were dissected and placed into 15 ml centrifuge tubes with 1000 µL homogenization buffer. The composition of the homogenization buffer is 90% MeOH, 9% water, and 1% acetic acid v/v/v. To homogenize the tissues, the probe homogenizer (Fisherbrand, Cat#FB120110) was operated at 10 Watts for 20 s on zebrafish tissues and 1 min for

mouse tissues. The heat generated in this procedure did not appear to have any influence on the results.

2.2.2 Experimental design

Optimizing SPE method

To optimize the composition of the solvent, GnRH1, mSN, and P4 were selected as tracers for the extraction and dissolved in 0.2% FA and 5% acetonitrile in water solution (1 pmol/μL) because they cover a wide range of sizes and hydrophobicities. The SPE plate was prepared with 10 mg of sorbent in each well. Activation buffer (0.2% FA and 50% acetonitrile) was added to each well 4 times with 200 μL each time. The filtered plate (Orochem OF1100-07PE) was centrifuged on top of the waste tray for 1 min at 500 cfm to remove the flow-through. To equilibrate the SPE plate, 200 μL equilibrium buffer (0.2% FA and 5% acetonitrile) was flushed through each SPE bed 8 times. A 1 min 500 cfm centrifugation was employed to accelerate the equilibration steps. After equilibrium, 50 μL of the indicator sample was loaded to each well followed by 4 times 200 μL washing using equilibrium buffer. There was 1 min of 1000 cfm centrifugation after the loading and each wash. All flow-through was flushed to waste. Then the SPE beds were eluted individually with 300 μL of each elution candidate buffer. The buffer candidates contain 0.2% FA and 70%, 75%, 80%, and 85% of acetonitrile. The elutions were collected and analyzed independently to determine the most appropriate elution buffer. A standard curve was used to estimate the recovery rates. When analyzing the data, the post-hoc comparisons were performed by comparing the recovery rate from every other group of elution buffer to the 70% acetonitrile group with Dunnett's test on 90% confidence intervals. The difference of 5 in one tail was selected as an equivalent level because most LC-MS/MS equipment can have a standard error of 10% (Figure 2.2). If the comparison resulted in non-equivalence, the 70% group for the tested compound was neglected. Then the post hoc measurements were performed by comparing the recovery rate from every other group of elution buffer to the 75% group with the Dunnett test on 90% confidence intervals.

To establish appropriate amounts, 3, 5, 10, 15, and 20 mg of sorbent were individually loaded into wells of a filtered well plate (N=5). To each extraction bed, the supernatant of 3 zebrafish brain homogenate was loaded with tracing chemicals. Note that these peptides are mammalian forms and P4 is low in the zebrafish brain, so they serve here as external calibrators for the endogenous

molecules of similar structure. The spiking compound recovery rates were analyzed after washing and elution.

The amount of elution buffer was determined by preparing an SPE plate same as stated above. In the elution step, 20 µL of the elution buffer was added individually multiple times. The number of elution times tested varied incrementally from 1 to 10. The total elution from each SPE well was collected and analyzed to establish the most appropriate times of elution. When analyzing the data, the difference of 5 in one tail was selected as an equivalent level because most LC-MS/MS equipment can have a standard error of 10 % (Figure 2.3).

Validation

The validation of this SPE method was focused on the reproducibility of each analyte in the actual tissue sample. To examine this, 20 pmol of each analyte was spiked into pooled homogenates of 5 zebrafish pituitaries. After centrifugation, the supernatant was lyophilized, resuspended, and aliquoted to 5 individual SPE experiments. The elutions from the 5 extractions were analyzed independently and compared to a standard curve to evaluate the variance of the recovered analyte.

2.3 Results and discussion

2.3.1 Amount of sorbent

The elution from all sorbent beds were analyzed by LC-MS/MS independently (N=5) and compared to the same standard curve. The recovery rate data for each indicator analyte was analyzed by one-way ANOVA followed by Dunnett's test with the 3 mg sorbent group as control. The results (Figure 2.1) indicated that the recovery rates for each analyte from the 5, 10, and 20 mg SPE beds were equivalent to the recovery rate from 3 mg beds separately. In other words, increasing the SPE bed volume did not make any considerable change to the recovery rates.

Mouse tissue samples will be eventually processed and analyzed using this method. To reduce method optimization steps procedures for mouse samples, the 10 mg was selected as a standard SPE bed volume. This amount of sorbent is about mid-range for commercial SPE cartridges (8-15 mg). The sorbent uses has a 10 µm particle size, which is smaller than that in most commercial cartridges (20-50 µm). This provides the SPE bed with a higher loading capacity and efficiency.

In the meantime, the smaller particle size requires a finer mesh in the frits. Both the smaller sorbent size and the finer frit can significantly increase the necessary pressure to operate the SPE experiment. It also makes the SPE system easier to experience clogging. The finer sorbent and frit, in the meantime, lead to better protection to the HPLC system.

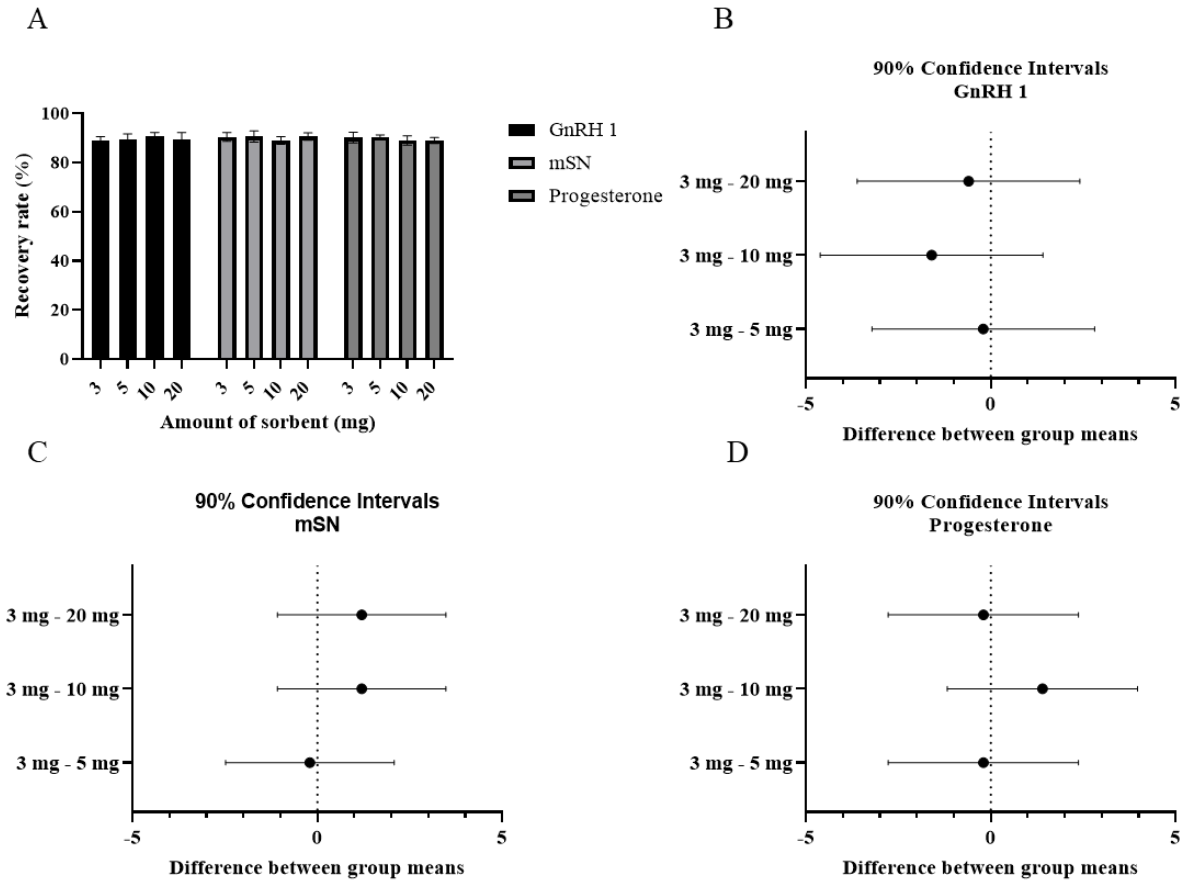

Figure 2-1 SPE recovery rates for indicator analytes (GnRH 1, mSN, and progesterone) on 3 mg, 5 mg, 10 mg, and 20 mg sorbent beds. A: Column diagram of the recovery rates of each analyte after SPE from different amounts of sorbent. The error bar represents the standard deviation (N=5). For each analyte, the recovery rate was analyzed by one-way ANOVA followed by Dunnett's test (90% confidence intervals). The difference of 5 in one tail was selected as equivalent level because most LC-MS/MS equipment can have a standard error of 10%.

2.3.2 Composition of elution buffer

The recovery rates of indicator analytes from each elution buffer composition were analyzed by LC-MS/MS and compared to the same standard curve. The overview of the recovery rate on each elution buffer is presented in Figure 2.2A. Comparing the recovery rate of 75%, 80%, and 85% acetonitrile to the 70% by 90% confidence intervals, only GnRH 1 was fully eluted by 300 µL of 70% acetonitrile (Figure 2.2B, C, E). Progesterone and mSN were fully eluted by 300 µL of 75% acetonitrile (Figure 2.2D, F) Therefore, 75% acetonitrile with 0.2% FA in water was selected as the elution buffer.

In this experiment, the 300 µL of elution buffer is relatively high compared to the void volume of the SPE bed. The biological samples in this project are very complex. This SPE would be the last step to simplify the sample before LC-MS/MS analysis. The HPLC used was a nanoscale HPLC system, which was an Agilent 1100 capillary HPLC modified in-house. The accumulation of fat molecules in the trap column can have a significant impact on the results. Therefore, in this SPE procedure, the elution needs to be stopped soon after the last analyte, P4. This is why the elution buffer was optimized to be as polar as possible with elution volume being as low as possible.

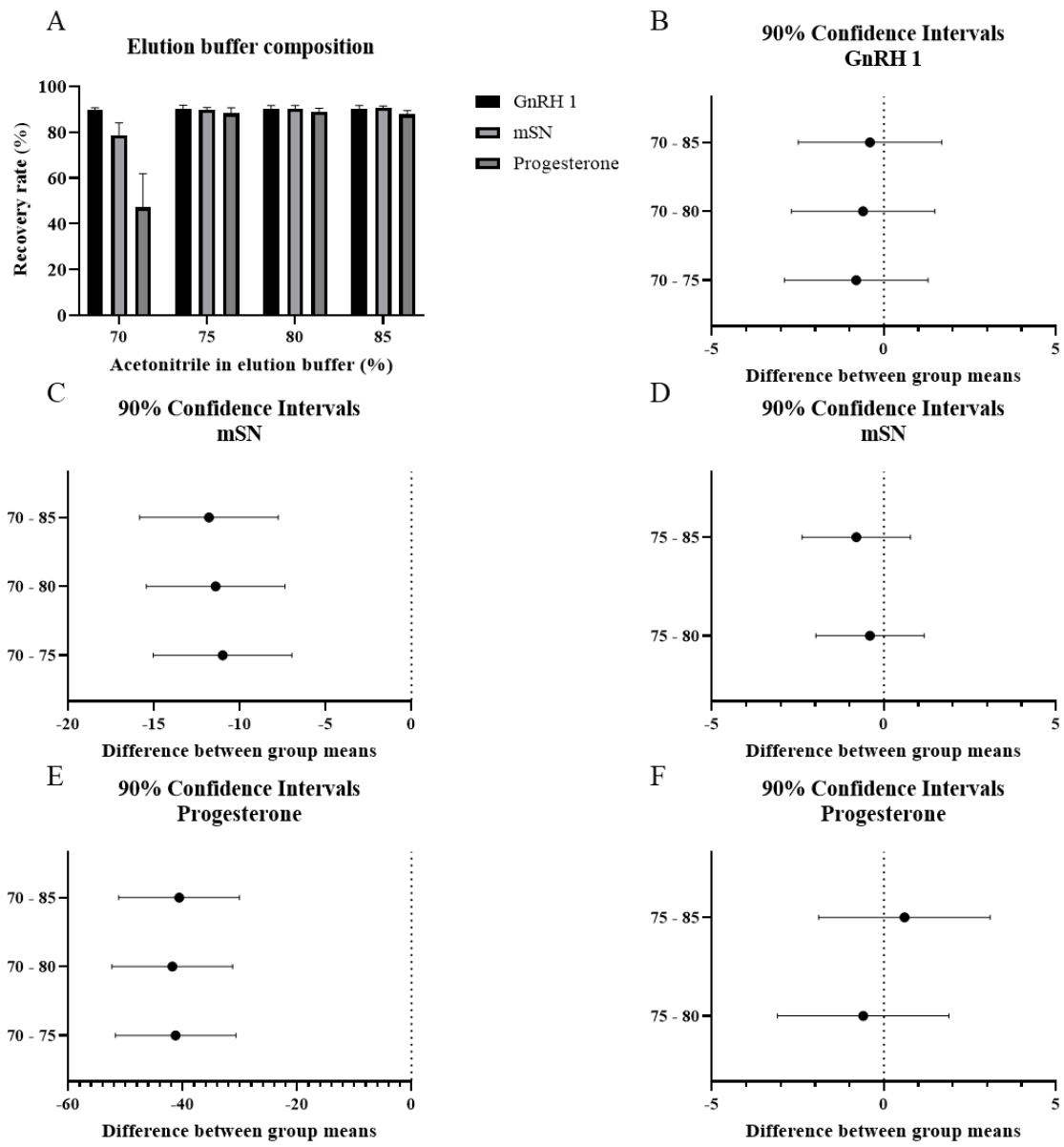

Figure 2-2 SPE recovery rates for indicator analytes (GnRH 1, mSN, and progesterone) for 70%, 75%, 80%, and 85% acetonitrile in the elution buffer (N=5). Figure 2.2A illustrates the recovery rates of each analyte after SPE from different elution buffers. In this diagram, the error bar represents the standard deviation. For each analyte, the recovery rate was analyzed by one-way ANOVA in Figure 2.2B, C, D. The post hoc measurements were performed by comparing the recovery rate from every other group of elution buffer to the 70% group with the Dunnett test on 90% confidence intervals. The results for GnRH 1 are in Figure 2.2B. The results for mSN are in Figure 2.2C and D. The results for progesterone are plotted in Figure 2.2E and F. The horizontal axis for B, D, and F are locked between -5 and +5 to represent the equivalence.

2.3.3 Elution times

To determine the minimum volume of elution buffer for an efficient elution, a ten times 75% acetonitrile elution experiment was conducted. According to Figure 2.3A, the total recovery rate reached a maximum after 5 elutions. Comparing the recovery rates of each analyte, the GnRH1 recovery rates for 4-10 elutions were equivalent to 3 elutions (Figure 2.3B). For mSN and P4, the recovery rates for 6-10 elutions were equivalent to 5 elutions (Figure 2.3C and D). For the final protocol, 6 rather than 5 elutions were chosen to overcome potential unforeseen minor variation or errors from buffer or matrix effects elution process was designed to be stepwise rather than 120 µL (6×20 µL) in one shot to maintain the composition of the elution buffer. The equilibrium buffer from the washing step can modify the composition of the elution buffer. The stepwise elution ensures that the composition of the later portion of the elution buffer is closer to the designated concentration.

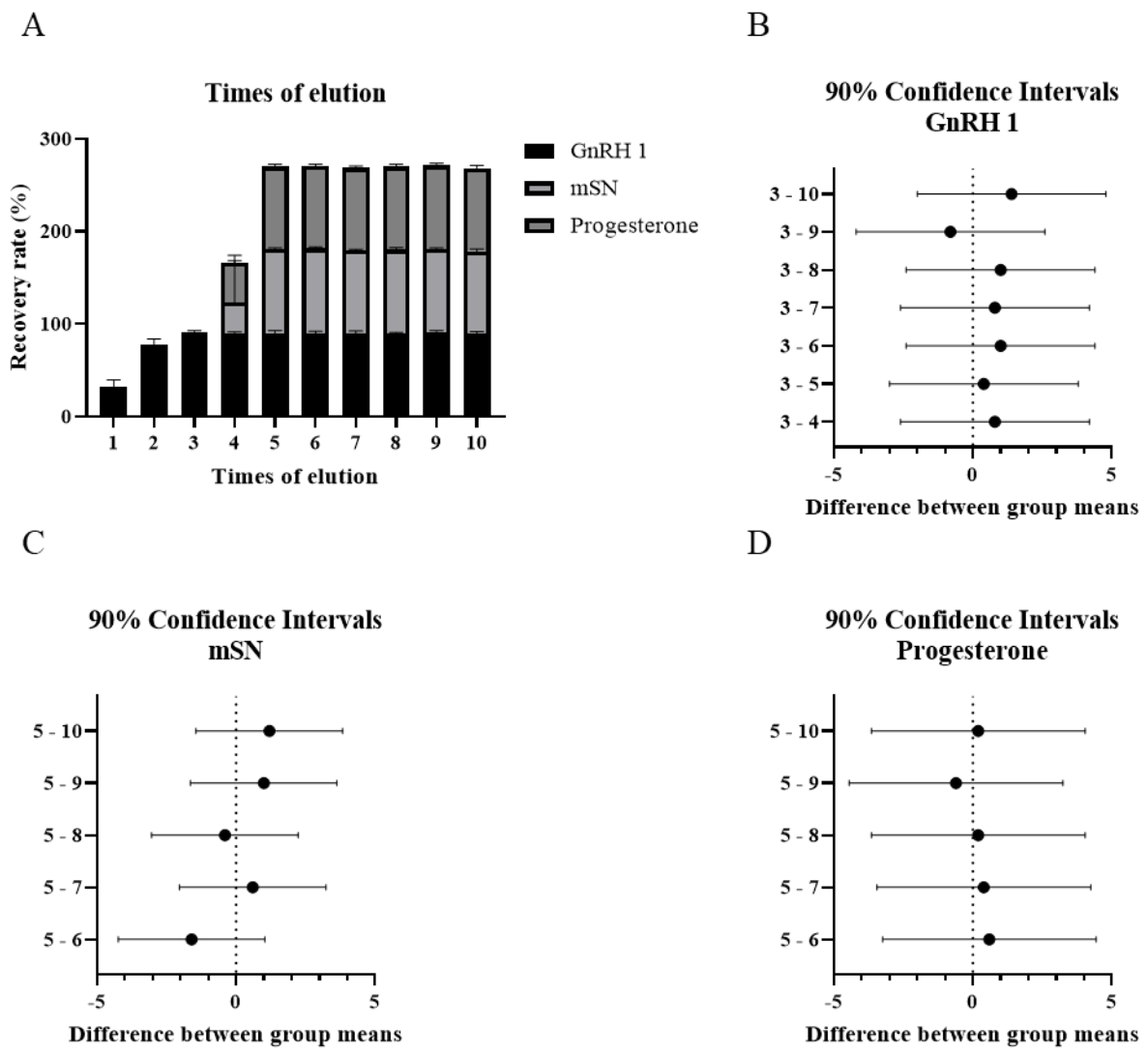

Figure 2-3 SPE recovery rates result for indicator analytes (GnRH 1, mSN, and progesterone) on 1 to 10 times elution by 0.1% formic acid, 75% acetonitrile (N=5). Figure 2.3A is a column diagram of the recovery rates of each analyte after SPE from different times of elution. In this diagram, the error bar represents the standard deviation. For each analyte, the recovery rate was analyzed by one-way ANOVA. The post hoc measurements of GnRH 1 were performed by comparing the recovery rate from every other group of elution times to the 3 times group with the Dunnett test on 90% confidence intervals in B. The test results for mSN, and progesterone is plotted in C and D in sequence by comparing every other group to the 5 times elution using Dunnett test on 90% confidence intervals. For B, C, and D, the horizontal axis is locked between -5 and +5.

2.3.4 Validation of the SPE method

The sorbent employed in this experiment was originally manufactured for packing HPLC columns (Dr. Maisch HPLC GmbH). The same sorbent with a smaller particle size was used to prepare the analytical and trap HPLC columns (Chapter III). This sorbent was highly suited to the current sample system. Due to the fluctuation of experimental conditions and potential human errors, minor parameters such as centrifugation strength, temperature, frit pore size, etc. were also adjusted to ensure reproducibility between each extraction.

After all optimizations, the LC-MS/MS results from extracted tissue samples were compared to the same standard curve for hormone quantification. The recovery rate was not applicable in this situation because of the interference from the endogenous analytes. Therefore, the coefficient of variation (relative standard deviation) was selected to evaluate the reproducibility. The intra-day coefficient of variation was 5-15% for the different analytes. Generally, later eluting compounds exhibited higher variation. There were no differences detected for inter-day analyses.

2.4 Discussion and Conclusions

For the first time, long and short peptides, and steroid hormones can be extracted at the same time and subjected to sensitive nano LC-MS/MS analysis. The extraction method provides high efficiency and reproducibility. This method makes it possible to simultaneously analyze multiple peptide and steroid hormones from single small tissues from species such as zebrafish (Table 6) and mouse (Chapter V). Due to the fact that this extraction method was developed and validated with the LC-MS/MS method as an intact package, the discussion on this method is combined with the LC-MS/MS method in Chapter III.

This SPE method has the potential to be expanded to generate a set of LC-MS/MS injectable samples for targeted and untargeted peptidomes and proteomics analysis from the same tissue sample as small as a single zebrafish pituitary. An overview flowchart of the entire set of SPE methods is presented in Figure 6.1 and the standard operation procedure (SOP) is provided in Appendix IV.

Chapter III Development of a sensitive nano LC-MS/MS method to simultaneously quantify SN, and other peptide and steroid hormones

3.1 Introduction

Simultaneously quantifying peptide and steroid hormones is an important step in the advancement of endocrine research. Not only does this increase efficiencies in many steps of the analysis, but it also permits the direct comparison of variations in the targeted hormones. The main challenge is that steroids are lipophilic, and peptides can range from hydrophobic to hydrophilic. They are traditionally isolated and quantified separately by incompatible approaches. In this new method, I set out to optimize the quantification of SN as the main goal, but in addition, the extraction and quantification of multiple other hormones in the same sample.

Peptide quantification by LC-MS/MS instruments can also be regarded as targeted peptidomics. The HPLC and mass spectrometer setups are slightly different among laboratories, but overall can be very similar. A C-18 reverse phase column is commonly employed. The mobile phase of the HPLC uses 0.1% FA in water as mobile phase A and 0.1% FA 80%-100% acetonitrile as mobile phase B. Samples are commonly injected at 1%-5% B. The gradient is often 20-45% of mobile phase B ramped up in 60-120 mins [124, 125]. The mass spectrometer setups in these studies share common concepts. Due to the fact on the size and charging state of peptides, orbitrap and time of flight analyzers are more common in peptide quantification studies. Regarding the data acquisition method, there is still a debate on data-dependent versus data-independent acquisition [62, 85, 104]. The appropriate setup depends on experimental design, types of equipment, coelution, charge states of the ions of interest, and numerous other parameters [125, 126].

Steroid quantification by LC-MS/MS instruments has been widely accepted. These experiments employ either positive or negative mode ionization, depending on the analytes of interest. For positive mode ionization, FA is commonly used as an ionization enhancer. In experiments with negative mode ionization, the enhancer can be ammonia, ammonium fluoride, or ammonium acetate [48, 60]. Steroids are relatively small molecules that are singly charged when ionized, therefore, a triple quadrupole mass spectrometer is more commonly used. These mass spectrometers have a very short duty cycle in multiple reaction monitoring (MRM). A steep gradient slope (over 80% B difference in 15 mins) performed by a UHPLC can improve the efficiency of the analysis. A C-18 column may be suitable for these experiments. Methanol instead

of acetonitrile can provide a better elution profile for steroids. The employment of UHPLC solves the backpressure issue from methanol at the same time [47, 52, 61].

Secretoneurin has been successfully detected from human blood samples and mouse tissue samples by LC-MS/MS experiments [12, 127]. Regarding the HPLC methods, the mobile phase systems, gradient slopes, and columns were similar to regular peptidomics analysis. These experiments were performed on high-resolution MS analyzers, either orbitrap or time of flight analyzers. In another word, in these studies, the sample volume is relatively large compared to this experiment and the amount was only estimated from human blood samples [12, 127]. Based on the important role of SN in angiogenesis, neuroinflammation, and as an emerging new reproductive hormone, a sensitive quantification method from small tissue samples from multiple species is crucial [8, 13, 128].

In this experiment, I have successfully quantified, in single small tissue samples, multiple peptides and steroid hormones by LCMSMS. I have also identified and solved a challenging matrix effect issue for the SNs which made their detection and quantification very difficult.

3.2 Experiments

3.2.1 Material and methods

HPLC

The two HPLC systems used were the Thermo Scientific EASY-nLC 1000 UHPLC system and an Agilent 1100 Series Capillary LC System. The Thermo system is an integrated system with all modules in one box. The Agilent 1100 nanoflow HPLC was achieved by combining a micro-mode Agilent 1100 system (stack with G1376A binary capillary pump, G1477A micro well-plate autosampler, and G1330A ALS thermostat).

Mass spectrometers

The two mass spectrometers used were Thermo Finnigan^{TM} LTQ^{TM} linear ion trap mass spectrometer and a Thermo Scientific Orbitrap Velos Pro^{TM} mass spectrometer.

3.2.2 Experimental design

To achieve the optimum LC-MS/MS results, various parameters needed to be optimized, and a variety of parts were selected or modified.

Analytical column: In this experiment, four RP-HPLC resins from Dr. Maisch were tested. They are ReproSil-Pur 120 C18-AQ, 3 µm (Cat#. R13.aq.); ReproSil-Pur 120 C18-AQ, 5 µm (Cat#. R15.aq.); ReproSil-Pur 300 ODS-3, 3 µm (Cat#. R33.93); and ReproSil-Pur 300 ODS-3, 5 µm (Cat#. R35.93.). On the most suitable HPLC resin, 2 column IDs (50 µm and 100 µm) and 3 column lengths (100 mm, 150 mm, and 200 mm) were tested [129, 130]

Trap column and loading flow rate: The packing resin in the trap column was the same as in the analytical column. The tested column IDs were 50 µm, 75 µm, and 100 µm. Various flow rates were tested with the trap columns to achieve optimum loading efficiency [130].

Nano-ESI spray tip and introducing HV electrode: The nano-ESI spray tip can be made on the HPLC column as one intact part. It can also be an individual part and connected to the column by a two-point connector. Both of these formats were tested. The HV charge for electron spray can be introduced at three positions, which are in between the column and the spray tip; in between the trap column and the analytical column; and before the trap column. The actual hardware setup to test these structures is shown in Figure 3.3. The advantages and disadvantages for each setup will be demonstrated in the result section.

Flow restrictor: Fused silica capillaries with 20 µm ID were selected to work as the flow restrictor. The length of the restriction capillary was determined using a positive mode mobile phase with 20 µL/min from HPLC. The flow rate from the HPLC in negative mode is decided according to the same restrictor [77, 131].

Fluidic Connections: Fused silica was manufactured by Molex LLC and distributed by Mouser Electronics. The Mouser catalog numbers for 20, 50, 75, 100 and 200 µm ID fused silica capillaries are 538-106815-0009, 538-106815-0017, 538-106815-0019, 538-106815-0023, and 538-106815-0204, respectively. The Tee connectors, cross connectors, and two-point connectors are purchased

from Idex-hs. PEEK MicroTee for 360 µm OD Tubing (Cat#. P-888), PEEK MicroCross for 360 µm OD Tubing (Cat#. 889), and PEEK Union for 360 µm OD Tubing (Cat#. P-772) are tested against Tee Assembly High-Pressure PEEK .020 thru-hole (Cat#. P-715), Cross Assembly PEEK .050 thru-hole, F-300 (Cat#. P-730), and Union Assembly PEEK 10-32 .050 Fittings (Cat#. P-760) with tubing Sleeve PEEK Orange 1/16 D x .016" x 1.3" (Cat#. F-230). To connect 360 µm OD fused silica capillaries to the 6-port valve on the Agilent 1100 sampler, the M4 Micro PEEK fitting (Cat#. 6000-360) was selected to work with PEEK Tubing 1/32" ID x .015" ID (Cat#. 1568L) as a sleeve.

Mobile phase and gradient: In this experiment, the positive mode and negative mode analyses have to run separately. The most appropriate mobile phase composition and gradient for each mode were optimized independently.

Data-dependent and independent acquisition in mass spectrometer: At the beginning of the project, the Finnigan LTQ mass spectrometer was used to develop the HPLC method and validate SPE methods. On that mass spectrometer, all analyses were run on a timetable operated SRM mode. The most stable transitions were confirmed by direct infusion of analyte in acetonitrile and water 1:1 with 0.1% FA. The SRM information is shown in Table 2. When developing the MS method for the Orbitrap MS, both timetables triggered data-independent MS2 acquisition and the mass list triggered data-dependent MS2 acquisition were evaluated [52, 132].

Nano ion source and spray tip

The nano-spray ion source was in-house assembled and modified from the University of Washington's Proteomics Resource (UWPR) open-source instructions (https://proteomicsresource.washington.edu/docs/protocols05/UWPR_NSI_Source.pdf). The list of parts is shown in Table 3. The HV cable provided a 2.5 kV constant voltage to the mobile phase through a 0.50mm diameter 99.95% platinum charging tip installed on the splitter. The nano-ESI tip was made by hand pulling fused silica under a butane torch. It was set to spray 5 mm away facing the MS orifice.

Table 2 List of charge state, precursor ion, collision energy, and product ions for various analytes. Quan represents quantitative, qual represents qualitative.

Compound	Precursor Ion	Precursor Ion Charge	Collision Energy (CID)	MS2 (Quan)	MS2 (Qual)
GnRH 1	592.3	M+2H	55	1011.3	934.3
GnRH 2	619.3	M+2H	55	1065.3	902.3
GnRH 3	1213.3	M+H	55	667.2	742.2
Mouse Oxytocin	504.6	M+2H	55	933.2	916.2
Mouse Vasopressin	544.1	M+2H	55	809.3	757.1
Zebrafish Isotocin	967.4	M+H	55	412.1	664.2
Zebrafish Kiss 1	664.0	M+2H	55	1145.5	972.3
Zebrafish Kiss 2	638.0	M+2H	55	1012.4	849.4
Mouse SN1-33	1217.9	M+3H	55	1597.3	1346.0
Zebrafish SNa1-34	1243.7	M+3H	55	1511.0	1697.5
Zebrafish SNb1-31	1152.7	M+3H	55	1277.0	1655.6
Zebrafish SNa1-14	832.4	M+2H	55	1320.6	1006.5
Zebrafish SNa1-18	1039.5	M+2H	55	1180.6	1308.6
Zebrafish SNa19-34	835.4	M+2H	55	1336.7	1078.6
Zebrafish SNb1-17	962.93	M+2H	55	1397.6	1025.5
Zebrafish SNb19-31	696.38	M+2H	55	1305.7	916.5
5α-DHT	291.3	M+H	55	255.2	273.3
Estradiol (E2)	271.3	M-H	55	145.0	225.2
Progesterone (P4)	315.3	M+H	55	109.2	279.2
Testosterone	289.3	M+H	55	109.1	271.2
Estrone (E1)	269.3	M-H	55	145.0	159.0
Estriol (E3)	287.4	M-H	55	171.1	257.0
11-KT	303.3	M+H	55	121.1	267.1
Cortisol	363.2	M+H	55	121.1	309.1
Cortisone	361.2	M+H	55	163.1	325.1
Corticosterone	347.2	M+H	55	121.1	293.1

Table 3 List of parts to assemble the nano-ion source.

Cat#	Description	Vendor
MB810	Aluminum Breadboard, 8" x 10" x 1/2", ¼-20 Threaded	Thorlabs
RLA1200	Imperial Dovetail Optical Rail, 12"	Thorlabs
RC1	Rail Carrier, Counterbored Hole 1"x 1"	Thorlabs
VC1	Small V-Clamp with PM3 Clamping Arm	Thorlabs
T711-250	Post Mountable Fiber Clamp, 250mm	Thorlabs
MS3R	Mini Series Mounting Posts, 6mm Diameter, 3" Long	Thorlabs
MS2R	Mini Series Mounting Posts, Ø6 mm, L = 2"	Thorlabs
MSA25	Thread Adapter, 1/4"-20 to #4-40	Thorlabs
ER90B	Mini-Post Right Angle Adapter	Thorlabs
9065-XYZ	Pint-Sized XYZ-Translation Stage	Newport
9301	Knob Adjustment Screw, Braked, 12.7 mm Travel, Ball Tip, 1/4-80	Newport
9022NF	e·z·Trac™ Rail, 2.5 in. Length	Newport
9025NF	e·z·Trac(TM) Stage Track Carrier	Newport
9020NF	e·z·Trac™ Rail, 12.0 in. Length	Newport
9101NF	Angle Plate, 1/4-20 Thru Slots, 8-32, and 1/4-20 Threads	Newport
CR-1	Construction Rail, 1 x 5 in.	Newport
SPH-2	Slim 1/2-in. Post Holder, 2-in. (50.8-mm) Ht.	Newport
SPH-3	Slim 1/2-in. Post Holder, 3-in. (76.2-mm) Ht.	Newport
MSPH-2	Miniature Optical Post Holder, 2.25 in., 1/4-20 (M6) Slotted Base	Newport
PHB-25	Open Slotted Base, 1/4-20 Thread, 0.25-in Thick	Newport
91035A430	18-8 SS Slotted Knurled Head Panel Screw 8-32 Thread, 1" Length	McMaster Carr
2706T16	PTFE Flanged Sleeve Bearing for 5/16" Shaft Diameter, 1/2" OD, 3/8" Overall Length	McMaster Carr
6362K233	Rulon LR Sleeve Bearing for 5/16" Shaft Diameter, 1/2" OD, 1/2" Length	McMaster Carr
2639T13	PTFE Sleeve Bearing for 3/8" Shaft Diameter, 1/2" OD, 1/2" Length	McMaster Carr
92185A116	Type 316 Stainless Steel Socket Head Cap Screw, 4-40 Thread, 1" Long, Fully Threaded	McMaster Carr
92313A109	Type 316 Stainless Steel Cup Point Set Screw, 4-40 Thread, 1/2" Long	McMaster Carr
1340088468	ROFPT000000 Round Wire Fine Platinum 1 pc Fine Pt N 4.202 g 1,000.00 mm 0.50 mm ROFPT000000 1/2 Hard ;	UMICORE
10334-02	THREADED PLASTIC FLANGE RECEPTACLE ASSEMBLY	Connectronics Corp.
066-031-14	#22 AWG, .180 O.D. silicone rubber insulated wire	Connectronics Corp.

3.3 Results and Discussion

3.3.1 Analytical column selection

The analytical column achieves the primary separation of all analytes. An appropriate analytical column can decrease the difficulties in downstream methods development. The Agilent HPLC was employed to determine the optimum packing sorbent and dimension of the column. In this step, buffer A is 0.1% FA in water, and buffer B is 0.1% FA in acetonitrile. All trap columns were made of the same packing material as the analytical column and trimmed to 40 mm in length. The ID of the trap columns was the same as the corresponding analytical column. Three compounds (GnRH 1, mSN, and P4) were selected as indicator compounds to determine the performance of the column.

In the experiment, 1 pmol of each of the three compounds in a mixture was loaded into the LC-MS/MS system. Restrictors were trimmed to various lengths for each column to have a flow rate of 350 nL/min for 75 µm ID columns and 160 nL/min for 50um ID columns at 50% B. The gradient was set to be 5% B to 95% B in 45 min and maintain at 95% B for 5 min. The results are shown in Table 4. It was determined that both of the ODS-3 packing resins were not suitable for this application because they did not retain polar peptides such as GnRH 1. Both of the C18-AQ HPLC resins can achieve a sufficient separation for the analytes. The backpressure generated by the 5 µm resin was much lower than the back pressure when loading samples into the trap column. This pressure fluctuation can cause the backflow of the packing resin from the trap column to the restrictor. It eventually caused a loss of trapping efficiency and plugging of the restrictor. Therefore, only C18-AQ 3 µm HPLC resin was selected to pack the analytical column. For the column dimensions, the 150 mm length column is more suitable for this experiment because the retention time of low polarity compounds in the 200 mm columns is dramatically longer. Regarding the ID of the column, the 50 µm columns have less mobile phase going through the emitter which contributes to higher sensitivity. When testing the spiked biological samples, the retention time and peak width stay the same as standard samples for both 50 µm and 75 µm ID columns. Therefore, the C18-AQ, 3 µm, 50 µm × 150 mm was selected as the analytical column for the rest of the experiments. The actual system back pressure (on 160 nL/min) for this column is measured to be 204 bar at 2% B, 210 bar at 50% B, and 161 bar at 95% B.

Table 4 List of experimental columns, corresponding backpressure, and the retention time of GnRH 1, mSN, and Progesterone.

Sorbents	Column Dimention	Retention time (min)			Pressure at 50% B (bar)
		GnRH 1	mSN	Progesterone	
C18-AQ, 3 µm	50µm X 150mm	18.5	33.3	42	210
	50µm X 200mm	19.1	34.1	46.5	245
	75µm X 150mm	19.2	34.5	43	205
	75µm X 200mm	20	37	49	244
C18-AQ, 5 µm	50µm X 150mm	14	28	38.5	163
	50µm X 200mm	17.3	32.8	39.1	197
	75µm X 150mm	15	28.5	38.8	162
	75µm X 200mm	18.7	33.4	39.8	197
ODS-3, 3 µm	50µm X 150mm	N/A	27.4	35.1	161
	50µm X 200mm	N/A	28.1	36	181
	75µm X 150mm	N/A	27.3	35.2	162
	75µm X 200mm	N/A	28.1	36.3	183
ODS-3, 5 µm	50µm X 150mm	N/A	26.9	33.1	140
	50µm X 200mm	N/A	27.1	33.7	157
	75µm X 150mm	N/A	26.9	33.5	141
	75µm X 200mm	N/A	27.3	33.6	160

3.3.2 Trap column and loading flow rate

Trap column choice was also important to the success of this project. During the loading step, they have to capture the analytes efficiently while allowing the salt contaminants to pass through quickly. They are also acting as a protective guard to the analytical column to trap dust and lipid contaminants. All trap columns were trimmed to 35 mm length, which is the minimum length for the connection hardware.

The results of varying trap column ID and flow rate are shown in Figure 3.1. The system backpressure is plotted against the flow rate for each tested trap column. Data were only collected for flow rate between 2-10 µL/min and backpressure between 140-400 bar. To generate minimum pressure fluctuation when the system switched between the loading and analyzing positions, the trap column should be operatable at around 200 bar. Therefore, the 3 µm particle size 50 µm ID and the 3 µm particle size 75 µm ID were not suitable for this experiment. At this stage, durability tests on 6 trap column candidates were undertaken.

In the durability test, the HPLC system loaded 1 µL of tissue extract 100 times to each trap column candidate. The HPLC maintains the loading position with the corresponding flow rate for 20 µL mobile phase flushing. There was 5 min of 80% B isocratic wash and a5 min of 2% B equilibrium in between each injection. The experiment was repeated 5 times. The HPLC was set to report an error and terminate the analysis when the backpressure exceeded 310 bar. The results of the durability test are shown in Figure 3.2. Three candidates passed the durability test. They did not get plugged within 100 injections. However, it was noted that the 200 µm ID trap columns are very easy to be snaped when working with the ferrules in connectors. Therefore, the 3 µm particle 200 µm ID and the 5 µm particle 200 µm ID trap columns failed the durability test even though they did not get easily plugged.

In conclusion, there was only one trap column candidate that passed both the flow rate and backpressure tests. Therefore, for the remainder of the experiments, the C18-AQ, 5 µm, 100 µm ID, and 35 mm capillary column was used as trap column. The flow rate for the loading position was chosen to be 6 µL/min and the loading time was 3 min (18 µL on volume).

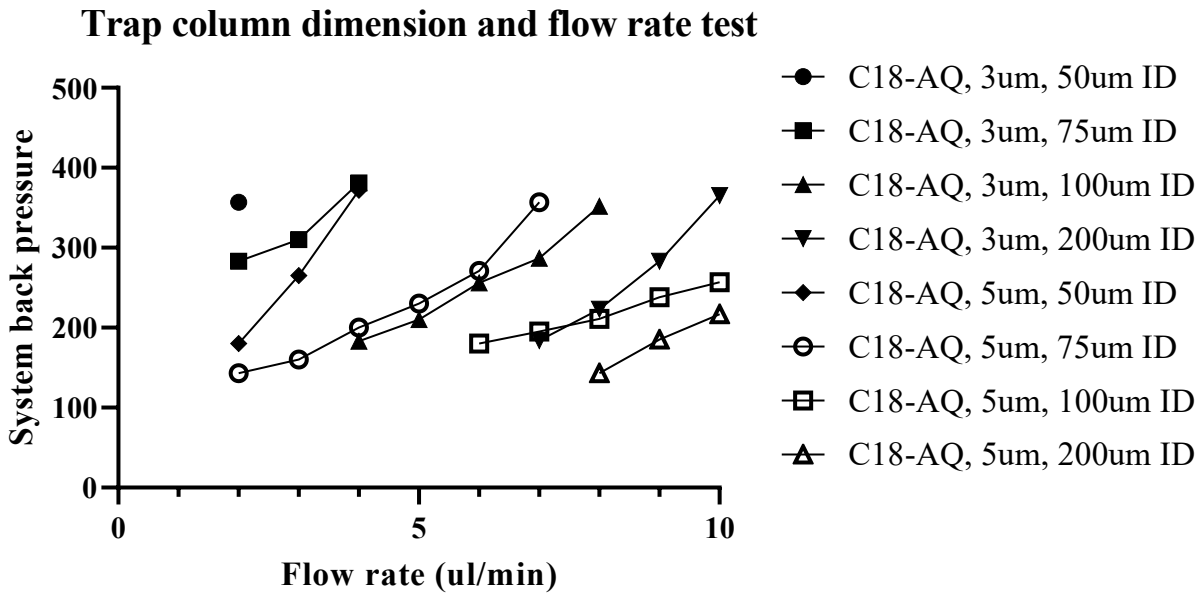

Figure 3-1 System back pressure was generated by each trap column candidate on various flow rates. Backpressure values were acquired directly from the Agilent HPLC system. Each trap column candidate was tested once.

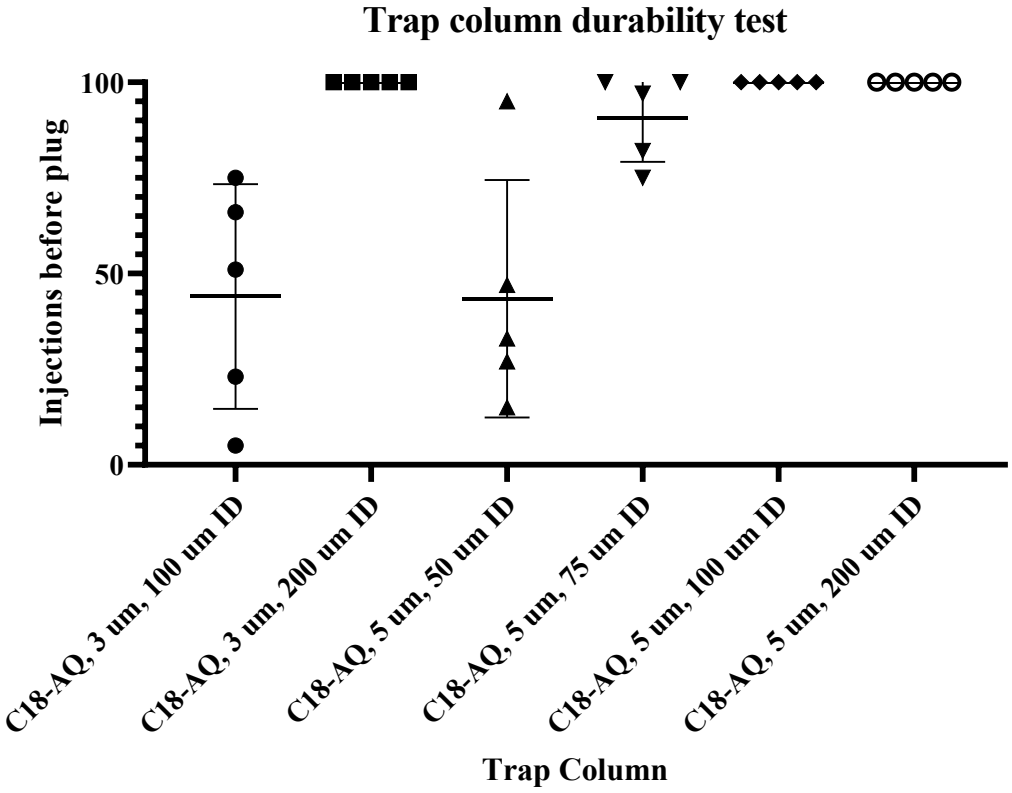

Figure 3-2 The durability of trap columns for repeated biological sample injections. The total number of injections was recorded for each column candidate until it jammed or reached 100 times. Each column candidate was tested 5 times. The testing flow rate for each column candidate was set according to the system backpressure between 180-200 bar before the first injection.

3.3.3 Nano-ESI spray tip and introducing HV electrode

The fluidic setups for using an Agilent capillary LC as a nano-LC have been reported as previously reviewed [84, 131, 133]. Most of them are for shotgun proteomics research, where the samples tend to be much cleaner than those in this thesis and where chromatographic peak shape is less important. In this project, the co-extraction of peptides and steroids will inevitably contaminate the sample with lipids and fine particles, which will plug not only the columns but also the connectors. In this section, I will review the fluidic connection layouts I have tested, which are depicted in Figure 3.3. The setup in Figure 3.3a permits both the trap column and analytical column to stay grounded through the analysis. The setup in Figure3.3 b and c allow the trap column to stay grounded. The setup in Figure 3.3A and 3.3B gives the flexibility to replace any part of the system

individually, when necessary. For the setup in Figure 3.3A, B, and C, chromatograms exhibit a severe peak tailing. This is probably caused by a trapped air pocket at the HV cable branch of the connector. The connector between the analytical column and spray tip (Figure 3.3a and b) became plugged frequently. The cross connector in setup Figure 3.3D was also plugged often. This issue was solved by expanding the thru-hole from 0.006" to 250 µm. This connector is placed before both columns, so the expansion did not have a significant effect on the peak shape in the chromatogram.

3.3.4 Electrophoresis in HPLC columns

When developing the HPLC method, I noticed that GnRH peptides and testosterone are not retained on C18 columns if HV is applied at the inlet point of the column with no grounding. This issue can be resolved by grounding the column to the MS instrument frame. Other analytes did not exhibit this issue. This interesting phenomenon is probably caused by electrophoresis. Most likely, without proper grounding, the HV generates an electric field in the C18 column. Some analytes are ionized when dissolved in the mobile phase. These ions may be pushed by Coulomb's force (electrostatic force) towards the MS orifice. The C18 column may not be able to retain these analytes when the hydrophobic interactions between analytes and C18 packing resin are weaker than the Coulomb's force from the electric field.

No publications about the presumed electrophoresis phenomenon in the HPLC column could be located. The HV charged HPLC columns do not exist in regular HPLC experiments. Their columns are usually grounded to the column oven of HPLC equipment. Regarding the strength of the interference, the electrostatic force can be calculated by Coulomb's law. However, the method to calculate hydrophobic interaction is still unknown. There are few publications proposing estimate equations, but they are insufficient to solve the issue in this experiment [134, 135].

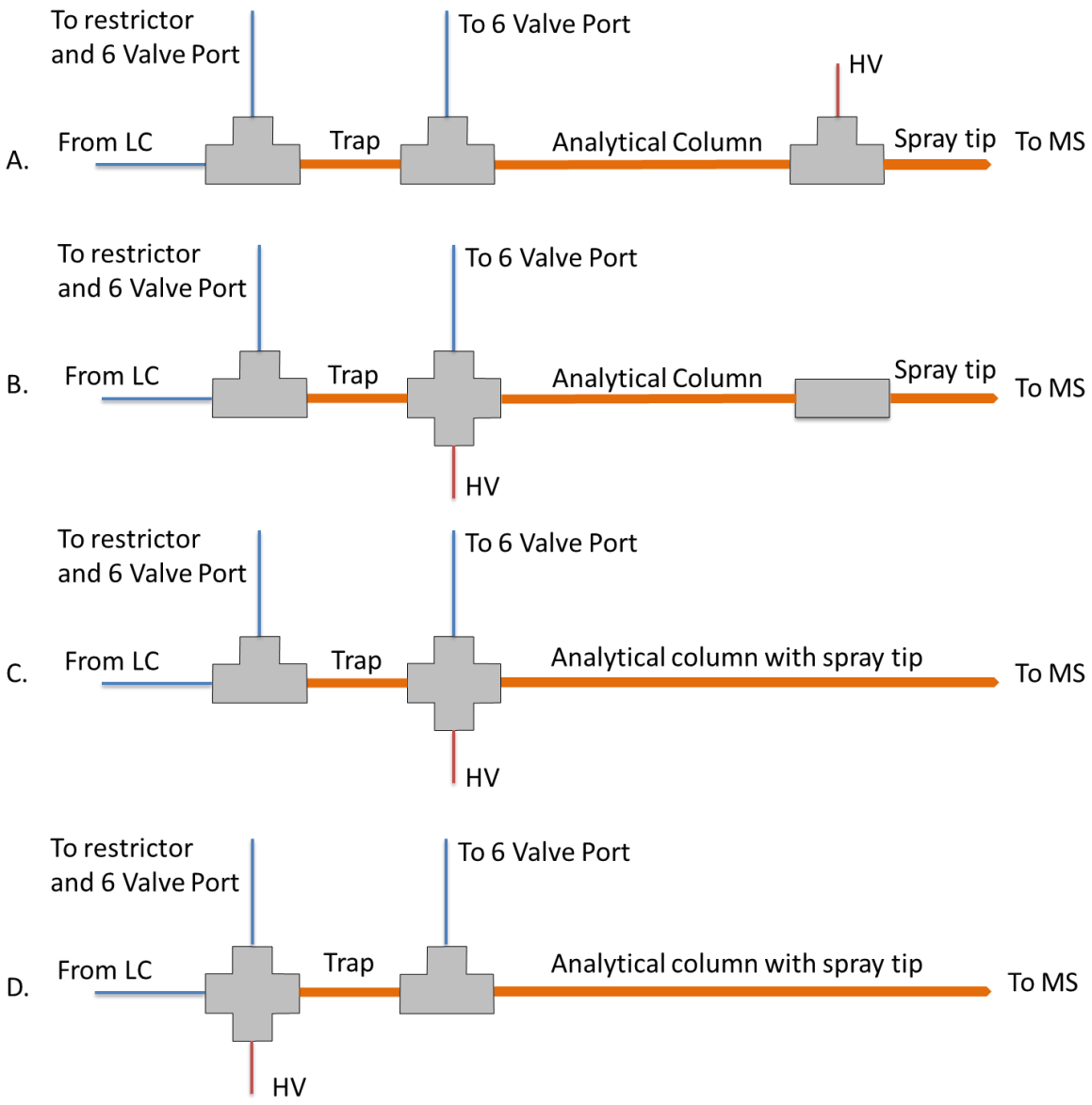

Figure 3-3 Fluidic connection setups for the splitter, trap column, analytical column spray tip, and high voltage electrode. HV represents the high voltage electrode.

3.3.5 Flow restrictor

The flow restrictor was selected on the mobile phase composition for positive mode analysis. After testing all the capillary lengths under various B1%, the 200 mm length was chosen. This restrictor has the narrowest range of pressure fluctuation through the gradient. The pressure surge when switching to equilibrium can reach 295 bar, which is still sufficiently lower than the 340 bar limit. To optimize the method for negative mode analysis, the same flow restrictor was used and the flow rate from EMPV was adjusted. Among all the tested flow rates, 15 µL/min is the maximum flow rate that the system can sustain. The EMPV flow rates below 15 µL/min could not generate reproducible chromatograms for estrogen analytes. Therefore, 15 µL/min was selected as the EMPV flow for negative mode analysis More details concerning the flow restrictor experiment and the negative mode EMPV flow rate are presented in Appendix III.

3.3.6 Mobile phase and gradient

There was an attenuation of the GnRH 1 signal after a week of mobile phase storage when 0.1% FA is used as an ionization enhancer. An increase of FA to 0.2% solved the issue. Therefore, the mobile phase portion of the positive mode analysis was optimized to be 0.2% FA in water as A1, and 0.2% FA in acetonitrile as B1. The gradient of B1 was from 20% to 90% in 30 mins. To achieve the optimum result for estrogens, the mobile phase of negative mode analysis was optimized to be 1 µM NH_4F in water as mobile phase A2 and 1µM NH_4F in 65% MeOH 30% acetonitrile 5% water as mobile phase B2. The gradient was set to be 50% to 90% B2 in 15 mins. More detailed mobile phase and gradient optimization data are in Appendix III

3.3.7 HPLC equipment

The decision on employing the Agilent capillary LC system as a nano-HPLC system was a major compromise. However, this was the system that was available for significant modification. This system setup used the restriction from the splitter and the column to realize a relatively reproducible flow rate during the gradient elution. However, after a large number of injections, the columns, connectors, and the splitter will inevitably get contaminated or plugged. There are still such incidents happening during my routine analysis. The most common incidents are:

- Fine particles and some macromolecules from samples can accumulate on the top of the trap column. They are so large that can not be eluted by chromatographic behavior in

chosen column. This continuously increases the restriction in the column system and decreases the actual flow rate in the column when injections go by. These fine particles are so small that their Brownian motion can not be neutralized by a low-speed centrifuge [136]. Ultracentrifugation can separate these particles from liquid samples but is not realistic in this experiment due to the balancing issue and throughput.

- When the system switches from the loading position to the analyzing position, the pressure inside the trap column can fluctuate. If the pressure ramps down in this procedure, the packing material in the trap column can backflow to the splitter. The 5 µm particle size is comparably large to the 20 µm ID of the fused silica capillary. This backflow can easily plug the splitter and shut down the system. Making the inlet side of the trap column fritted is not a solution because the fine particles (previously mentioned) can plug the frit much quicker than plugging the packing resin.
- Any incidents that change the back pressure can have an influence on the actual flow rate in the column. These changes can lead to severe consequences on the chromatograms including peak shape, peak area, and even retention time. The ideal solution to these issues was to let the nano-scale flow be directly controlled by the HPLC system. If the flow rate inside the column is consistently and precisely controlled, these incidents would not exist. This is the reason that I attempted to employ the Thermo easy-nLC system. Unfortunately, the issues caused by non-specific binding of SN were also evident in the Thermo system, and still require a solution. The digested BSA spiking did not improve this issue, even though it solved a similar issue in the Agilent LC system. The required troubleshooting can lead to future work. These non-specific binding (matrix effect) of the SN peptides are discussed in the next paragraph and also in Appendix III.

3.3.8 Matrix effects for the SN family of peptides

In this experiment, the detection and quantification of SNs exhibited a matrix effect. All SN peptides tested had a relatively high non-specific binding to the HPLC system. This binding was weakened by the addition of digested BSA in the Agilent system. The non-specific binding match the publications on peptidomics which discovered fragments of SNs rather than intact SNs [11, 14]. Without a high level of precaution, intact SNs have rarely been measured in LC-MS/MS experiments published to date.

The Thermo LC system has a different mechanism for injection compared to the Agilent setup. In the Thermo LC system, the elution buffer flow path did not include the injector needle, needle tube sampler valve, and the sampler loop. In another word, if any analyte did not get loaded into the column system during the loading procedure, it would be washed into waste. Therefore the digested BSA spike could not solve the matrix effect issue of SNs. The corresponding solution to this problem for the Thermo LC system is still unknown. More details on discovering the issue and possible solutions are presented in Appendix III.

3.3.9 Data-dependent acquisition

The mass spectrometer was set to collect data on data-dependent acquisition mode. The master scan was performed by the orbitrap analyzer. There were four master scans, a 150-1500 m/z scan on FWHM 60,000, a 1243.95 m/z SIM with 1 m/z on FWHM 30,000, a 1152.90 m/z SIM with 1m/z on FWHM 30,000, and a 1217.95 m/z SIM with 1 m/z on FWHM 30,000. The three SIM scans were only carried out between 25-30 mins after injection. The MS2 scans were triggered by a mass list and conducted 3 times. Dynamic exclusion time was set to be 1.5 mins. Details of the setup can be found in Appendix II.

3.3.10 Quantification ranges and calibration curves

The lower limit of quantification (LLOQ) and higher limit of quantification (HLOQ) are important because they are the main determinants of the suitability of a method for the samples under consideration [42, 59, 62]. The tissue samples in this project are small. The actual analyte amounts were determined to be closer to the LLOQ. The actual HLOQ was not determined. The level of each analyte in the most concentrated calibration solution (1× in the standard curve) is therefore presented as an estimate of HLOQ.

For standard curves, all compounds were stored individually at 1nmol/μL as a stock solution in either methanol or DMSO at -20 ºC. To achieve the LLOQ (except for the SNs), 1 μL of stock solution for each analyte was mixed to form a standard compound mixture, 25 μL in total. This mixture was diluted 10 times with 0.1% FA water to form a solution with each compound at 4 pmol/μL. This solution underwent 24 2-fold serial dilutions to form a standard curve. These are the standard samples used to determine the LLOQ of each compound. Each concentration in the standard curve was injected into the LC-MS/MS system 5 times repeatedly. The LLOQ was

determined by the lowest calibration range that covers 5 data points with $R^2 \geq 0.99$. The results are listed in Table 5

3.3.11 Analyzing efficiencies for peptide and steroid compounds.

Regarding the performance of the SPE and LC-MS/MS method, this thesis is the first attempt to analyze steroids and peptides from the same tissue at the same time. Therefore, the total efficiency of peptides and steroids is discussed separately.

Peptides: The analyzed peptides in this thesis cover a wide range of polarity and size. On the small hydrophilic side, I quantified low to high pmol/tissue GnRH peptides from the zebrafish pituitary. Weiming Li's group quantified low ng/ml from sea lamprey brain which is within the same range [23]. In the sea lamprey study, they quantified multiple gonadotropin-releasing and gonadotropin-inhibitory hormones by LC-MS/MS. Their homogenization method has the same concept as mime although the homogenization buffer has a slightly different recipe since they do not need to consider steroid co-extraction. Li's study employed a commercialized SPE kit from Waters company, which represents the SPE kit developed in this project exhibits similar to the Waters one for small hydrophilic peptides. In a separate study, oxytocin was measured to be at 50-200 ng/mg from the monkey pituitary [137]. This result was acquired by LC-MS/MS analysis following SPE on pituitary tissue. It is about 1000 times higher than the amount I quantified from the mouse pituitary (Figure 5.2), which is most likely caused by the difference in the size of the animal. The monkey experiment employed Strata × Drug B, 60 mg/6ml SPE columns from Phenomenex, which is relatively large for a monkey pituitary (80 mg according to the same article). This represents a lower efficiency on the SPE sorbent, which can lead to loss of analyte. For most other peptide analytes, this thesis is the first attempt to quantify through LC-MS/MS following SPE, regardless collectively with each other and steroids.

Steroids: Successful examples of quantifying steroid hormones by LC-MS/MS are more common than peptides. Denslow et.al. quantified cortisol, 11-KT, testosterone, P4, and E2 from zebrafish whole-body extracts [61]. The result in this article was described in pg/mg protein, therefore it is difficult to compare to my data. Multistage two-phase liquid-liquid extraction was employed, which explained higher viability on recovery ratio. In 2021, Li et. Al. developed an LC-MS/MS based steroid quantification method with samples prepared by SPE cartridges from Waters [138].

The LLOQ reported was lower with a similar reproducibility to this thesis (Table 5). This suggests that with a more advanced LC-MS/MS system the method developed in this study could reach a better performance.

Overall, the development of this novel LC-MS/MS method was successful. To the best of my knowledge, this is the first time that steroids and peptides have been analyzed in the same HPLC injection. Both the HPLC and mass spectrometry equipment were acquired from the secondary market as retired machines, which makes this method more accessible to many research laboratories. The main limitation of this method is that the splitting flow setup needs an experienced operator. It has a plugging issue in the flow restrictor tube more often than regular HPLC setups.

The outlined extraction and quantification of peptides and steroids in a major model organism, the zebrafish was achieved. The approach was used to study periovulatory variations in hormone levels by another Ph.D. student (Peng, D. 2022. Characterization and Role of Secretoneurin in the Ovulatory Cycle of Zebrafish, Ph.D. Thesis, University of Ottawa, pp. 160), and will be applied to the laboratory mouse in Chapter V. An overview of the zebrafish result is presented in Table 6.

Table 5 The lower limit of quantification (LLOQ), the higher limit of quantification (HLOQ), and the working ranges of the standard curves for each analyte. The ranges were estimated by fmol analyte injections. The table was generated from the brain, pituitary, and gonads of single female (N=42), male (N=12) zebrafish, and single female mouse (N=72)

Compound	LLOQ (pmol/tissue)	HLOQ (pmol/tissue)	Working Range (pmol/tissue)
11-KT	0.488281	175	0.171-2.734
5a-DHT	0.244141	175	0.244-175
Corticosterone	0.030518	175	0.031-175
Cortisol	0.015259	175	0.015-175
Cortisone	0.015259	175	0.015-175
Estradiol	0.244141	175	0.342-10.94
Estriol	0.976563	175	1.37-43.84
Estrone	1.953125	1750	3.418-109.4
GnRH 1	0.015259	175	0.015-175
GnRH 2	0.015259	175	0.175-21.85
GnRH 3	0.244141	175	0.342-43.78
Mouse Oxytocin	0.488281	1750	0.489-1750
Mouse SN1-33	750	10000	750-10000
Mouse Vasopressin	0.976563	1750	0.977-2.734
Progesterone	1.953125	175	0.171-2.734
Testosterone	0.244141	175	0.342-21.88
Zebrafish Isotocin	1.953125	1750	3.418-1750
Zebrafish Kiss 1	0.030518	175	0.171-2.734
Zebrafish Kiss 2	0.015259	175	0.171-2.734
Zebrafish SNa1-14	0.003815	1750	6.836-109.4
Zebrafish SNa1-18	0.12207	175	0.171-2.734
Zebrafish SNa1-34	391	52600	822-13150
Zebrafish SNa19-34	0.061035	175	0.171-21.875
Zebrafish SNb1-17	0.488281	175	0.684-21.875
Zebrafish SNb1-31	195	52600	822-13150
Zebrafish SNb19-31	0.007629	175	0.684-21.875
Zebrafish Vasotocin	0.976563	175	1.367-43.74

Table 6 The minimum, maximum amount, and mean of each compound (pmol/tissue) from brain, pituitary, and gonads of single female (N=42) and male (N=12) zebrafish.

		Female (42)			Male (12)		
		Min	Max	Mean	Min	Max	Mean
SNa1-34	Brain	105230	448290	256577.5	3032	180954	78717.6
	Pituitary	50782	178126	116969.3	50782	113238	82421.5
	Gonads	3032	202403	100543.8	3032	154602	656025.7
SNa1-14	Brain	204.5	6127	1434.1	204.5	8724	1803.2
	Pituitary	204.5	1865	1413.8	204.5	3209	1920.4
	Gonads	204.5	2526.5	1313.9	204.5	4068	1996.1
SNa1-18	Brain	0.5	41.5	12.6	13.5	74.5	24.9
	Pituitary	0.5	33.5	12.4	13.5	34	16.6
	Gonads	0.5	73.5	16.4	13.5	80.5	25.5
SNa19-34	Brain	5.5	22.5	9.1	10.5	55	18.4
	Pituitary	4.5	474.5	28.4	10.5	48	18.1
	Gonads	5	283	65.8	5	351.5	38.3
SNb1-31	Brain	176623	204334	193869.6	39485	113950	60501.7
	Pituitary	182217	184475	183119.6	39595	56069	44874.9
	Gonads	39485	185663	164157.8	39485	53584	44418.2
SNb1-17	Brain	56	489	262.9	56	282	129.4
	Pituitary	56	103	72.3	56	82	61.2
	Gonads	56	137.5	80.3	56	85	63.4
SNb19-31	Brain	34.5	328.5	129.7	1	154	50.6
	Pituitary	33	211.5	87.3	1	139.5	51.47
	Gonads	1	642.5	156.9	1	415	100.1
Gnrh2	Brain	0.5	576.5	200.9	0.5	1033.5	245.6
	Pituitary	0.5	39.5	16.2	1	46	7.5
	Gonads	0.5	99.5	23	0.5	119	15.3
Gnrh3	Brain	3.5	1757	683.9	34	436.5	219
	Pituitary	6.5	78.5	26.1	3.5	65	27.3
	Gonads	3.5	556.5	143.8	3.5	135	45.8

Oxytocin	Brain	8.5	5723	1728.3	8.5	2432	921.9
	Pituitary	8.5	165997	40961	8.5	65132	20553.2
	Gonads	8.5	180.5	86.9	8.5	384	56
Vasopressi	Brain	194	328	213.2	194	289	214.8
n	Pituitary	194	4013.5	1405.4	194	1348.5	642.6
	Gonads	194	888.5	285.2	194	305	201.4
Kiss1	Brain	0.5	99.5	32.6	0.5	243	76.7
	Pituitary	0.5	53	17.6	0.5	32.5	11.8
	Gonads	0.5	141	14.4	0.5	86	11.8
Kiss2	Brain	0.5	119.5	24.2	0.5	117.5	21
	Pituitary	0.5	100	36.5	0.5	87	25.5
	Gonads	0.5	1516	133.3	0.5	182	32.7
E1	Brain	0.5	7936	711.7	0.5	1576.5	354
	Pituitary	0.5	1102	289.8	0.5	587	69.2
	Gonads	0.5	3487	489.3	0.5	922.5	71.3
E2	Brain	0.5	2634	293.7	0.5	330	67.7
	Pituitary	0.5	973.5	151.3	0.5	587	69.3
	Gonads	0.5	7936	828.8	0.5	205.5	26.3
E3	Brain	82	4786	830.7	82	4517.5	459.2
	Pituitary	82	4743	470.4	82	4785	368.15
	Gonads	82	4775.5	992.8	82	1717	184.4
T	Brain	15.5	36	18.1	16.5	65	22.3
	Pituitary	16	52.5	18.5	16.5	74	21
	Gonads	1.5	67	11.7	16.5	816	175.8
11-KT	Brain	0.5	44.5	5	0.5	60	37.2
	Pituitary	0.5	19	4.35	0.5	60	43.2
	Gonads	0.5	225.5	41.47	0.5	446.5	56

3.4 Conclusion

The original intention of this LC-MS/MS method is to quantify various peptides and steroids in low abundance from tissue extract. The method needs to be not only accurate but also sustainable and high throughput. This LC-MS/MS method has been successfully developed and tested by various experimenters from my research group. During the development process, there were a large number of technical difficulties. Most have been overcome, however, there were still a few that led to compromises.

Due to the non-specific binding between SN peptides and HPLC fluidic system (more details in Appendix III), a BSA solution was inevitably applied, which caused the co-elution of P4. In this project, discovering the level of SN peptides was more important than quantification of P4. Therefore, the sensitivity on P4 was the trade-off for more sensitive measurement of SN peptides. In addition, the Thermo nano-UHPLC system was made to have a higher chromatographic resolution and reproducibility than the Agilent system. It can also run the elution gradient faster. However, an effective solution for non-specific binding of the SN peptides is still missing for the Thermo nano-UHPLC system. Therefore, the Agilent system was employed rather than the Thermo system.

The Agilent HPLC system had a much lower pressure rating than the Thermo system and run with an external 6-port valve and a flow restrictor. Therefore a sorbent larger than the analytical column was used to prepare the trap column. This material generated lower backpressure, in the meantime, theoretically decreased the chromatographic resolution.

Chapter IV Preparation of standard peptides by FMOC chemistry and HPLC purification to characterize peptide sequences by targeted and untargeted peptidomics analysis

4.1 Introduction

Researchers have developed various approaches to acquire peptidic compounds to fill their rapidly expanding demand in the scientific and pharmaceutic industries. These methods include chemical synthesis (liquid and solid chemistry), extraction from vertebrate tissues, expression in genetically modified organisms, or a combination of these techniques [139, 140]. This study requires a small amount (1-5 mg) of highly purified peptide samples with various sequences. These sequences range from 5 to 35 amino acids in length and various modifications, which makes the SPPS technique more suitable.

There are two main goals of this research. First, high-quality commercial standard peptides are not readily available in some cases, or not available at all in others. Therefore, I set out to synthesize all targeted peptides. Many are well-characterized peptides and were quantified under experimental conditions in both zebrafish and mice. However, those in the SN family are largely unknown and have never been quantified accurately. The second main objective was to employ untargeted peptidomics to discover naturally existing SNa and SNb fragments in zebrafish. Thereafter, targeted peptidomics was used to confirm the existence and structure of intact zebrafish SNa and SNb peptides with synthetic standard compounds.

4.2 Experiment

Materials and methods

For SPPS, Fmoc/tBu protected amino acids and coupling reagent (HBTU) were purchased from P3 BioSystems (Louisville, KY, USA). The Rink-amide linker Tentagel peptide synthesis resin was purchased from Rapp Polymere GmbH (Tuebingen, Germany). NMM, TFA, triisopropylsilane, piperidine, Iodine, and other SPPS-related chemicals were purchased from MilliporeSigma Canada Co. (Oakville, Ontario). ACN, DMF, NMP, and other related solvents were purchased from Fisher Scientific Company (Ottawa, Ontario). The water used in peptide synthesis and RP-HPLC purification was produced by the MiliQ water purification system (Oakville, Ontario) with 18.2 MΩ·cm resistivity at 25 °C.

SPPS

Standard peptide samples were assembled on the Intavis Multipeptide peptide synthesis machine (model RSi) using Fmoc peptide synthesis chemistry. The sequence of each peptide is listed in Table 7. In general, a Rink-amide linker on 90 μm Tentagel resin with 0.2 - 0.27 mmol/g loading capacity was used as solid-phase synthesis support. For deprotection, 2 times 5 min 20% piperidine treatment was employed to remove the Fmoc group on the N-terminus of each amino acid [113]. Standard coupling reactions were set as 40 mins treatment with 4-fold of HBTU (0.5 M), 4.4 fold of amino acids (0.6 M), and 4 fold of NMM (4 M). Two times coupling reactions were used to attach each amino acid when the sequence length was below or equal to 15, while three times coupling reactions were for sequence length over 15 [108, 111]. At the end of the synthesis, the resin was treated in the cleavage cocktail, TFA-triisopropylsilane–H_2O (95:2.5:2.5), for two hours to harvest crude peptides. For oxytocin, isotocin, vasotocin, and vasopressin, Fmoc-Cys(Acm)-OH and Fmoc-Cys(Trt)-OH were used to introduce cysteine into the peptide sequence. The Acm-protected cysteine was for on-resin oxidation and the Trt-protected cysteine was for in-solution oxidation. For on-resin oxidation, the disulfide bridge was built by suspending the synthesis resin in 4 M Iodine/DMF solution with mild mixing for 2.5 h before cleavage. For in-solution oxidation, the peptides were kept in the cleavage cocktail under air blow for 4 hrs. To introduce pyroglutamic acid (Pyr), both Boc-Pyr-OH and H-Pyr-OH were used with standard coupling protocol. The crude peptides were precipitated by ethyl ether on ice, dissolved in 50% ACN water, and lyophilized. Lyopholizezed crude peptide samples were stored at -20 °C for purification.

Purification

Peptide purification was performed on an Agilent 1100 HPLC system (consisted of G1322A vacuum degasser, G1311A quaternary pump, G1313A autosampler, G1316A column compartment, G1315B diode array detector, and G1364C analytical fraction collector). Purification methods used a Luna Omega 5 μm 100 Å PS C18 RP-HPLC column (250×10 mm) at a flow rate of 4 ml/min. The mobile phases consisted of 0.1% TFA in water (buffer A) and 0.1% TFA in ACN (buffer B). The column oven was set at 50 °C. To purify each peptide, the HPLC gradients were adjusted to have the target peptide elute at least 7.5 min after the gradient started. The fraction collector was set to start collection 7.5 min after the gradient started on 400 mAU threshold, 500 mAU/s upslope, and 200 mAU/s downslope according to the 214 nm chromatogram.

The collected fractions were chilled in liquid nitrogen for 5 min and lyophilized accordingly. Lyophilized purified peptide powders were stored at -20 °C. The molecular weight of each peptide was confirmed on LC-MS/MS. In this step, samples were loaded on the column by the initial mobile phase containing 0.1% FA, 2% ACN, and water. The HPLC was set to run a linear gradient from 90% B to 40% B in 25 min. Mass spectrometry was set to collect data through the entire gradient time on the normal scan mode between 150 and 2000 m/z.

Peptidomics

MS analyses were accomplished using HPLC-ESI-MS/MS. The system consisted of an Agilent 1100 micro-HPLC system (Agilent Technologies, Santa Clara, CA, USA) coupled with an LTQ-Orbitrap mass spectrometer (ThermoFisher Scientific, San Jose, CA) equipped with a nano-electrospray interface operated in positive ion mode. The mobile phases consisted of 0.1%(v/v) FA in water as buffer A and 0.1% (v/v) FA in acetonitrile as buffer B. Peptide separation was performed on a 75μm × 100 mm analytical column packed in-house with reverse-phase Magic C18AQ resins (1.9μm; 120-Å pore size; Dr. Maisch GmbH, Ammerbuch, Germany). Briefly, the sample was loaded on the column using 98% buffer A at a flow rate of 1.5μL/min for 15min. Then, a gradient from 5% to 35% buffer B was performed in 120 min at a flow rate of ~300nL/min obtained from splitting a 20 μL/min through a restrictor. The MS method consisted of one full MS scan from 300 to 1700 m/z followed by a data-dependent MS/MS scan of the 5 most intense ions, with dynamic exclusion repeat count of 2, and repeat duration of 90 s. As well, for the experiments on the Orbitrap MS the full MS was performed in the Orbitrap analyzer with R = 60,000 defined at m/z 400, while the MS/MS analysis was performed in the LTQ. To improve the mass accuracy, all the measurements in Orbitrap mass analyzer were performed with internal recalibration ("Lock Mass"). On the Orbitrap, the charge state rejection function was enabled, with single and "unassigned" charge states rejected.

The raw files generated by the LTQ-Orbitrap were processed and analyzed using MaxQuant, Version 1.2.2.5 using the Uniprot protein FASTA database (2012, July version), including commonly observed contaminants. The following parameters were used: methionine oxidation, protein N-terminal acetylation, and no enzyme digestion. Precursor ion mass tolerances were 7 ppm, and fragment ion mass tolerance was 0.8 Da for MS/MS spectra. The false discovery rate

(FDR) for peptide and protein was set at 1% and a minimum length of six amino acids was used for peptides identification.

4.3 Results

The average mass value of the synthetic peptides was calculated by ExPASy PeptideMass online calculation server [141]. The m/z of each peptide was compared to the calculated value in Table 9. These results confirm the accuracy of peptide synthesis and purification. The optimized gradients for each peptide are shown in Table 7.

The on-resin oxidations were successful with initial purity of over 50% for each cyclic peptide. The in-solution oxidations led to a severe self-aggregation issue with initial purity below 50%. The cyclic peptides prepared by in-solution oxidation were discarded without further purification. The pyroglutamic acid was successfully introduced by Boc-Pyr-OH for GnRH peptides with initial purity of more than 50%. When introducing the H-Pyr-OH with standard coupling protocol, the product peptide ended up with multiple pyroglutamic acids. The initial purity was less than 50% and the products were discarded without further purification.

The targeted peptidomics confirmed the existence of intact zebrafish SNa and SNb. The synthetic peptide was identical to the natural peptide on retention time, MS1, and more than 3 most intense ions on MS2. The untargeted peptidomics identified 24 SN peptide fragments, which naturally occur in zebrafish brain and pituitary. The intact SNa1-34 and SNb1-31 peptides were also identified. The SN peptide fragments are listed in Table 8.

Table 7 The list of synthetic peptide sequences and the corresponding mobile phase gradients of RP-HPLC purification methods. B% represents the starting and ending point of the slope gradient on the percentage of buffer B in RP-HPLC purification. The time column represents the timespan of the slope gradient. All RP-HPLC purification methods contained 5 min purging at 95% buffer B and 5 min re-equilibration at 5% buffer B, which are not shown in this table.

Peptide Name	Sequence	B%	Time (min)
GnRH 1	Pyr-HWSYGLRPG-CONH2	15-30	15
GnRH 2	Pyr-HWSHGWYPG-CONH2	15-30	15
GnRH 3	H-Pyr-HWSYGWLPG-CONH2	25-50	15
Mouse Oxytocin	H-CYIQNCPLG-CONH2 [Disulfide C1-C6]	15-30	15
Mouse Vasopressin	H-CYFQNCPRG-CONH2 [Disulfide C1-C6]	15-30	15
Mouse Kiss 1	H-Y(PO3)NWNSFGLRY-CONH2	20-30	10
Zebrafish Isotocin	H-CYISNCPIG-CONH2 [Disulfide C1-C6]	15-30	15
Zebrafish Vasotocin	H-CYIQNCPRG-CONH2 [Disulfide C1-C6]	10-20	10
Zebrafish Kiss 1	H-Y(PO3)NLNSFGLRY-CONH2	15-30	15
Zebrafish Kiss 2	H-FNYNPFGLRF-CONH2	25-50	15
Mouse SN1-33	H-TNEIVEEQTYPQSLATLESVFQELGKLTGPSNQ-CONH2	45-60	15
Zebrafish SNa1-34	H-TNENAEEQYTPQKLATLQSVFEELSGIASSKTNT-CONH2	45-60	15
Zebrafish SNb1-31	H-ATEDLDEQYTPQSLANMRSIFEELGKLSAAQ-CONH2	45-60	15
Zebrafish SNa1-14	H-TNENAEEQYTPQKL-CONH2	10-20	10
Zebrafish SNa1-18	H-TNENAEEQYTPQKLATLQ-CONH2	15-30	15
Zebrafish SNa19-34	H-SVFEELSGIASSKTNT-CONH2	15-30	15
Zebrafish SNb1-17	H-ATEDLDEQYTPQSLANM-CONH2	15-30	15
Zebrafish SNb19-31	H-SIFEELGKLSAAQ-CONH2	25-50	15

Table 8 Identified secretoneurin fragments from zebrafish brain and pituitary by untargeted peptidomics.

Name	Sequence	Modification
SNa 1-34	**T N E N A E E Q Y T P Q K L A T L Q S V F E E L S G I A S S K T N T**	
SNa 1-19	T N E N A E E Q Y T P Q K L A T L Q S	
SNa 1-18	T N E N A E E Q Y T P Q K L A T L Q	
SNa 1-14	T N E N A E E Q Y T P Q K L	
SNa 1-12	T N E N A E E Q Y T P Q	
SNa 1-9	T N E N A E E Q Y	
SNb 1-31	**A T E D L D E Q Y T P Q S L A N M R S I F E E L G K L S A A Q**	
SNb 1-19	A T E D L D E Q Y T P Q S L A N M R S	
SNb 1-18	A T E D L D E Q Y T P Q S L A N M R	
SNb 1-18	A T E D L D E Q Y T P Q S L A N M R	Oxidation (M)
SNb 1-17	A T E D L D E Q Y T P Q S L A N M	
SNb 1-17	A T E D L D E Q Y T P Q S L A N M	Oxidation (M)
SNb 1-16	A T E D L D E Q Y T P Q S L A N	
SNb 1-15	A T E D L D E Q Y T P Q S L A	
SNb 1-14	A T E D L D E Q Y T P Q S L	
SNb 1-13	A T E D L D E Q Y T P Q S	
SNb 1-12	A T E D L D E Q Y T P Q	
SNb 1-11	A T E D L D E Q Y T P	
SNb 1-10	A T E D L D E Q Y T	
SNb 1-9	A T E D L D E Q Y	
SNb 12-31	Q S L A N M R S I F E E L G K L S A A Q	
SNb 19-31	S I F E E L G K L S A A Q	
SNb 20-31	I F E E L G K L S A A Q	
SNb 19-30	S I F E E L G K L S A A	
SNb 19-29	S I F E E L G K L S A	
SNb 19-28	S I F E E L G K L S	

Table 9 The average molar mass and the observed m/z of each synthetic peptide

Peptide	Average Molar Mass	$[M+H]^{+}$	$[M+2H]^{2+}$	$[M+3H]^{3+}$	$[M+4H]^{4+}$
GnRH 1	1182.3	1182.8	592.3	N/A	N/A
GnRH 2	1236.3	1236.8	619.3	N/A	N/A
GnRH 3	1212.3	1213.3	N/A	N/A	N/A
Mouse Oxytocin	1007.2	1008.3	504.6	N/A	N/A
Mouse Vasopressin	1084.2	1085.6	544.1	N/A	N/A
Mouse Kiss 1	1325.4	1325.7	664.0	N/A	N/A
Zebrafish Isotocin	966.1	967.4	484.0	N/A	N/A
Zebrafish Vasotocin	1050.2	1051.26	526.05	N/A	N/A
Zebrafish Kiss 1	1325.4	1325.7	664.0	N/A	N/A
Zebrafish Kiss 2	1273.4	1273.9	638.0	N/A	N/A
Mouse SN1-33	3650.0	N/A	1825.6	1217.9	913.7
Zebrafish SNa1-34	3729.0	N/A	1864.7	1243.7	933.2
Zebrafish SNb1-31	3455.8	N/A	1728.0	1152.7	N/A
Zebrafish SNa1-14	1663.8	N/A	832.4	N/A	N/A
Zebrafish SNa1-18	2077.2	N/A	1039.5	N/A	N/A
Zebrafish SNa19-34	1668.8	N/A	835.4	N/A	N/A
Zebrafish SNb1-17	1925.1	N/A	962.93	N/A	N/A
Zebrafish SNb19-31	1391.6	N/A	696.38	N/A	N/A

4.4 Discussion

Briefly outlined here are some of the challenges and solutions relating to peptide synthesis and purification.

Disulfide bond: The in-solution oxidation of cyclic peptides failed. It is probably because the peptide concentration in the cleavage cocktail was too high so there was not enough time for the 'naturally folding' to happen before aggregation. It may be solved by introducing the Acm-protected cysteine, which can remain protected in TFA. Then the Acm-removal and oxidation can proceed in much a lower peptide concentration. Since the on-resin oxidation was successful, this theory was not tested.

Coupling pyroglutamic acid: The secondary amine on pyroglutamic acid was significantly more reactive than I expected. Therefore, it caused self-aggregation. It was solved by using the Boc group to protect the secondary amine. This solution increased the cost of the entire synthesis by around 1/3. There is another untested solution, which decreases the amount of pyroglutamic acid and HBTU to one-fold of the resin loading amount.

Challenges with SN synthesis: The peptide synthesizer employed in this experiment is an Intavis Multipep model. This peptide synthesizer is equipped with a two Gilson syringe pump which can deliver derivative solutions (in high viscosity) accurately. This allows me to prepare the derivative and activator solutions in 0.6M concentration to acquire a higher yield in each coupling. However, this equipment does not come with an agitation function which limits the mass transfer within the reactor (plate wells). Therefore, a longer reacting time is needed to let every coupling reaction reach equilibrium. When dealing with short peptide sequences (within 15 amino acid length), the entire synthesis program can be completed within 3 days (4 hrs per amino acid). However, for longer peptide-like SN, the last few amino acids can be coupled on the 5^{th} or 6^{th} day after the program is initialized. This requests the operator to replace all derivative solutions on the 4^{th} day after the synthesis starts. According to my experience, replacing the derivative solution can significantly increase the initial purity and decrease the purification work (data not shown).

Peptidomics: The SN peptides in Table 8 is the most complete SN profile so far that have been found to naturally exists in zebrafish brain and pituitary. In this list, the SNb 19-33 was reported

when zebrafish was studied as a Parkinson's disease and a brain intracellular peptide characterization model [142, 143]. In a discovery study that intended to search for zebrafish neuropeptides, SNb 1-16 and SNb 1-17 with no SNa fragments were reported. This proves the SPE method I developed is more efficient than commercialized kits. The connection and relationship between SN processing and physiology are pending further discoveries.

4.5 Conclusion

All of the peptides are successfully synthesized and purified. HPLC re-injection of the purified peptides did not show any impurity peak with the method 2 times shallower than the purification method.

Chapter V Periovulatory variations in the peptides and steroids of the hypothalamic-pituitary-ovarian axis during the mouse estrous cycle

5.1 Introduction

The neuroendocrine control of ovulation underlies the successful reproduction of vertebrate animals. In this regard, both rodent and fish models have proven invaluable, and neuropeptide regulation LH release from the pituitary has been the focus for many decades [26, 144-146]. The fundamental concept emerging in the last decade is that GnRH neurons receive inputs from classical neurotransmitters and other neuropeptides that generate a pulsatile release of GnRH that in turn drives LH release, and in the periovulatory period, the surge release of LH that causes ovulation. While the focus in the last two decades has been on the paramount role of the mammalian kisspeptin neuronal systems mediating the positive and negative feedback actions of ovarian steroids, there are numerous other known and newly implicated neuropeptides that are also important [147-149].

Evidence suggests some involvement of the hypothalamic nonapeptides oxytocin and vasopressin. Oxytocin is well-known for controlling uterine contractions at birth, the release of milk during lactation, and the modulation of multiple socio-sexual behaviors [150, 151]. However, oxytocin is likely involved in stimulating GnRH and LH release [152, 153]. For example, oxytocin antibody administered in the brain inhibits the proestrus LH surge [154], oxytocin induces GnRH release from hypothalamic explants on the afternoon of proestrus [155], and some GnRH neurons in rats express oxytocin receptors [152]. Moreover, vasopressin, best known as the osmoregulatory antidiuretic hormone acting on the kidneys, may also have a role in mammalian reproduction [156]. For example, vasopressin infusion into the brain can induce the LH surge in rats [157]. This stimulatory effect of vasopressin is highest in proestrus around the time of peak blood E2 levels just before the preovulatory LH surge [156]. A subset of GnRH neurons expresses vasopressin receptors in female mice [158].

In this regard, the neuropeptide secretoneurin (SN), derived from the selective processing of the larger secretogranin-2 precursor protein should be more carefully considered. Secretoneurin is a 31-42 amino acid segment that is well-conserved from sharks to mammals. It is widely distributed

in neuroendocrine neurons and pituitary cells [13], and in particular, it colocalizes with oxytocin and vasopressin in some hypothalamic magnocellular cells in rats [159, 160]. Using goldfish and zebrafish as experimental models, our laboratory has shown that SN plays a critical role in the HPG axis. In goldfish, for example, SNa stimulates LH production and secretion [2, 3, 9]. Moreover, this appears to be conserved in evolution because mouse SN stimulates the production and secretion of LH independent from GnRH in the mouse LβT2 gonadotroph tumor cell line [4]. Recently, we demonstrated that mutations in the SCG2a and SCG2b precursors reduce the ability of zebrafish to reproduce normally. For example, in animals carrying mutations in both genes, only 10% spawn. This defect was partially rescued by in vivo injections of SNa that I synthesized [9]. These observations are highly suggestive of a role for SN in ovulation. To begin addressing this possibility, I set out to measure known reproductive hormones in comparison to mSN in the hypothalamus, pituitary, and ovaries of mice.

In this experiment, I sampled female mouse hypothalamus, pituitary, and ovaries in the diestrus, proestrus, and estrus stages of the estrous cycle. Then I employed the recently developed extraction and quantification method to estimate the level of each hormone analyte. Comparing fluctuations in these hormones, I discovered that the mSN level was changing in the hypothalamus and pituitary through the estrous cycle following a similar trend as GnRH 1. I also found that mSN levels and vasopressin levels were changing following a similar trend in the hypothalamus and pituitary. The change in the average level of mSN and P4 and E2 in ovaries did not follow the same trend, however, the sample-specific regression of mSN against P4 and E2 individually showed they were weekly related. This is the first report which simultaneously measures SN and other reproductive hormones in the mouse estrous cycle. The correlation between mSN and GnRH 1 in hypothalamus is R^2=0.61 in linear regression which indicated that the levels of these two hormones are related. This lays the foundation for the very first studies on the role of SN in mammalian reproduction.

5.2 Experiments

Material and methods

Chemicals

Peptide standards were in-house prepared by Fmoc chemistry and purified by RP-HPLC (See Chapter III). Steroid standards were purchased from Sigma-Aldrich. Solvents were purchased from Fisher Scientific. Other chemicals were purchased from Sigma-Aldrich.

Tissue sample collection

Female CD1 mice were obtained from Charles River Laboratories (St-Constant, Québec) at 3-5 weeks of age. Mice were housed in all-female rooms in groups of 4 per cage in polycarbonate nit-picky cages measuring 17 cm × 28 cm × 12 cm (width × length × height) and contained corn cob bedding (Cat# 7097, Envigo, Mississauga, CA), one cardboard hut (CAT# XKA2455, Ketchum, Brockville, CA), and one piece of nestlet (Cat# NES3600, Ancare, Bellmore, USA). Mice had ad libitum access to food (Teklad Global Diets, Envigo) and water. The vivarium was maintained on a 14 h light and 10 h dark cycle (lights off at 10:00 am, and lights on at 8:00 pm) at a constant temperature of 24°C (±2°C) and 40% (±5%) humidity. Dusk and dawn were gradually induced over 1 h. All experimental procedures were approved by the Animal Care Committee of the University of Ottawa. A vaginal lavage was used to determine estrous stages using sterile phosphate-buffered saline (PBS) in a Fisher brand graduated transfer pipette [161]. The PBS solution was transferred onto a Fisher brand Super frost Plus microscope slide and covered slip for cytology. The ratio of cornified, epithelial, and leukocyte cells determined proestrus, estrus, metestrus, or diestrus. Mice were euthanized at three timepoints: 1hr before lights off on diestrus, 1.5 hrs after lights off in proestrus, and 2 hrs after lights off in estrus (Figure 5.1). Mice were euthanized by carbon dioxide (CO_2) asphyxiation. After that, the hypothalamus, pituitary, and ovary were collected separately and immediately placed in the homogenization buffer (Chapter II)

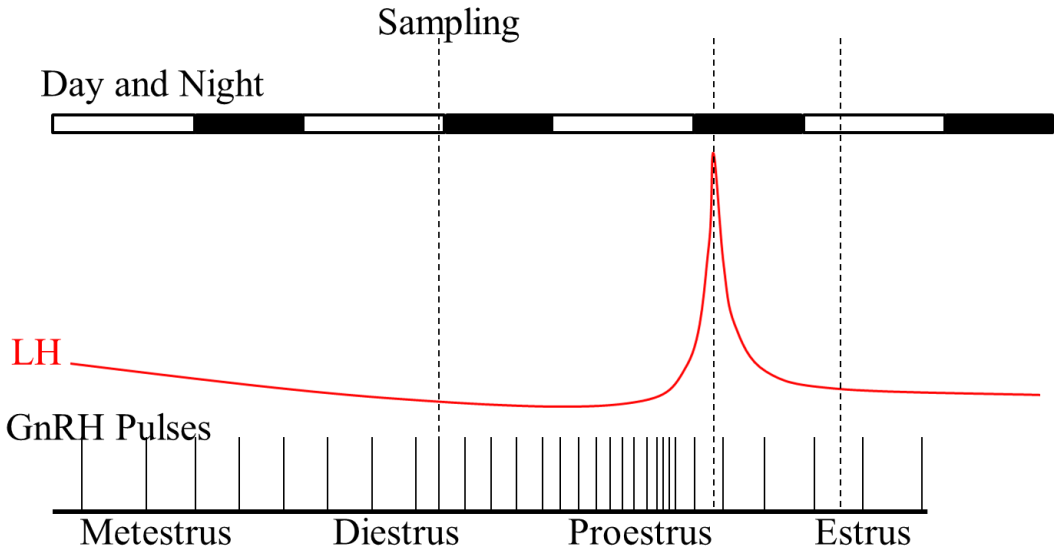

Figure 5-1 Diagram for the mouse estrous cycle experiment. The dashed vertical lines indicate the time of tissue sampling.

Solid-phase extraction (SPE)

Solid-phase extraction (SPE) was performed by in-house prepared SPE cartridges with 10 mg sorbent (Dr. Maisch Cat#. r10.aq). Before loading the sample, the SPE bed was prepared with 5 times 200 µL 50% acetonitrile activation and 5 times 200 µL 5% acetonitrile equilibrium. Samples were loaded with 5% acetonitrile as a loading buffer. Then the SPE cartridges were washed 5 times 200 µL 5% acetonitrile and eluted 6 times 20 µL 75% acetonitrile. The eluted sample was evaporated in a speed vac. All buffers in this section were deionized water solutions with 0.2% FA as additive. Please see details in Chapter II.

Nano LC-MS/MS

The details for the LC-MS/MS method are presented in Chapter III. The nano LC-MS/MS system consisted of Agilent 1100 nanoflow HPLC system (stack with G1376A binary capillary pump, G1477A micro well-plate autosampler, and G1330A ALS thermostat).and a Thermo Scientific Orbitrap Velos Pro^{TM} mass spectrometer. The LC was run in micro mode with a pre-column splitter

on load and elute modes. The 50 µm × 150 mm analytical column was in-house prepared using 3 µm C18-AQ sorbent from Dr. Maisch. The mobile phase for positive mode analysis consisted of 0.2% formic acid in water (A1) and 0.2% formic acid in 80% acetonitrile and 20% water (B1). The mobile phase for positive mode analysis consisted of 1 µM NH_4F in water (A2) and 1µM NH_4F in 65% MeOH 30% acetonitrile 5% water (B2). The gradient for positive mode analysis was 20%-90% B1 in 30 mins and the gradient for negative mode analysis was 50% -90% B2 in 15 mins.

The mass spectrometer was set to run on data-dependent acquisition. The orbitrap analyzer performed the master scan at resolution 60,000 (FWHM). The linear ion-trap analyzer performed the fragmentation and secondary MS scan according to the mass list and master scan. Data acquisition and analysis were performed on Thermo Xcalibur software, version 2.2.

5.3 Results

Oxytocin

Nine female mice were sacrificed, and tissue samples were collected at the diestrus, proestrus, and estrus stage of the estrus cycle. Tissue homogenates were processed at the same time and analyzed by LC-MS/MS. Oxytocin was detected in all tissues through the estrus cycle. There were no changes measured as a function of time (Figure 5.2). The highest levels were found in the pituitary, followed by the hypothalamus and ovary,

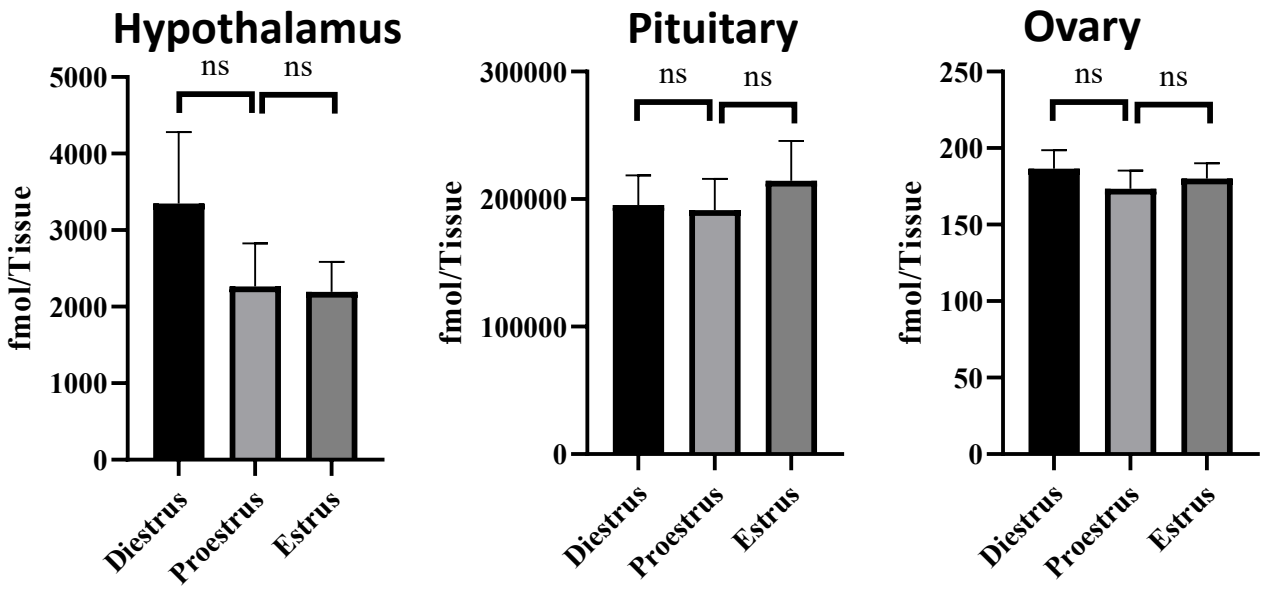

Figure 5-2 Periovulatory changes in oxytocin level during the estrous cycle of mice (n=9). Values represent mean ± SEM (n=9). Statistical analysis was performed using one-way ANOVA followed by Tukey's post-hoc (ns: not significant; *P<0.05; **P<0.01)

Vasopressin

Vasopressin was detected in all the tissues through the entire estrous cycle. The total levels of vasopressin were higher in the hypothalamus than in the pituitary and ovary (Figure 5.3). In both the hypothalamus and pituitary, the vasopressin level was significantly higher at the proestrus stage compared to the diestrus and estrus stages. In the ovary, there were no significant changes in vasopressin through the estrous cycle.

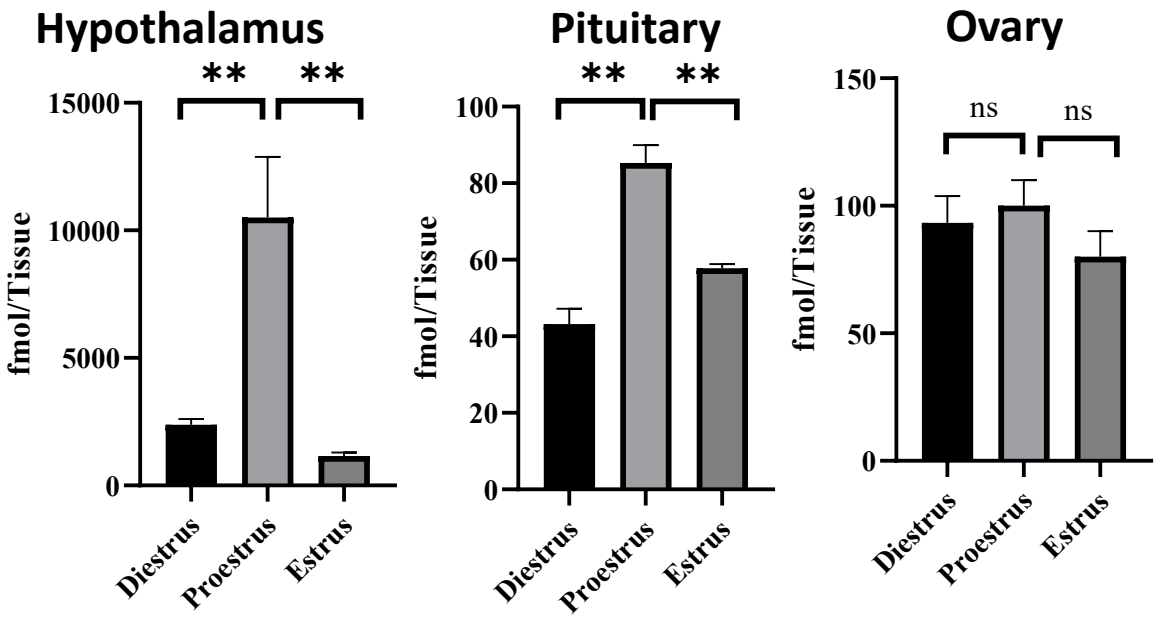

Figure 5-3 Periovulatory changes in vasopressin level during the estrous cycle of mice (n=9). Values represent mean ± SEM (n=9). Statistical analysis was performed using one-way ANOVA followed by Tukey's post-hoc (ns: not significant; *P<0.05; **P<0.01)

GnRH 1

Levels of GnRH1 in the hypothalamus at the proestrus and estrus stages were l significantly higher than at the diestrus stage (Figure 5.4). There was no significant difference in the GnRH 1 level between the proestrus and estrus stages. In the pituitary (Figure 5.3), the level of GnRH 1 was significantly higher at the proestrus stage compared to the diestrus and estrus stages. GnRH 1 was not detected in the ovary.

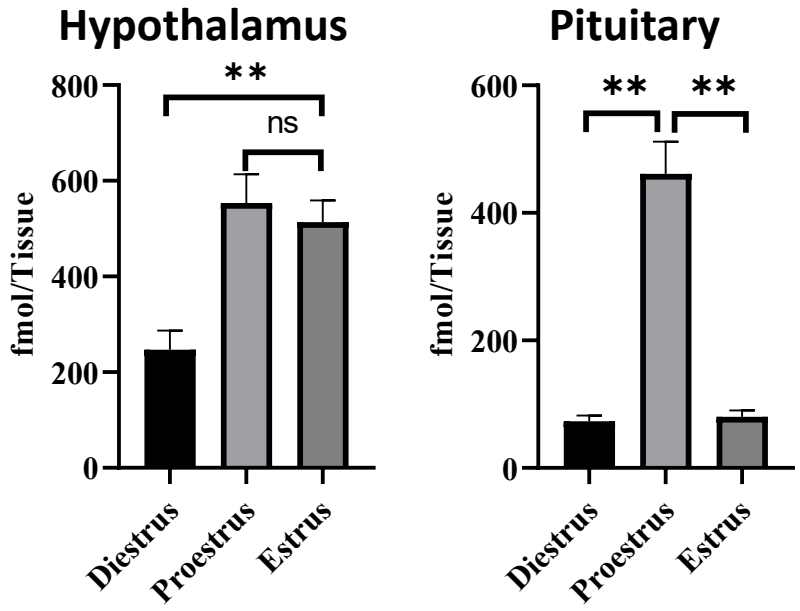

Figure 5-4 Periovulatory changes in GnRH 1 level during the estrous cycle of mice (n=9). Values represent mean ± SEM (n=9). Statistical analysis was performed using one-way ANOVA followed by Tukey's post-hoc (ns: not significant; *P<0.05; **P<0.01)

Secretoneurin

Secretoneurn (SN) was detected in all three tissues through the entire estrous cycle (Figure 5.5). In the hypothalamus, mSN levels were significantly higher at the proestrus stage compared to the diestrus and estrus stages. In the pituitary, the mSN level was also high at the proestrus stage compared to the diestrus and estrus stages. The difference between diestrus and proestrus was significant. Due to the highly variable data at the estrus stage, the difference between the proestrus and the estrus stages was not significant. The ovarian levels of mSN were low and close to the detection limit. The standard deviation was overestimated because of this variability in the detection rate.

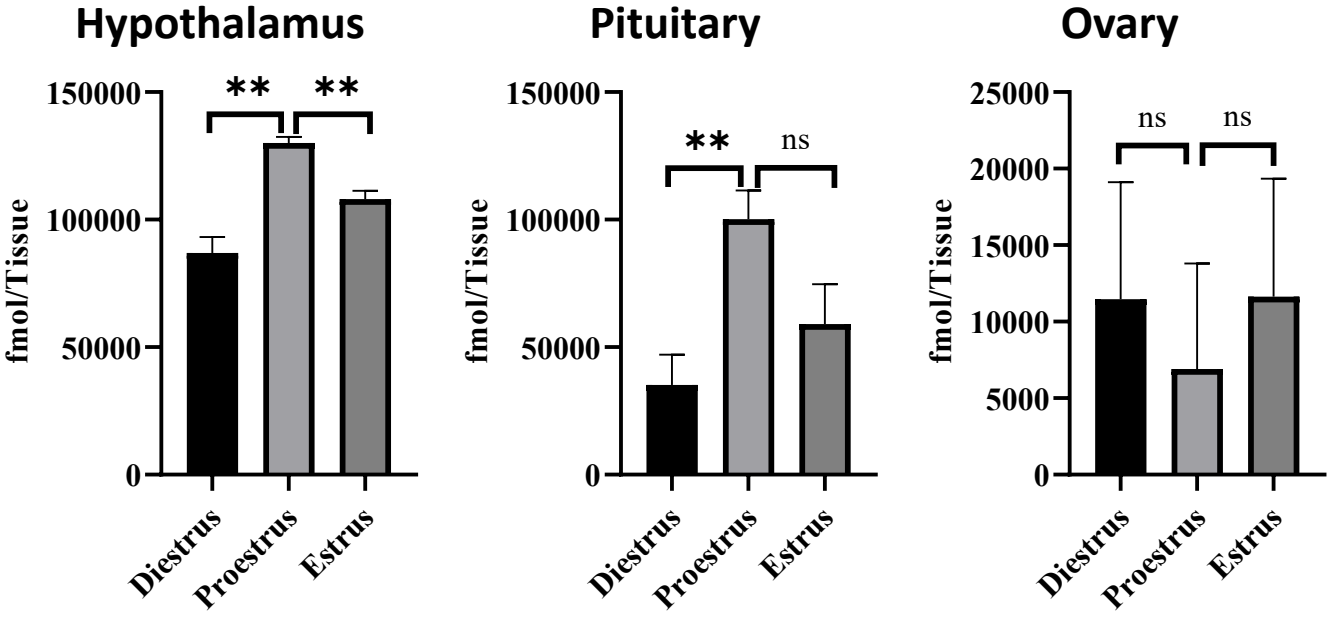

Figure 5-5 Periovulatory changes in secretoneurin level during the estrous cycle of mice (n=9). Values represent mean ± SEM (n=9). Statistical analysis was performed using one-way ANOVA followed by Tukey's post-hoc (ns: not significant; *P<0.05; **P<0.01)

Estradiol

Estradiol was detected in the pituitary and ovary through the estrus cycle (Figure 5.6) but was below detection limits in the hypothalamus. The pituitary E2 levels remained low through the estrous cycle. In the ovary, the E2 levels were high at the diestrus stage and remained low at the proestrus and estrus stages. There was no significant difference in estradiol levels between the proestrus and estrus stages.

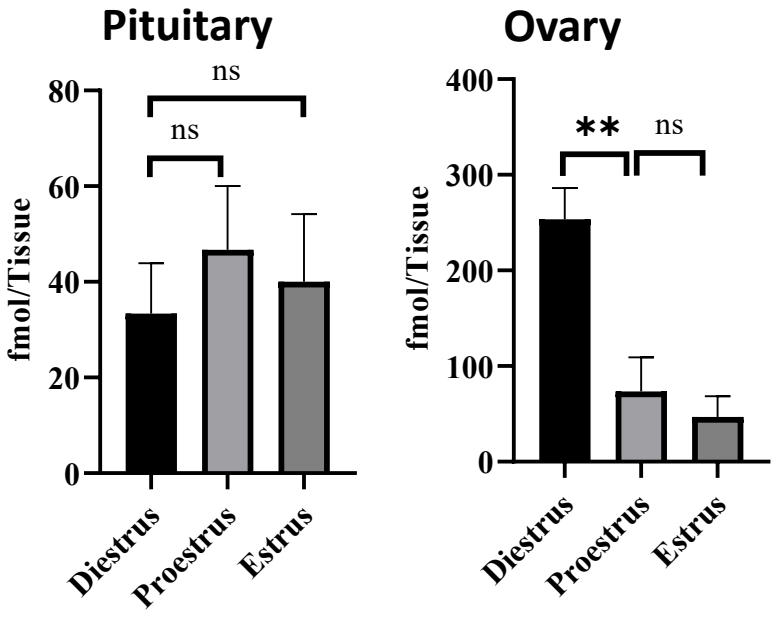

Figure 5-6 Periovulatory changes in estradiol level during the estrous cycle of mice (n=9). Values represent mean ± SEM (n=9). Statistical analysis was performed using one-way ANOVA followed by Tukey's post-hoc (ns: not significant; *P<0.05; **P<0.01)

Progesterone

Progesterone was detectable in all three tissues through the estrus cycle (Figure 5.7). In the hypothalamus, the P4 level at the diestrus stage was significantly higher than at the proestrus and estrus stages. There was no significant difference in the level of hypothalamic P4 between the proestrus and estrus stages. In the pituitary, the level of P4 stayed low and was highly variable throughout the estrous cycle. In the ovary, the level of P4 was about 4 times higher at proestrus than at diestrus and estrus stages.

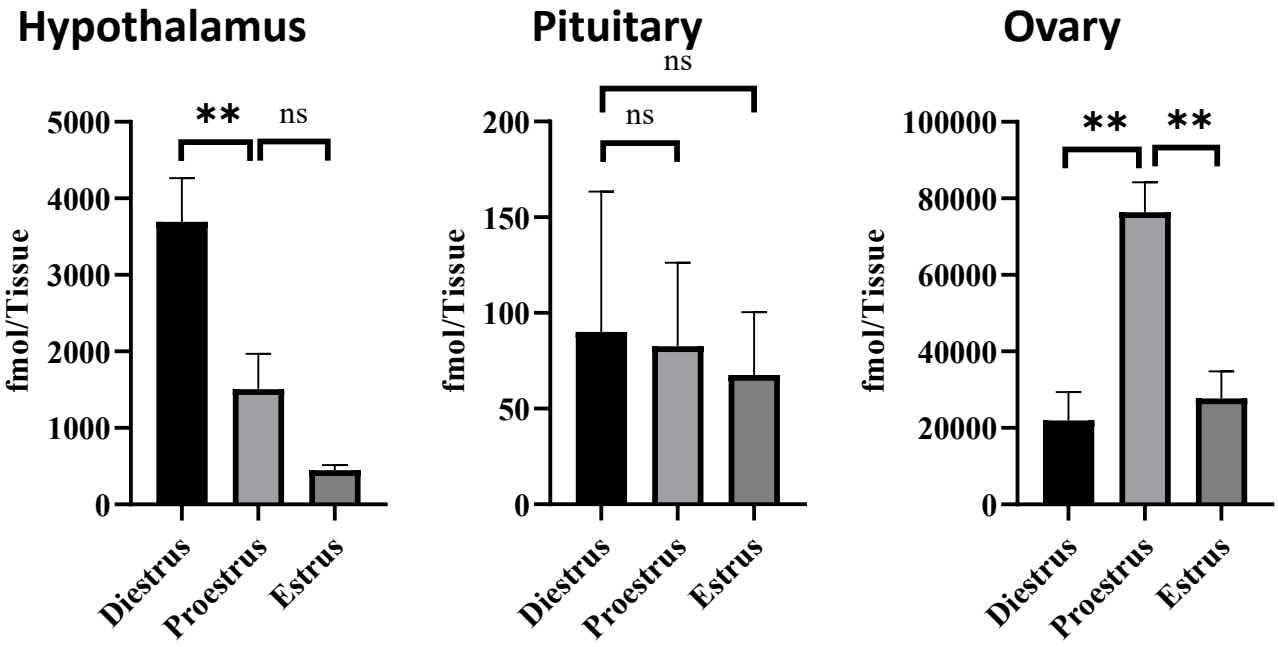

Figure 5-7 Periovulatory changes in progesterone levels during the estrous cycle of mice (n=9). Values represent mean ± SEM (n=9). Statistical analysis was performed using one-way ANOVA followed by Tukey's post-hoc (ns: not significant; *P<0.05; **P<0.01)

5.4 Regression

Visual analysis of the trends in mean hormone levels suggested several possible scenarios for co-variation during the estrous cycle. Linear regression analysis was applied to the level of mSN against all other analytes in each tissue over the 3 time points. The results are presented as R^2 values to reveal the goodness of fit. If the R2 value < 0.3, it is considered as not related; if 0.3 < R2 < 0.5, it is considered as weakly related; if 0.5 < R2 < 0.7, it is considered as moderately related; if R2 value > 0.7, it is considered as strongly related [162]. The R^2 values of mSN against each analyte are presented in Tabe 8. In the hypothalamus, mSN level was moderately related to the GnRH 1 level through the estrous cycle with R^2=0.6100. In the pituitary, the mSN level was weakly related to vasopressin with R^2=0.4030. In the ovary, the mSN levels were weakly related to P4 and E2 with R^2=0.3206 and R^2=0.3615, respectively.

Table 10. Linear regression coefficients (R^2) of SN against other analytes through estrous cycles in each tissue.

	Hypothalmus	Pituitary	Ovary
Vasopressin	0.2791	**0.4030**	0.0101
GnRH 1	**0.6100**	0.0173	N/A
Oxytocin	0.0264	0.00796	0.1254
Progesterone (P4)	0.1113	N/A	**0.3206**
Estradiol (E2)	N/A	0.03004	**0.3615**

5.5 Discussion

Numerous reproductive hormones were detected in the hypothalamus, pituitary, and ovaries during the periovulatory period of the female CD-1 mouse using LC-MS/MS. We investigated the hormonal fluctuation of the peptide hormones including GnRH 1, oxytocin, vasopressin and SN, and steroids such as progesterone and the estrogens. The results revealed that GnRH 1, vasopressin, and SN as well as the steroid hormones E2 and P4 varied during the periovulatory period while other hormones such as oxytocin were relatively more stable.

GnRH 1

In this experiment, I discovered that GnRH 1 was highest in the hypothalamus and pituitary at the proestrus stage. It is well-known that GnRH 1 pulsatile release becomes very frequent during the proestrus stage to trigger the LH surge that subsequently leads to ovulation. At the estrus stage, tissue GnRH 1 level remained relatively high in the hypothalamus but decreased in the pituitary. This is probably because of the quick processing and release of GnRH 1 around the time of the LH surge. The GnRH 1 measured in the pituitary is likely that which was released to the median eminence-portal blood system at the expected time [32]. The levels of GnRH 1 receptor in the pituitary is also high in proestrus compared to diestrus and estrus stages [30]. In female sheep, increased GnRH receptor mRNA and GnRH receptor binding in the pituitary prior to the LH surge, coincident with increased levels of E2 in ovarian follicles that drive positive feedback and the LH surge [163]. There is another possibility that the feedback of E2 and P4 decreased the secretion of GnRH 1 at the end of the proestrus stage, which led to the accumulation of GnRH 1 in the hypothalamus and low GnRH 1 in the pituitary. GnRH 1 can also be produced in the ovary to exert local paracrine actions on steroid production [164]. Relative to the pituitary, ovarian GnRH 1 levels are low. Indeed, I could not detect any biologically active form of GnRH 1 in any stage of the estrous cycle. This may be caused by the expression being very low and the actual GnRH 1 hormone level was below the detection limit. Alternatively, the GnRH 1 produced in the ovary may have been quickly processed and degraded. While I measured whole tissue levels of GnRH 1, the general pattern of hypothalamic production fits the model proposed by Herbison [148] for the

regulation of the pituitary-ovarian cycle by GnRH 1 in the mouse. It is also clear that the pituitary content of GnRH 1 was highest when it is known that pituitary sensitivity to GnRH 1 is high [165].

Progesterone

Progesterone was detected in all tissues across the estrous cycle. It is well-known to regulate GnRH 1 and LH and is usually considered in relation to blood levels and feedback actions on the hypothalamus and pituitary. Ovarian levels of P4 were highest at proestrus, being much lower at diestrus and estrus. This is somewhat different from circulating P4 patterns. In the mouse, it was found that blood P4 was highest in diestrus, lowest at estrus, and intermediate at proestrus [166]. However, hypothalamic P4 progressively decreased from high diestrus levels to the lowest concentrations at estrus, being very similar to that observed in circulating P4 in a previous study [166]. Moreover, hypothalamic P4 levels followed a similar pattern to ovarian E2 levels in my study. This is potentially important because circulating E2 can stimulate de novo P4 synthesis in hypothalamic astrocytes (glial cells), that in turn plays an important role to increase GnRH 1 release via kisspeptin neurons [167]. Thus, it may be that the total P4 content of the hypothalamus reflects both local production and P4 taken up from the circulation. Nevertheless, the role of P4 in the control of GnRH 1 and LH is paramount [148, 166, 168]. In marked contrast to the hypothalamus and ovary, pituitary P4 was relatively stable. This suggests that P4 mediated alternations in GnRH 1 receptor numbers and thus sensitivity to released GnRH 1 was not changing [169, 170].

Estradiol

The levels of E2 were highest in the ovarian tissue as expected. It is known that the mammalian brain can produce estrogens because of the presence of aromatase in the hypothalamus and E2 was not found in hypothalamic tissues [171]. Therefore the level was below the limits of detection (0.98 pmol/tissue). While E2 was measured in the pituitary, levels were stable and close to the detection limit at the time points assessed in the study. In the ovary, E2 content was high in diestrus compared to proestrus and estrus. The levels of ovarian E2 we measured corresponded to mRNA levels of the key estrogen synthesis enzyme aromatase documented for the rat across the estrous

cycle, whereas ovarian aromatase enzyme activities were highest at proestrus [172]. Thus the majority of E2 was produced in the ovary, and the overall pattern of variation fit expectations that ovarian E2 is critical to the control of the GnRH 1 pulse generator during the estrous cycle [173, 174].

Oxytocin and Vasopressin

While both oxytocin and vasopressin have been reported to have a role in the generation of the LH surge, they are rarely measured in the context of the estrous cycle. Contrary to expectations, oxytocin levels, while detectable in all 3 tissues, did not vary at the 3 time points analyzed. In contrast, vasopressin was high during the proestrus stages in the hypothalamus and pituitary. The various data point to an important stimulatory role for vasopressin in the LH surge, and coincident increases at proestrus in the hypothalamus and pituitary along with GnRH 1 in the hypothalamus and pituitary at the time of the expected proestrus LH surge indirectly support this proposal. Vasopressin can induce the LH [157], an effect that is maximal in proestrus around the time of peak blood E2 levels just prior to the preovulatory LH surge [156]. Some GnRH 1 neurons express vasopressin receptors in female mouse [158]. This is confirmed by another study that used mutant mice to reveal a critical role of vasopressin in the LH surge. In that study, the proestrus LH surge was absent when the level of vasopressin in the hypothalamus was decreased by Clock mutation [175]. Another study discovered that vasopressin controls LH surge through preoptic kisspeptin neurons in the female mouse [176]. My study is the first to measure the levels of vasopressin through the estrous cycle by LC-MS/MS.

Secretoneurin

The main objective of this work was to compare the levels of SN with known hypothalamic regulators to further attempt to characterize potential relationships to reproduction. It was found for the first time that SN was highest in both the hypothalamus and pituitary during proestrus. In other experiments, SN was detected by shotgun peptidomics multiple times in mouse and rat hypothalamus [12, 43, 177]. Another study on bovines discovered a change in secretoneurin processing in the pituitary before and after puberty [11]. The SN peptide was also detected at low

levels in the ovary, supporting the proposal that ovarian SN may regulate blood vessel formation in the primate and human ovary at the time of ovulation [178].

The levels of GnRH 1, vasopressin, and SN were all highest in the hypothalamus and pituitary at proestrus strongly implicates SN in the ovulatory cycle. It is known that SN stimulated LH release from mouse LβT2 cells [4] and that both SNa and SNb can stimulate GnRH 2 expression in the brain of the orange-spotted groupers, a commercially important fish species [179]. Moreover, mutations in the Scg2 genes of zebrafish lead to a decrease in GnRH 3 expression in the hypothalamus of females [9]. Moreover, SNa stimulated GnRH 3 and the type 2 GnRH receptor mRNA coincident with increased pituitary LHβ mRNA in the female zebrafish [9]. This led me to conduct regression analysis to determine potential relationships between SN, vasopressin, and GnRH 1 in the hypothalamus and pituitary. Of these, and remarkably, only GnRH 1 and SN appeared to co-vary within individuals across the estrous cycle. The moderate relationship (R^2=0.61) is very suggestive of an important stimulatory relationship between SN and GnRH 1, strongly supported by the aforementioned data in fish models.

Other analytes

The level of testosterone, E1 and E3 were measured in this experiment, however, the levels of these compounds were below the LLOQ in most samples. This issue may be solved by loading a larger amount of sample in each analysis. Due to technical issues, this can not be solved in the current experiment. It is also possible that a different sampling time can achieve higher levels of these compounds in the samples, which can lead to future work.

5.6 Conclusion

This is the first simultaneous measurement of peptide and steroid hormones in tissue samples during the estrous cycle. The extraction and quantification methods were optimized for SN detection in individual small tissues such as the hypothalamus, pituitary, and ovaries. This permitted direct comparison of variations in the known neuropeptides and steroids regulating ovulation with the emerging reproductive hormone SN. This is the first time that SN has been measured in the mouse estrous cycle that is moderately correlated to the levels of GnRH 1. This

strongly implicates SN in the regulation of GnRH neurons and the LH surge in the mouse. These data further suggest an important role for the SN peptides in vertebrate reproduction.

Chapter VI Conclusions, applications, and future work

6.1 The first time to analyze different types of hormones simultaneously

In this project, the hypothesis that the levels of peptide and steroid hormones can be analyzed from the same tissue sample simultaneously was successfully tested. The performance of the optimized method in measuring both peptide and steroid were similar to the previous report on peptide or steroid individually [61, 137, 138]. Although not discussed in detail I detected LHβ using untargeted proteomics (general method shown in Figure 6.1) in protein pellets obtained from pituitary samples. Detailed data is not included in this thesis because I did not have time to repeat and optimize conditions. However, the possibility of including protein analytes into this package of methods is certain. Analyzing the two (three) categories of the hormone at the same time can not only help physiologists to have a better understanding of the endocrine system but also make contributions to clinical testing and improved diagnosis of complex endocrine disorders. When I design the package of the methods, I employed the 96-well plate as a platform to make it possible to motorize the sample processing procedure and downstream analysis. With minimum optimization, this package of methods can be used for high throughput routine analysis in large research institutes or clinical test centers.

6.2 The SPE method is reusable and compatible with ELISA kits.

The SPE method alone is now widely employed in the Trudeau lab to extract peptides and steroid samples. It has been proved to be compatible with some ELISA kits on the market. Having a reusable SPE plate in a small-scale research laboratory that serves multiple different ELISA tests can not only save on research funds but also significantly decrease the plastic waste it generates. In addition, it can decrease the variability between different batches of SPE kits.

6.3 The matrix effect of SN peptides and better solutions are still needed.

When testing this hypothesis, I discovered that the strong matrix effect was the reason for the past SN peptides quantification frailer [14]. Although the BSA spikes and customed parts solved the issue, it can only work on the Agilent HPLC system. A solution for the Thermo HPLC system is still pending development. Due to the higher impact of dead volume, most of the nanoscale HPLC

equipment is designed to have an offline needle and sample loop. All nano-HPLC equipment may end with the same issue when working with SN peptides. Therefore, an easier and universal solution for matrix effects must be found if we are to explore more aspects of SN.

6.4 The first time to reveal the relationship between SN and GnRH 1

This is the first to reveal that, through an estrous cycle, SN and GnRH 1 were moderately related in the mouse hypothalamus. Moreover, SN and vasopressin were weekly related in the pituitary, SN and P4 were weekly related in the ovary, and SN and E2were weekly related in the ovary (Table 10). This strongly implicates SN in the regulation of the HPG axis of the mouse model/ A similar study (Peng, D. 2022. Characterization and Role of Secretoneurin in the Ovulatory Cycle of Zebrafish, Ph.D. Thesis, University of Ottawa, pp. 160) using the same package of methods discovered that SN and GnRH 3 were strongly related in zebrafish hypothalamus during the ovulatory cycle. These results support our proposal that SN is an important reproductive hormone [13]. Unfortunately, there was not sufficient time to optimize the protein extraction and analysis method. The relationship between SN and LH in the pituitary is still missing.

6.5 SN peptide processing.

In the peptidomics results (Table 8), both SNa and SNb had multiple naturally occurring fragmentations. Some of these fragments were highly abundant and changed throughout the zebrafish ovulatory cycle (Peng, D. 2022. Characterization and Role of Secretoneurin in the Ovulatory Cycle of Zebrafish, Ph.D. Thesis, University of Ottawa, pp. 160). Similar results were reported on the bovine model before and after puberty using untargeted peptidomics [11]. This requests further study on SN peptide processing and the functions of truncated SN peptides. An efficient way to answer this question will be to prepare a peptide analog library to generate many standards for the measurement and quantification of SN peptide derivatives during various physiological experiments.

6.6 Untargeted peptidomics with steroid and peptide quantification.

When the LC-MS/MS system operated for steroid and peptide quantification, the ion trap analyzer stayed idle most of the time. This meant that the machine had free analyzing power to acquire more MS2 information for untargeted peptidomics. I attempted to utilize this analyzing power for untargeted peptidomics. To do the untargeted peptidomics, I commanded the MS equipment to analyze MS2 for all ions with more than 2 proton charges when there is no ion triggering the mass list. The preliminary data was promising (not shown in the thesis), but further optimization work is needed. The digested BSA was a major interference from the sample and a mass exclusion list had to be established to eliminate the BSA signal.

6.7 Application in other industries

Peptide and steroid measurements are important not only in physiology research but also in other industries such as food safety evaluation and environmental assessment. For dietary supplements, collagen hydrolysate peptide profile consistency is important for nutrition, while determining steroid levels is important for safety [180, 181]. If the peptide profile and steroid levels are tested at the same time, food safety authorities could make inspections more efficient and less costly. Monitoring the levels of steroid hormones, especially synthetic and potent analogs, is crucial to monitoring pollution and endocrine-disrupting chemicals in the aquatic environment [182]. Additionally, formylmethionyl-peptides are key indicators of the level of bacteria [183]. Measuring these two categories of compounds together would permit ecotoxicologists to better understand chemical threats to ecosystems and human health. In addition to the food safety evaluation and environmental assessment, the method developed in this project may also make contributions to clinical tests and pharmaceutical research. All of these require further development.

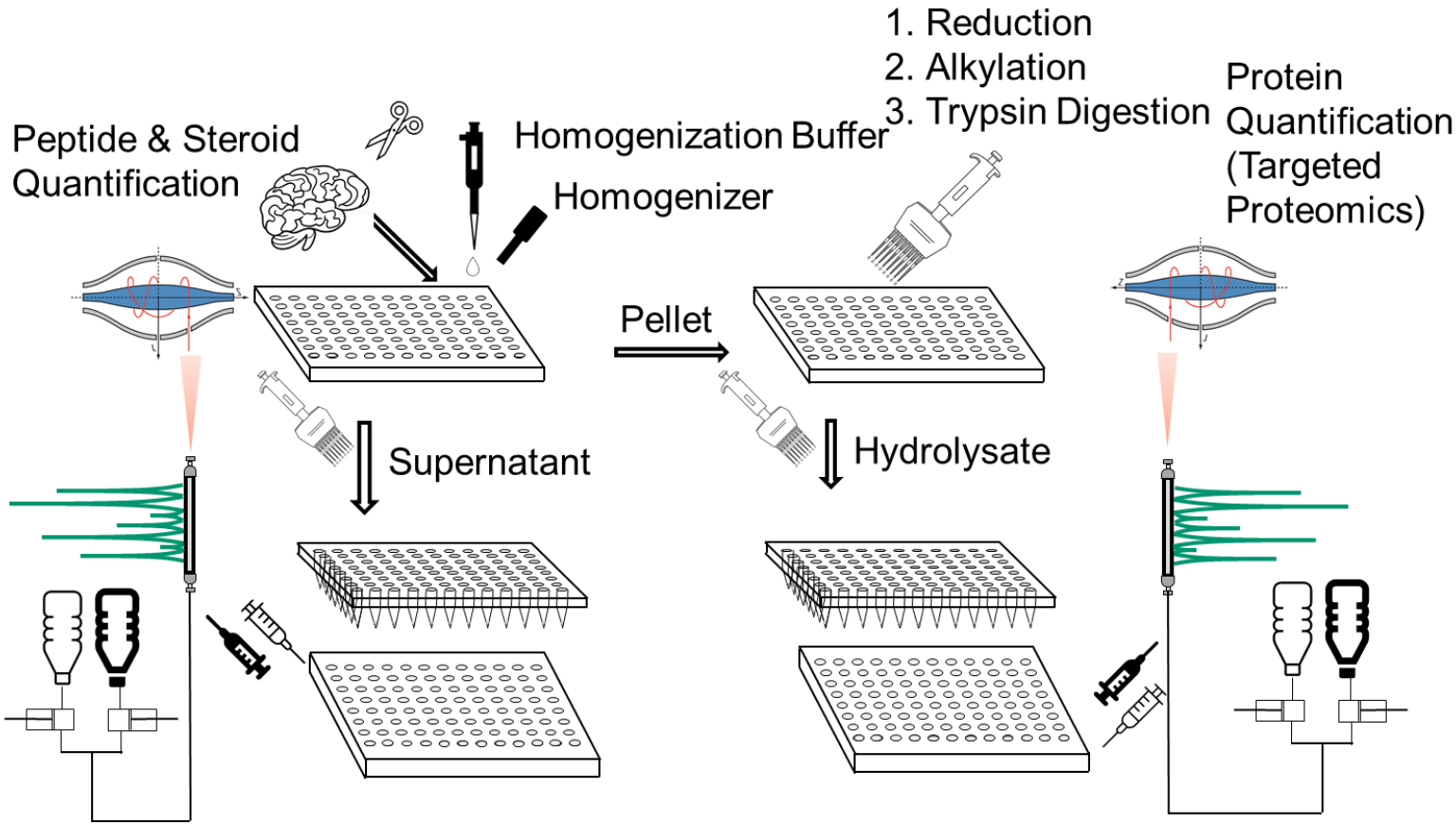

Figure 6-1 Overview of the entire package of methods and future work using the 96-well plates as a platform.

Chapter VII Appendix I In-house packing for nanoscale HPLC columns

An HPLC column is a tube with HPLC resin packed firmly in it. Packing a regular HPLC column is not feasible in most biology laboratories. To let silica packing resin generate a condensed and equally distributed packed bed, the necessary pressure is tremendous. If the loading force is not sufficient, the sheer force from the wall of column hardware and between resin particles can lead to a looser packing on the edge of the packed bed and channel-through within the bed. This unequally distributed bed would dramatically decrease the number of theoretical plates [184].

When working with nanoscale HPLC, the column ID is only 10-100 times the packing particle size. The sorbent particles tend to form an equally distributed packed bed when flushing with an HPLC pump. In addition, the amount of sample loaded to the column is comparably large relative to the column. When working with biological samples, a nanoscale column can be easily blocked. Therefore, in-lab packing nano-columns are technically feasible, practical, and cost-effective [185].

Nanoscale HPLC columns can be packed by a pressure cell. The design of the pressure cell varies between labs but they share the same concept. In this project, the pressure cell was fabricated by the machine shop of the University of Ottawa. As shown in Figure 7.1, the major function of these pressure cells is to maintain the pressure in the cell chamber so that the continuously mixed slurry can escape from the fused silica capillary. The frit at the end of the capillary stops the beads from running through while allowing the liquid to pass. In this way, the beads (packing material) form a packed bed (column). In this step, the column can be packed longer than desired. It is then flushed by an HPLC pump on high-pressure overnight to become firm and stable. During this period, the bed could be pressed to be denser and shorter. If the column is still longer than expected after the flushing, it can be trimmed to desired length [185, 186].

The frit of the column is also important to the success of a nano-HPLC experiment. It has to stop the packing particles from leaching out of the column with a minimum contribution to total

backpressure. Instead of having an actual stainless-steel frit locked by column hardware, nano-scale LC columns tend to have a polymer frit prepared inside the fused silica capillary at the end of the column. These frits are generated by chemical reactions. Figure 7.2 represents the reaction I employed to prepare the frit in this project [187, 188].

In some cases, the opening of a nano electron spray emitter is narrow enough to work as a frit. In this situation, the chromatography resins can be packed directly into the fused silica emitters. In consequence, the column and the electron spray emitter become one intact piece in the HPLC flow path [185].

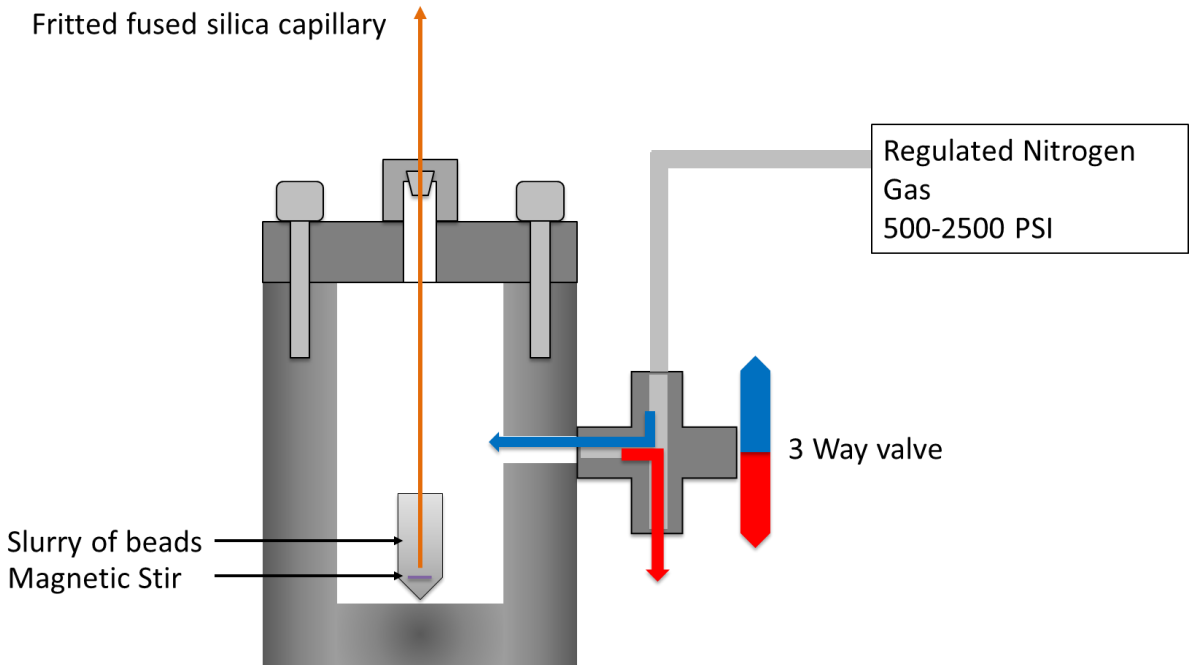

Figure 7-1 Schematic diagram of the pressure cell

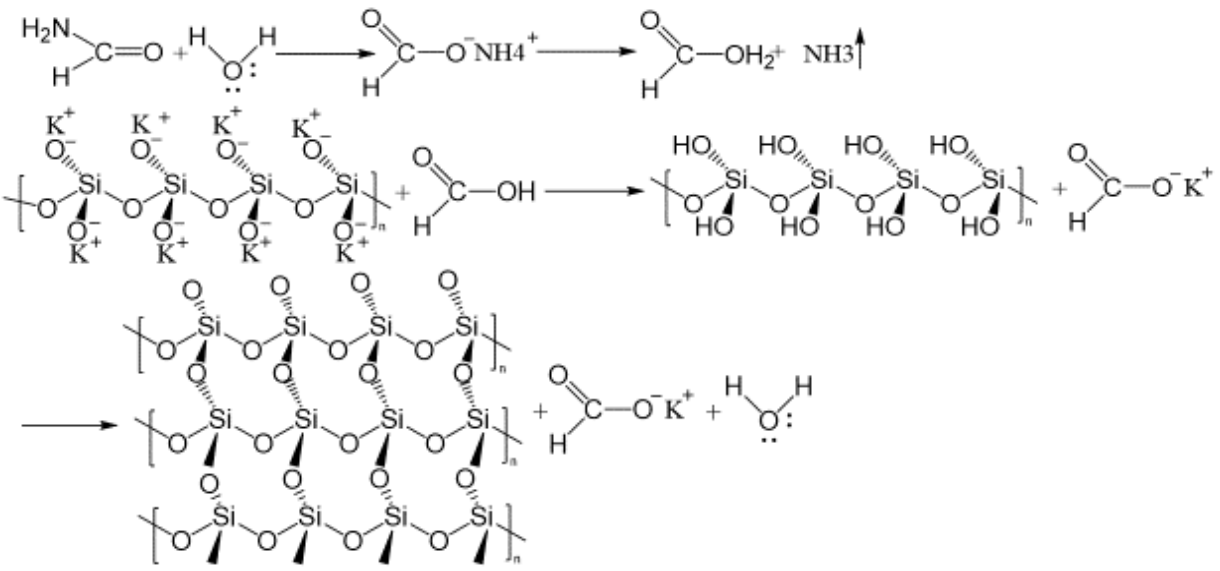

Figure 7-2 The chemical reaction to prepare frits using potassium silicate and formamide

Chapter VIII Appendix II Untargeted and targeted peptidomics

Untargeted peptidomics

LC-MS/MS based peptidomics can run as untargeted or targeted. The untargeted peptidomics gives a broad overview of the peptide components in the biological sample. It is optimized to provide a list of identified peptides. This list should be as complete as possible but not focus on any particular peptide compound. It is often employed in discovery experiments, for example to link changes in peptide production to environmental factors, nutrition, behaviors, or physiological states [189, 190].

From the technical point of view, during chromatographic elution, the MS machine repeatedly and quickly selects several most intense peptide ions (master scan); perform multiple MS2 scans to these ions (data-dependent scan); marks these ions as a temporary exclusion for a certain period (a few minutes). The data from the MS machine can be compared to the database to identify peptides. Using this technique, the identified peptides are the ones with higher MS1 responses and better MS2 profiles, which is not necessarily relevant to the abundance.

Targeted peptidomics

Targeted peptidomics also relies on the LC-MS/MS equipment but is set up to focus on specifically targeted analytes. The MS machines are set to proceed with certain MS transitions on a timetable basis (data-independent) or data-dependent. In this way, the full analyzing power is dedicated to the target analyte to achieve optimum sensitivity [191]. Targeted peptidomics needs standard compounds, such as chemically synthesized peptides.

Chapter IX Appendix III LC-MS/MS method development.

Flow restrictor:

The flow restrictor plays a key role in this LC-MS/MS method As previously demonstrated, it not only generates a nano-scale flow rate but also makes a critical contribution to chromatogram reproducibility. There were 7 lengths of restriction capillaries selected as candidates. To obtain a stabilized backpressure for each length in various B% (positive mode mobile phase system), the HPLC pump is set to run isocratic for 10 min on 5%, 30%, 50%, 75%, and 90% B individually. The backpressure is read at the end of each leave. The backpressure of the system in each B% is plotted against the capillary length in Figure 9.1.

The HPLC system was initially set to run at around 300 bar back pressure with a 280 mm fused silica capillary, for plugging resistance purposes. However, due to the modification on the rotor and the stator of the injector valve, the HPLC system could only have a pressure rating of 340 bar max. When the mobile phase ramps from high B1% to low B1% for equilibrium, the backpressure surges up to 360 bar with the 280 mm fused silica capillary as the restrictor. This generated a leak and triggered a leaking sensor. Therefore, the system was eventually set to run at around 200 bar backpressure with 200 mm fused silica capillary as a restrictor. This setup has the narrowest range of pressure fluctuation through the gradient. The pressure surge when switching to equilibrium can go up to 295 bar, which is still far from the 340 bar limit [192].

When analyzing in negative mode, the change in mobile phase composition increases the system backpressure. To minimize the hardware modifications required when switching between positive and negative mode analysis, the flow rate from the electromagnetic proportion valve (EMPV) has to be adjusted. To achieve the most suitable flow rate from EMPV for negative mode analysis, the system is set to run isocratic at 5%, 30%, 50%, 75%, and 90% B for 10 min on EMPV flow rate 10 µL/min, 13 µL/min, 15 µL/min 18 µL/min and 20 µL/min individually. In Figure 9.2, the system back pressure is plotted against B% for each flow rate from EMPV. According to Figure 9.2, 15 µL/min is the maximum flow rate that the system can sustain. The EMPV flow rates below

15 µL/min couldn't generate reproducible chromatograms for estrogen analytes. Therefore, 15 µL/min is selected as the EMPV flow for negative mode analysis.

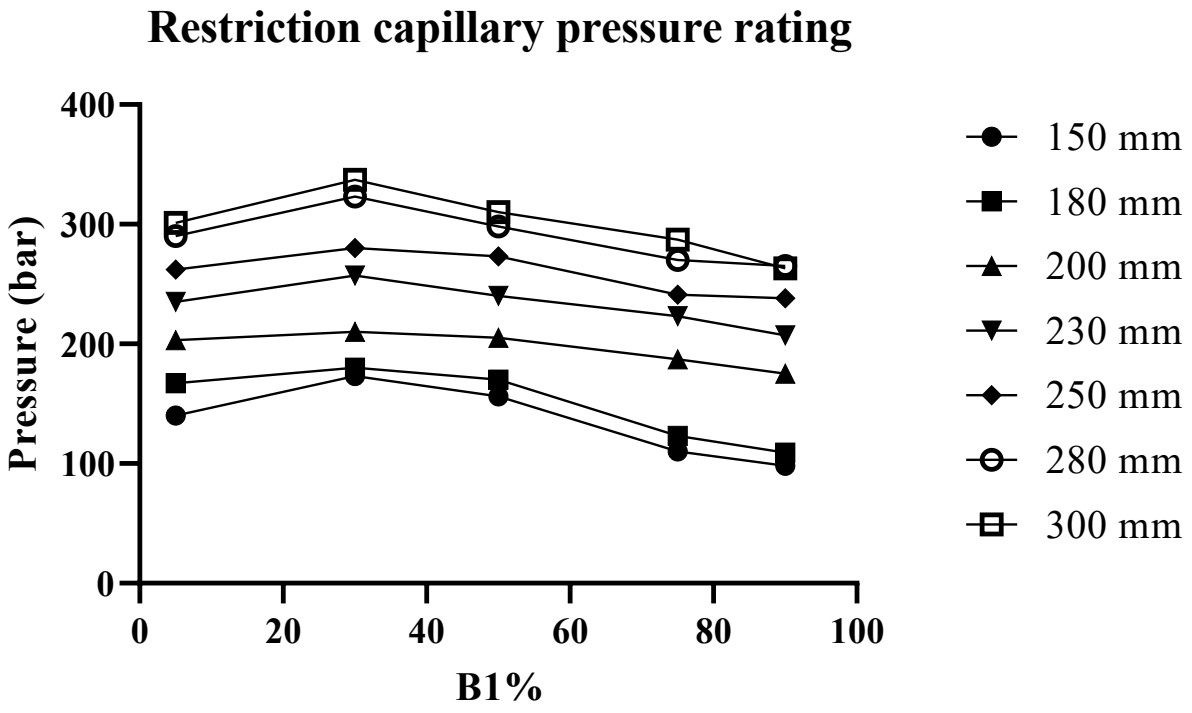

Figure 9-1 The HPLC system backpressure for 5%, 30%, 50%, 75%, and 90% of mobile phase B1 of each restriction capillary length. Mobile phase system A1 and B1 were employed. The EMPV flow rate was maintained at 20 µL/min. Each backpressure was recorded from the Agilent operation system once after the system maintained on isocratic conditions for 10 mins.

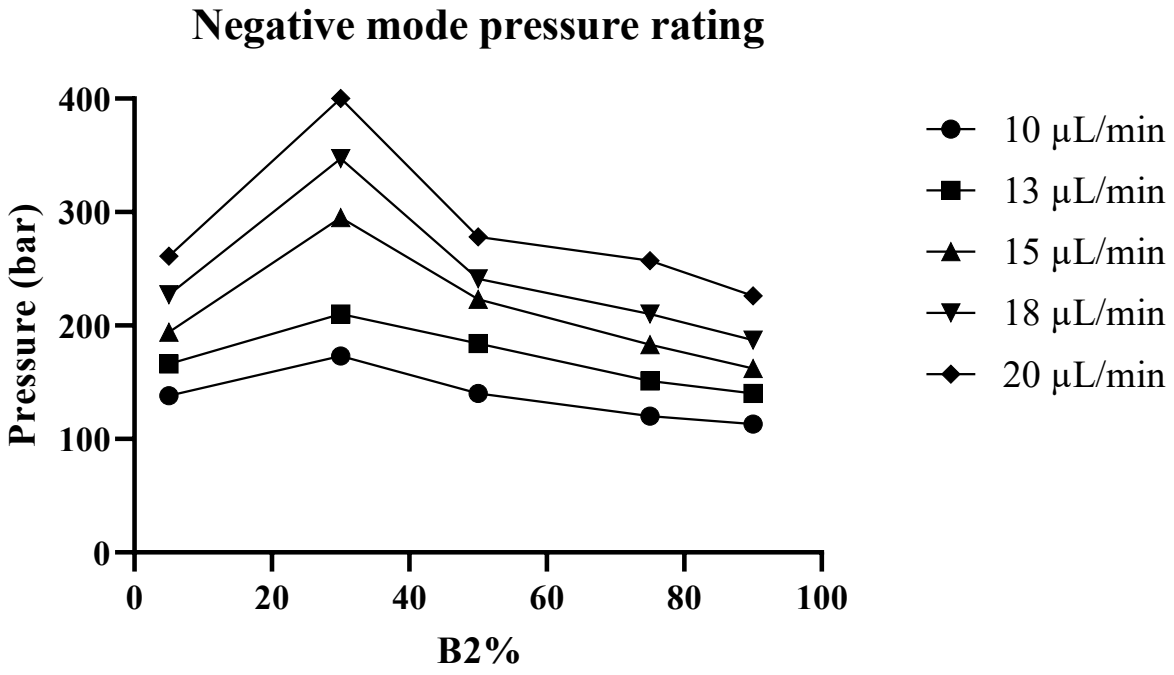

Figure 9-2 The HPLC system backpressure for 5%, 30%, 50%, 75%, and 90% of mobile phase B2 of each EMPV flow rate, 10 µL/min, 13 µL/min, 15 µL/min, 18 µL/min, and 20 µL/min. Mobile phase systems A2 and B2 were used. The restriction capillary employed was 20 µm ID, 200 mm length. Each backpressure was recorded from the Agilent operation system once after the system was maintained on isocratic conditions for 10 mins. The system was set to trigger an error at 400 bar.

Mobile phase and gradient

Positive mode ionization analysis

When developing the HPLC method for the positive mode ionization analysis, formic acid (FA) was selected as an additive to the mobile phase. In the experiment, the mass spectrum peak intensity of GnRH 1 was found to be pH-dependent. Given a bottle of FA-water mobile phase (mobile phase A1), with time going by, FA evaporates and the pH value of the solution rises. To guarantee the reproducibility of GnRH 1 measurements through time, four concentrations of mobile phase A1 were prepared on the first day of the experiment, which are 0.1%, 0.2%, 0.3%, and 0.4% v/v. At the same time every day, 1 pmol of GnRH 1 is injected into the LC-MS/MS system. This was repeated five times a day for 10 days with each A1 candidate. In this experiment, the chromatogram peak intensity is plotted against time by day in Figure 9.3.

According to Figure 9.3, the GnRH 1 mass spectrum signal decreases and variation increases after the 7^{th} day of the experiment when 0.1% FA is used as a mobile phase additive. There was no mass spectrum acquired on the 10^{th} day of the experiment for the mobile phase with 0.1% FA as additive. For other mobile phase candidates, 0.2% FA additive shows an increment of signal strength which is stable through the 10-day experiment; 0.3% and 0.4% FA additive could also keep the signal strength stable through the 10 days' experiment. However, the 0.3% and 0.4% FA additive slightly subtracted the signal strength. Therefore, the 0.2% FA was selected as the additive for the mobile phase in positive mode analysis. There is no other analyte that had mass spectrum signal decay under the conditions discussed.

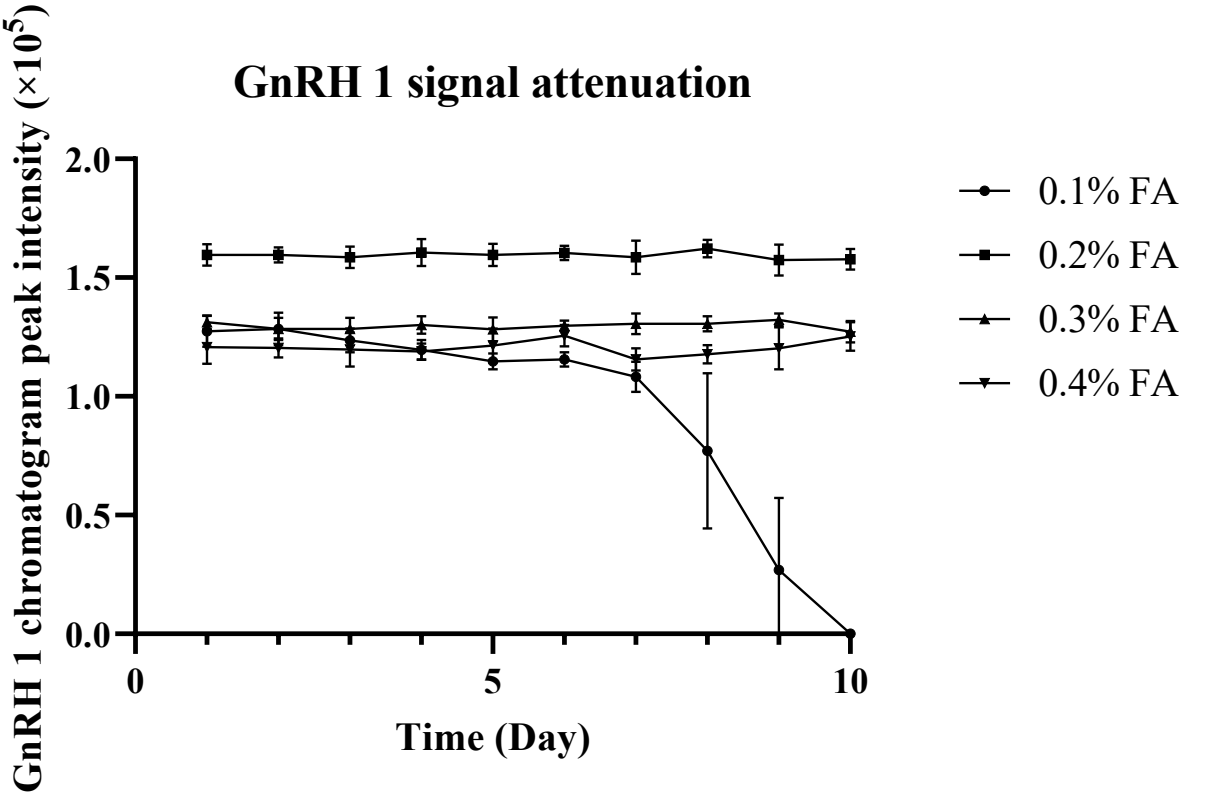

Figure 9-3 The attenuation of GnRH 1 chromatographic peak intensity on various mobile phase additives. One pmol of GnRH 1 was injected to the LC-MS/MS system 5 times on each mobile phase additive concentrations every day for 10 continuous days. The chromatogram peak intensities of GnRH 1 were plotted against time. The experimented additive concentrations are 0.1%, 0.2%, 0.3% and 0.4% FA (formic acid). The error bars represent the standard deviation on each data point (N=5).

Negative mode ionization analysis

The negative mode ionization methods for estrogen analysis have been reported multiple times. There are a few commonly used mobile phase compositions. Mobile phase A is usually water with NH_4F or, NH_4OH as an additive. The mobile phase B can be a mixture of water, acetonitrile, and MeOH with the same additive as mobile phase A. In this experiment, I initially attempted to run positive mode analysis and negative mode analysis in the same HPLC injection. It was abandoned eventually but still a very valuable attempt. It will be demonstrated in a later section.

To optimize the mobile phase composition for estrogens in negative mode analysis, I selected four mobile phase compositions as a candidate. They are:

I. 1 μM NH_4OH in water as mobile phase A and 1 μM NH_4OH in water as mobile phase B [59, 193].
II. 10 μM NH_4OH in water as mobile phase A and 10 μM NH_4OH in acetonitrile as mobile phase B [59, 193].
III. 1 μM NH4F in water as mobile phase A and 1μM NH_4F in 90% acetonitrile 10% water as mobile phase B [193-195].
IV. 1 μM NH4F in water as mobile phase A and 1μM NH_4F in 65%MeOH 30% acetonitrile 5% water as mobile phase B [193-195].

One microliter of 1 pmol/ μL estradiol, estriol, and estrone mixture was loaded into the system individually running with the previously mentioned 4 mobile phase systems. The gradient was set as 5% B to 95% B in 45 min. The flow rate from HPLC was set as 20 μL/min. In this experiment, the mobile phase system, I only have a chromatographic peak of estrone; the mobile phase system II has a chromatographic peak of estrone and estradiol; the mobile phase system III has chromatographic peaks of all three compounds but the FWHM for estriol is over 2 minutes; the mobile phase system IV have chromatographic peaks of all three compounds but the backpressure goes over 350 bar during the gradient which is discussed in other parts of this thesis. In the end, the mobile phase composition IV is selected for the negative mode analysis. In this composition, mobile phase A is named A2, the mobile phase B is named B2.

Gradient

The gradients for both positive and negative ion mode analysis were optimized to be as short as possible. When analyzing in positive mode, the system was maintained at the loading position for 3 mins. The capillary pump delivered 95% A1 and 5% B1 on a flow rate of 6 μL/min during the loading period. The injection volume was 1 μL for all analyses. When the system switched to the analyzing position, the capillary pump quickly ramped to a 20 μL/min flow rate with 80% A1 and

20% B1, and then maintained for two minutes. Gradient elution was done from 20% B1 to 90% B1 in 30 mins.

When analyzing in negative mode, the system was maintained at the loading position for 5 mins. The capillary pump delivered 90% A2 and 10% B2 on a flow rate of 3 µL/min through the loading period. The injection volume was 1 µL for all samples. When the system switched to the analyzing position, the capillary pump quickly ramped to a 15 µL/min flow rate with 50% A2 and 50% B2, and then maintained for 5 mins. Gradient elution was done from 50% B2 to 90% B2 in 15 mins.

Mass spectrometry

MS data collection method

Setting up the data collection method for a mass spectrometer is important to the success of an LC-MS/MS experiment. In this project, the MS equipment is required to collect enough mass information to confirm the structure of eluted molecules and to have more than 5 data points to plot a chromatogram. All mass spectrometers have a limitation on duty cycles. They can only perform a certain amount of scans every second. For the same machine, the higher the resolution of a scan, the longer time the scan will take.

The Finnigan LTQ system was employed to develop the HPLC methods. Purified standards were loaded into the MS system by direct infusion to confirm MS2 ions. The primary ions and product ions for qualification (Qual) and quantification (Quan) are listed in Table 2. During the method development step, the MS equipment was operated in SRM mode for all analyte ions with timetable triggered segments. The timetable was designed to guarantee that no more than 7 transitions are analyzed at the same time. This setup ensures the MS system collects at least one data point per second for each analyte when they elute from the column.

When running biological samples, the Velos Orbitrap system was employed to achieve optimum sensitivity and accuracy. In the beginning, when transferring the MS method from the LTQ to the Orbitrap system, I attempted to set the orbitrap analyzer to collect MS1 information at high resolution (FWHM 60,000) at 1 Hz, while the ion trap analyzer collected the MS2 information at low resolution (FWHM 1,000) at 10 Hz. With a similar timetable as the Finnigan LTQ, the system should finish one high-resolution full scan for quantification and 10 MS2 scans for qualification every second. However, the MS system did not behave as described. When one mass analyzer is occupied (either ion trap or orbitrap), the other mass analyzer does not operate independently. Instead, it stays idle. In consequence, the system can only collect one MS1 data point every 2 seconds. For a chromatographic peak of fewer than 10 seconds, the data points would not be sufficient for reliable quantification.

To acquire sufficient data points for chromatographic quantification, the Velos Orbitrap equipment had to be operated in a data-dependent acquisition mode. During analysis, the mass spectrometer performs the following events repeatedly:

Event 1. The orbitrap analyzer performs a full scan (master scan) at 150-1500 m/z with resolution FWHM 60,000.

Event 2. Using event 1 as a master scan, the LTQ analyzer performs data-dependent ETD MS2 full scans on the most intense ion on the preset mass list three times. The threshold to trigger this MS2 scan is 5×10^3 counts. The parent ion sampling is assisted by the onboard chromatographic peak top detection function. The same parent ion would not trigger MS2 analysis for 1.5 mins.

Event 3. Using event 1 as a master scan, the LTQ analyzer performs data-dependent ETD MS2 full scans on the second most ion on the preset mass list three times. The threshold to trigger this MS2 scan is 5×10^3 counts. The parent ion sampling is assisted by the onboard chromatographic peak top detection function. The same parent ion would not trigger MS2 analysis for 1.5 mins.

Event 4. Using event 1 as a master scan, the LTQ analyzer performs data-dependent ETD MS2 full scans on the third most intense ion on the preset mass list three times. The threshold to trigger this MS2 scan is 5×10^3 counts. The parent ion sampling is assisted by the onboard chromatographic peak top detection function. The same parent ion would not trigger MS2 analysis for 1.5 mins.

Event 5. At 25-30 mins after injection, the orbitrap analyzer performs a single ion monitoring scan on 1243.95 m/z with scan width 1 m/z on resolution FWHM 30,000.

Event 6. At 25-30 mins after injection, the orbitrap analyzer performs a single ion monitoring scan on 1152.90 m/z with scan width 1 m/z on resolution FWHM 30,000.

Event 7 At 25-30 mins after injection, the orbitrap analyzer performs a single ion monitoring scan on 1217.95 m/z with scan width 1 m/z on resolution FWHM 30,000.

Event 8. Using event 5 as a master scan, the LTQ analyzer performs data-dependent ETD MS2 full scans on the most intense ion on the preset mass list three times. The threshold to trigger this MS2 scan is 5×10^3 counts. The parent ion sampling is assisted by the onboard chromatographic peak top detection function. The same parent ion would not trigger MS2 analysis for 1.5 mins.

Event 9. Using event 6 as a master scan, the LTQ analyzer performs data-dependent ETD MS2 full scans on the most intense ion on the preset mass list three times. The threshold to trigger this MS2 scan is 5×10^3 counts. The parent ion sampling is assisted by the onboard chromatographic peak top detection function. The same parent ion would not trigger MS2 analysis for 1.5 mins.

Event 10. Using event 7 as a master scan, the LTQ analyzer performs data-dependent ETD MS2 full scans on the most intense ion on the preset mass list three times. The threshold to trigger this MS2 scan is 5×10^3 counts. The parent ion sampling is assisted by the onboard chromatographic peak top detection function. The same parent ion would not trigger MS2 analysis for 1.5 mins.

The mass list is set according to Table 2 (page 60). When the mass spectrometer executes this method, the LTQ analyzer performs all MS2 scans while the orbitrap analyzer performs the Fourier transform analysis for MS1. Therefore, the system collects both MS1 and MS2 information at the same time. The resulting file can have enough data points to plot a chromatogram from high-resolution MS1 and sufficient MS2 information for each peak to identify the molecule.

Matrix effects for SN detection required machine modification for reliable detection

Even though secretoneurins have been compounds of interest in many research projects, a successful MS-based quantification essay has not been reported [13, 196]. When I was developing the method to quantify SNs using LC-MS/MS, I realized that the non-specific binding of SNs is the major barrier to a reliable sensitive quantification assay.

Matrix effects

In this experiment, purified SNs are loaded to the mass spectrometer through the LC-MS/MS system and direct infusion independently. The LC-MS/MS had a detection limit of around 1 µL of 10 pmol/µL for all SN samples. The 1 µL of 10 pmol/µL injection can have a 1×10^5 to 3×10^5 LC-MS/MS peak strength. That falls into the middle of the full mass analyzer range which is 1×10^1 to 9×10^8. However, a 1 µL injection of 5 pmol/ µL standard and SNs (2-fold dilution) did not produce any chromatographic peak. In the meantime, the direct infusion can detect a 100 fmol/µL solution at a 300 nL/min flow rate.

To investigate the issue, I designed the following experiment. One zebrafish brain and pituitary were dissected and extracted by SPE. The lyophilized extract was re-suspended in 40 µL 0.1 % FA and 2 % ACN water. From this solution, 12 µL was used for 2 × dilutions, 12 µL was taken out for 1 pmol/µL SNa and SNb spikes, and 12 µL was injected as is. These samples run through the LC-MS/MS system. Chromatograms were plotted by accurate MS1 of SN peptides with 10 ppm mass tolerance. The Normalization Level (NL) was recorded from each chromatogram taking the most intense SNs accurate mass intensity as 100%. When there were over 5 data points to form a chromatographic peak for the SNs, the peak area was recorded [197]. All samples were injected 3 times. These results are compared in Figure 9.4. When diluting the purified SNs from 10 pmol/µL to 5 pmol/µL, the mass spectra not only significantly decrease in intensity, but also in the number of spectral frames that contain SN signals. The 5 pmol/µL SN injections did not produce enough data points to plot a chromatographic peak. In tissue extracts, the 1 pmol/µL spike of the purified SNa and SNb significantly increased both mass spectrum intensity and peak area. The 2 fold dilution of tissue extracts decreased the peak area and spectrum intensity, but there are still over 5 data points to plot the chromatographic peak for all diluted tissue extract injections. This decrement

is significant with different probability levels on NL. It may not be significant in peak areas due to the sample size. The diluted tissue extracts have a significantly higher NL compared to the 5 pmol/μL SNs. This represents the two-fold dilution of 10 pmol/μL purified SN peptides is not the only factor causing mass spectrum signal decrement. The difference in matrix effect between biological samples and purified peptide samples is important as well. Matrix effects can reduce or increase the mass spectrum signals by co-elution [198]. For the SNs, the matrix effects from tissue extracts prevent the mass spectrum signals from subtraction unrelated to chromatographic behavior.

This experiment was conducted on both the Agilent 1100 HPLC and the Thermo Easy nLC individually coupled with the Velos Pro Orbitrap mass spectrometer. The results discussed above are from the Agilent 1100 HPLC. The results from the Thermo Easy nLC are on a similar trend and the matrix effect is more severe. This issue is still unresolved for the Thermo Easy nLC and will not be discussed further in this thesis.

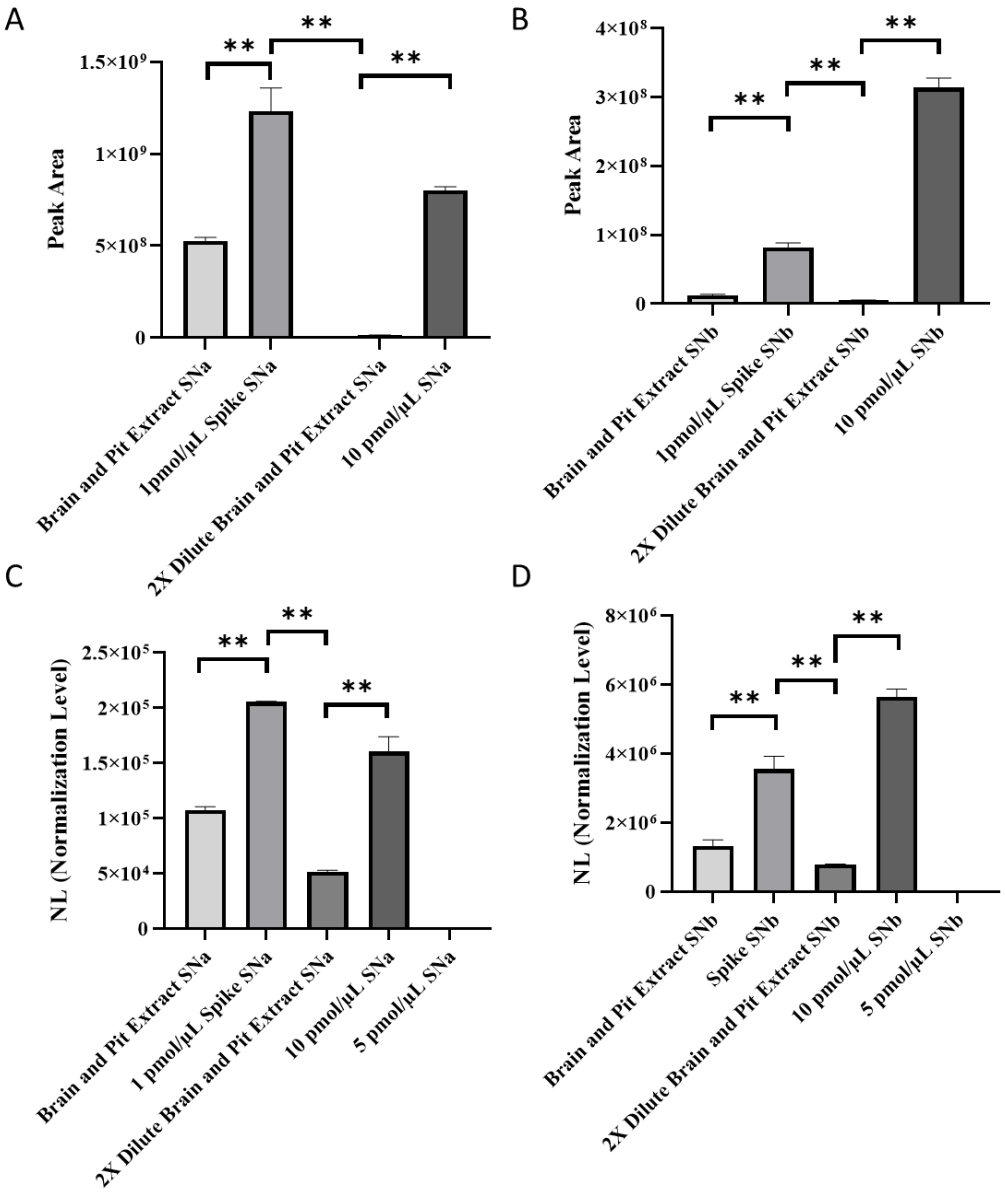

Figure 9-4 Matrix effects for SNa and SNb in LC-MS/MS experiments (N=5). Chromatogram peaks were plotted with a minimum of 5 data points. The experimental groups measured SNa/b levels in brain and pituitary extract; 1 pmol/µL SNa/b in tissue extract; 2 × of tissue extracts; 10 pmol/µL SNa/b of pure peptide samples. Standard bars represent standard deviations. A and B are plotted by chromatogram peak area. 5 pmol/µL SNa and SNb did not have sufficient mass spec data points to plot a chromatogram. C and D are plotted by the normalization level of the most intense mass spectrometry peak.

Non-specific binding

To discover the origin of this matrix effect, the following experiments were conducted. To a well-cleaned LC-MS/MS system, 1 µL of purified SNa and SNb of various concentrations were injected and run through the quantification method. There were 25 injections of 1 µL water following each of the SN injections and run through the quantification method. The SN injection was registered as injection #0 and the 25 water injections were registered as injection #1 to injection #25. In Figure 9.6, the logarithmic value of NL for the SN chromatographic peaks were plotted against the injection number. When SN peptides were injected into the LC-MS/MS system at 10 pmol/µL, they carried over to the next water injection by less than 10% of signal strength. These peptides get cleared out of the HPLC system after 2 water injections. When the SN peptides were injected into the LC-MS/MS system at 100 pmol/µL, they were carried over for 5 injections. There was no more carryover of the SN peptides by the 6^{th} water injection. When the SN was injected into the LC-MS/MS system at 1000 pmol/µL, both SNa and SNb signals lasted over 25 water injections. There are no trends or patterns observed that this SNs leaching may follow. The SN carryover issue and the previously described pure sample dilution issue are both caused by non-specific binding. It was hypothesized that the SNs should non-specifically bind to one or multiple parts of the HPLC system, which led to detection problems at low concentrations and leaching for a long time when a high concentration is loaded.

After loading 1000 pmol/µL SN peptides into the system, all parts on the fluidic channel were replaced one after another, and run water inject to locate the position where the SNs bind. The parts were replaced sequentially, from the spray tip to the sample loop. Eventually, the only parts that bound the SN were the rotor and the stator on the 6-port valve of the auto-injector. The rotor is made from Vespel® (a polyimide-based plastic from DuPont) and the stator is made from stainless steel with Vespel® coating (Figure 9.5). There is no other material in the rotor that is made from Vespel and an in-house machined rotor I constructed from polyetheretherketone (PEEK) can not match the system. In the end, the Vespel coating on the stator was polished off and the rotor was left in place. This did not solve the issue completely but improved it dramatically.

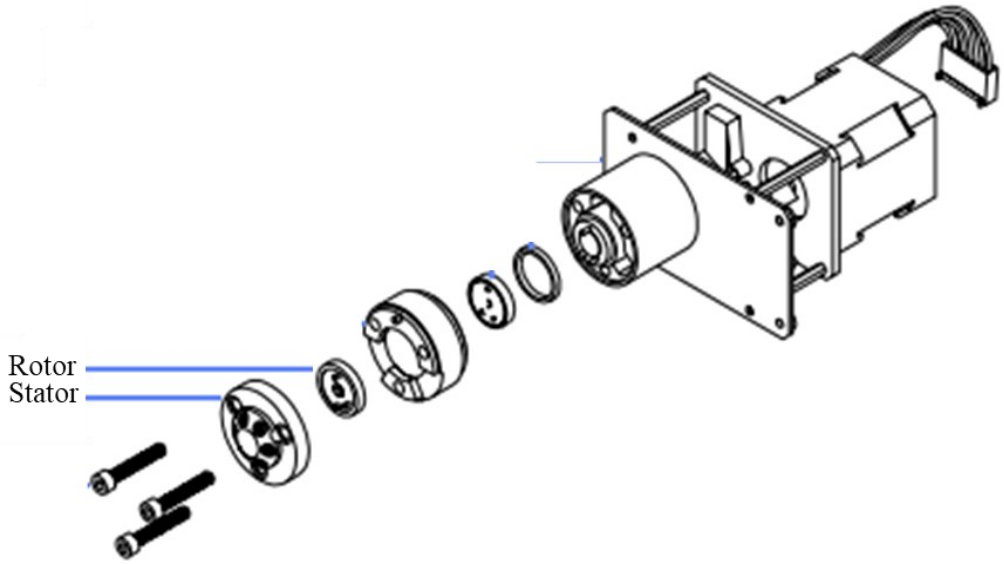

Figure 9-5 The assembling diagram represents the mechanism of the microinjection valve assembly. This diagram is modified from the Agilent manual Edition 08/2002 Figure 21. The rotor and stator that bind to SNs are highlighted in the diagram.

Another method to improve the issue is introducing a foreign matrix. Trypsin digested BSA was added to all samples at 1μg/μL as a foreign matrix [199]. This foreign matrix, working with the polished stator, made the dilution and carryover issue manageable. On the other hand, these two methods also decrease the lifetime of the trap column (replaced every 100 injections) and the pressure rating of the whole system (from 400 bar to 340 bar).

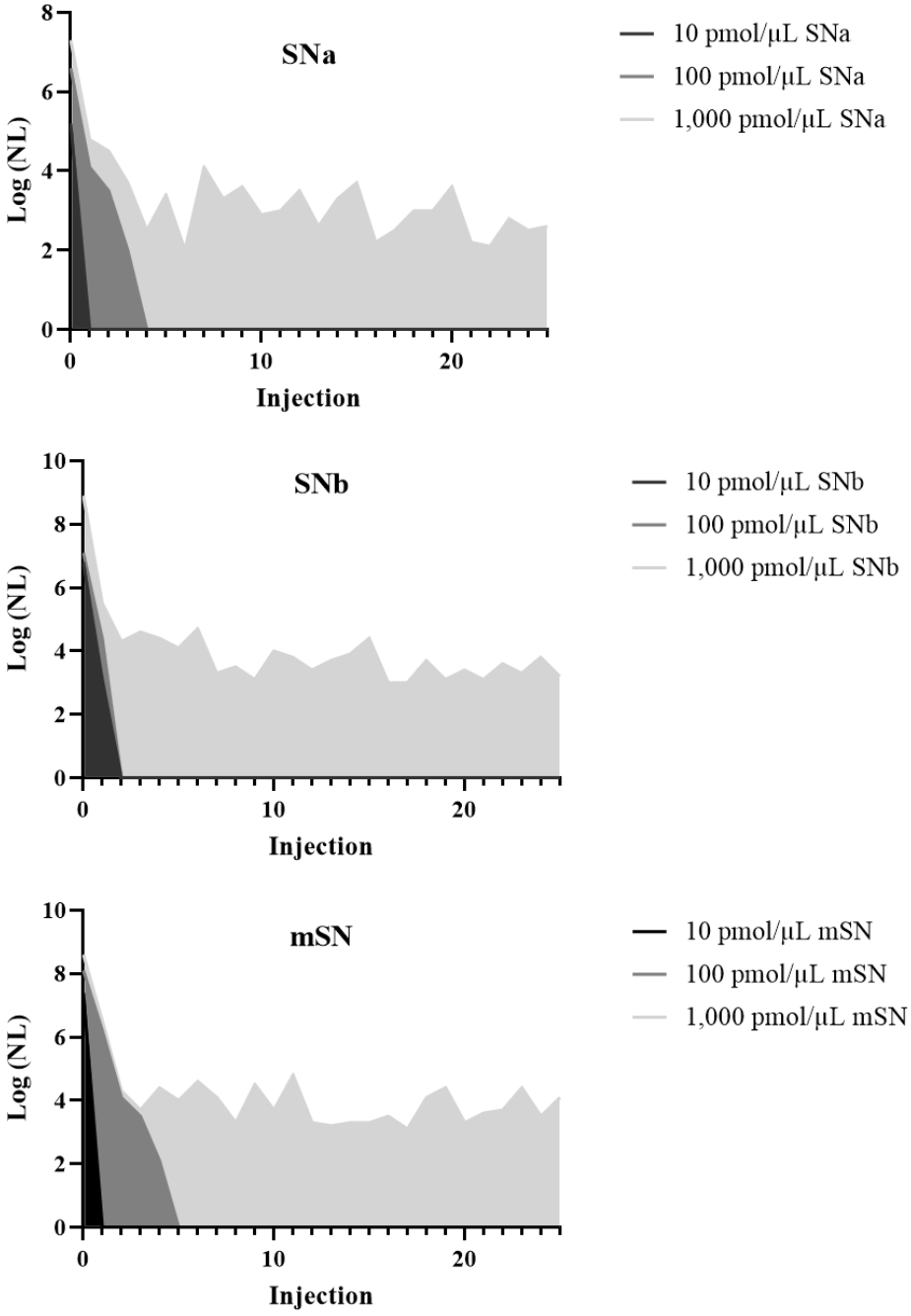

Figure 9-6 SNs carry over on water injections after different concentrations of SNs loaded into LC-MS/MS equipment. Charts are plotted by the logarithm number of HPLC peak intensity against injection times (N=1). SNa represents secretoneurin A in zebrafish. SNb represents secretoneurin B in zebrafish. mSN represents mouse secretoneurin.

The addition of foreign matrix and stator polishing together significantly improved the quantification limit and accuracy. Figures 9.7-9.12 represent the chromatograms and mass spectra of the various SNs when 1 µL serial dilution of purified SN samples are loaded with the polished stator and digested BSA as sampling solvent. The chromatograms were plotted on 20 ppm mass tolerance by MS1 base peak recorded from FTMS. NL is normalized according to the strongest mass intensity. Each data point was plotted by a vertical line. The mass spectra were plotted by averaging the total ions from the FTMS MS1 within 0.1 min on each side of the chromatogram peak top.

As shown in Figure 9.7, the chromatographic peak height of SNa decreased slowly between 25 pmol/ µL and 1.56 pmol/uL. The chromatographic peak height decreased 8 times when the sample concentration decreased 16 times. In the meantime, the average intensity of the most intense SNa ion decreases four times (Figure 9.8). When the SNa concentration was below 1.56 pmol/uL, every 2-fold dilution caused a 3-fold decrement in chromatogram peak height. The SNa MS peaks were absent on the averaged mass spectrum when the concentration was lower than 1.56 pmol/uL. In practical terms, this means the SNa signals were not consistent and got subtracted as background.

As shown in Figure 9.9. the chromatographic peak height of SNb decreased evenly between 25 pmol/µL and 0.78 pmol/µL. The chromatographic peak height decreased 100 times when the sample concentration decreased 32 times. In Figure 9.10, the average intensity of the most intense SNb ion decreased 10 times when the sample concentration decreased 8 times from 25 pmol/µL to 3.1 pmol/µL. When the SNb concentration was reduced from 3.1 pmol/µL to 1.6 pmol/µL, the most intense SNb ion signal decreased 25 times. This decay on signal strength goes up to 39 times when the concentration of SNb decreased from 1.6 pmol/µL to 1.8 pmol/µL. Even though the absolute intensity of 1152.9 m/z ions for SNb is 4.09×10^3 for a concentration of 0.781 pmol/µL, it vanishes with another 2-fold dilution.

Regarding mSN, (Figure 9.11, 9.12) both chromatographic peak intensity and average mass peak intensity decreased quickly when the sample was diluted from 6 pmol/µL to 0.75 pmol/µL. They also vanished together when the concentration was lower than 0.75 pmol/µL.

Modifying the part made of Vespel and using digested BSA as a foreign matrix improved the SN non-specific binding issue, however, the issue still affected SN quantifications. The actual SNs measured were between 1-10 pmol/uL. Therefore, when plotting the standard curve in the 1-10 pmol/μL range, the point-to-point curve method is used. There is no fitting that can comprehensively demonstrate the trend.

The strong matrix effects of SNs in HPLC experiments have not been reported previously. The non-specific binding of other peptides and plastic surfaces has been reported multiple times [200-202]. The recovery of low abundance peptides from plastic containers has been difficult for researchers for a long time. A common method to increase the recovery rate is to add detergent and BSA. However, in this LC-MS/MS experiment, detergent and BSA are not applicable. Using digested BSA as an additive is not a perfect solution. It still needs to improve, but it is the most ideal method I could achieve within a limited time. The troubleshooting and machine modifications reported took over 8 months.

Another promising additive to solve the SN matrix effect issue could be the addition of different SN peptide analogs. A shorter piece of SN peptide as an additive could potentially displace the SN-plastic binding more efficiently. In a previous study, the 15 C-terminal amino acids of SN could effectively displace the specific binding of SN peptides to the human monocytic cell line [203]. The displacement effect of this SN fragment in the HPLC system is still pending. Other fragments may have a better effect to neutralize the matrix effects of SNs in the LC-MS/MS experiment. This can lead to a promising project for a better SN quantification method.

Chromatograms of SNa Serial Dilution

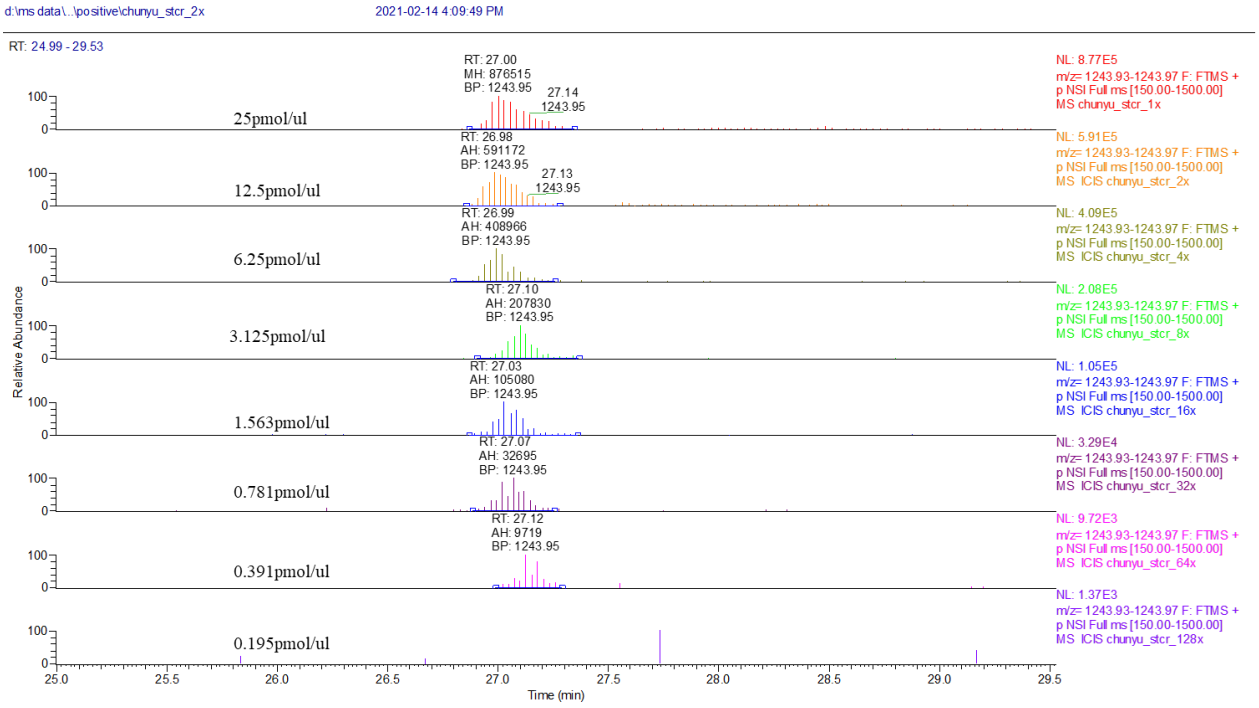

Figure 9-7 Chromatograms of SNa serial dilutions from 25 pmol/µL to 0.195 pmol/µL. Each vertical line in the chromatogram represents the MS signal strength on 1243.93-1243.97 m/z. RT represents retention time, MH represents manual integration peak height, AH represents automatic integration peak height, and BP represents the base peak.

Mass Spectra of SNa serial dilution

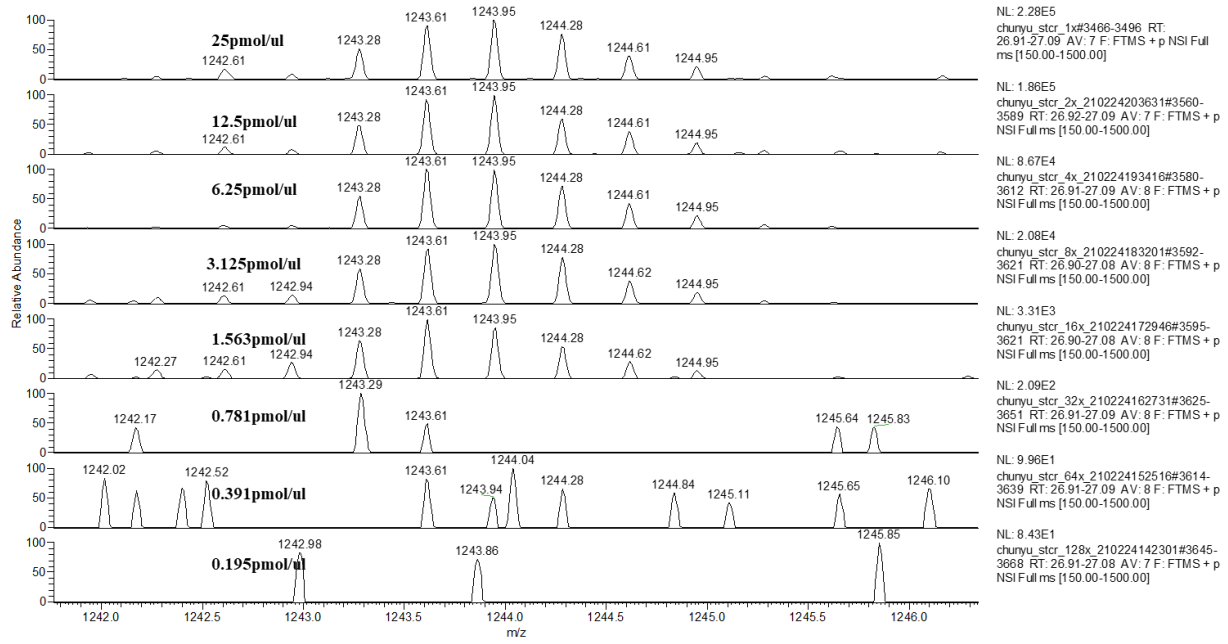

Figure 9-8 Mass spectra of SNa serial dilution from 25 pmol/μL to 0.195 pmol/μL. Mass spectra were the averages of spectrums between retention time between 26.9-27.1 min

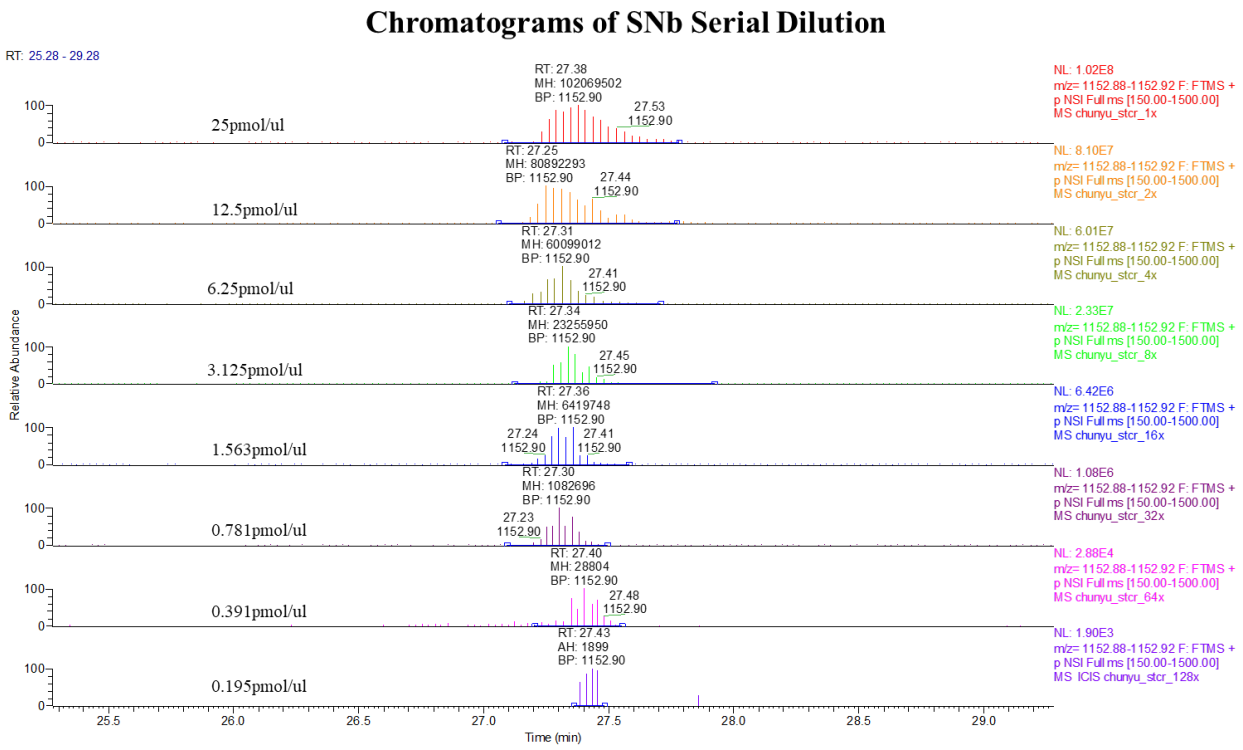

Figure 9-9 Chromatograms of SNb serial dilutions from 25 pmol/µL to 0.195 pmol/µL. Each vertical line in the chromatogram represents the MS signal strength on 1152.88-1152.93 m/z. RT represents retention time, MH represents manual integration peak height, AH represents automatic integration peak height, and BP represents the base peak.

Mass spectra of SNb serial dilution

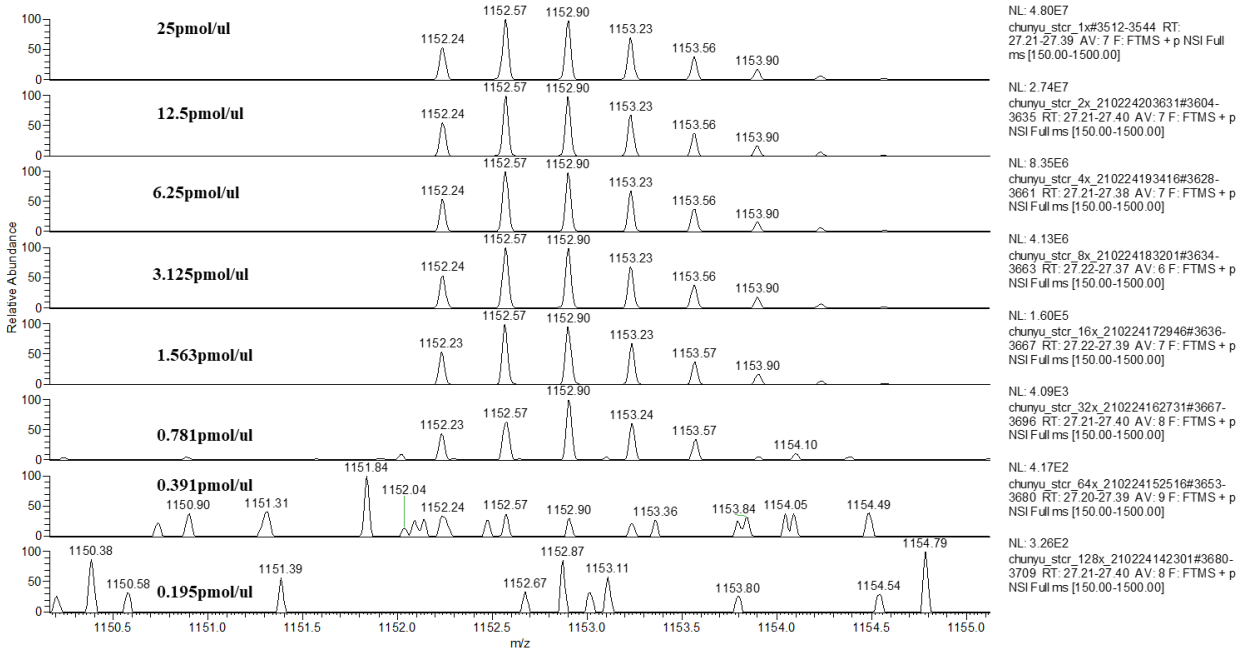

Figure 9-10 Mass spectra of SNb serial dilution from 25 pmol/µL to 0.195 pmol/µL. Mass spectra were the averages of spectrums between retention time between 27.2-27.4 min.

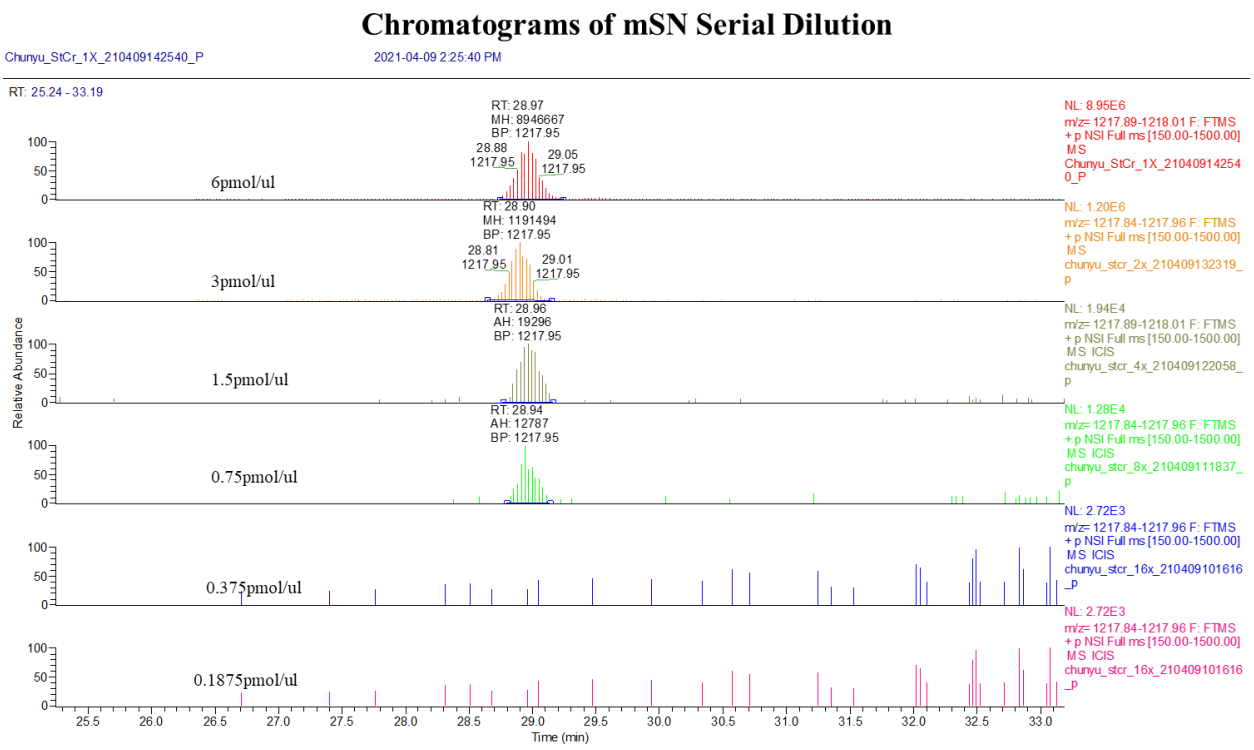

Figure 9-11 Chromatograms of mSN serial dilutions from 25 pmol/µL to 0.195 pmol/µL. Each vertical line in the chromatogram represents the MS signal strength on 1217.89-1218.01 m/z. RT represents retention time, MH represents manual integration peak height, AH represents automatic integration peak height, and BP represents the base peak.

Mass spectra of mSN serial dilutions

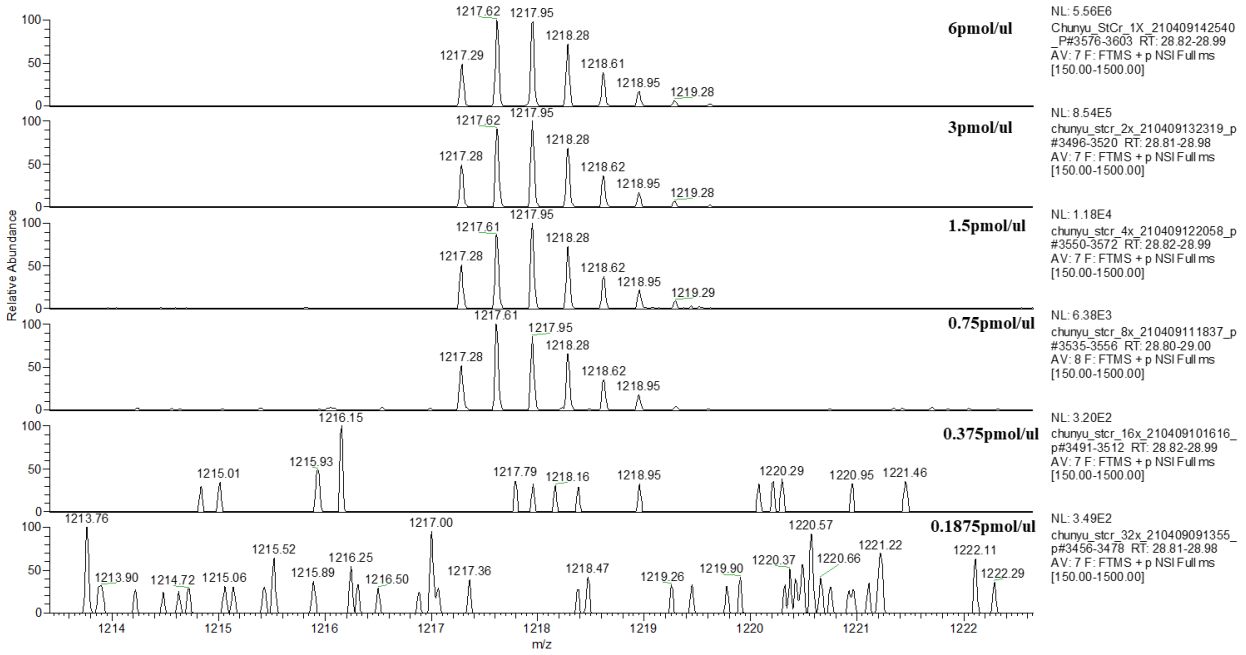

Figure 9-12 Mass spectra for mSN serial dilution from 25 pmol/µL to 0.195 pmol/µL. Mass spectra were the averages of spectrums between retention time between 28.8-26 min.

Chapter X Appendix IV SPE

SPE Standard operation procedure (SOP)

Packing an SPE plate

1. Measure 1 g of sorbent, and place in 20 ml flat bottom glass flask with a magnetic stir bar in.
2. Add 10 ml of HPLC grade acetonitrile and agitate with magnetic mixing to generate an evenly distributed slurry.
3. Place a filtered well plate on the waste collection tray.
4. Aliquot 100 µL of the slurry in each well of the filtered well plate by 100 µL or 200 µL pipettor with the flask agitation on.

The slurry leftover can be stored in the flask with airtight cap at room temperature. The stir bar can remain in the flask with to agitation. When packing another SPE plate, sorbent and acetonitrile can be added to the flask by the same ratio. It is not necessary to empty or clean the flask in between of two experiments. The SPE plate can be packed on an independent day to the actual extraction experiment. The plate can be stored at room temperature with an aluminum foil cover to prevent dust.

Extraction

Pre-condition swing bucket centrifuge to 4 ºC.

Prepare equilibrium buffer (0.2% formic acid, 5% acetonitrile, 95% water); activation buffer (0.2% formic acid, 50% acetonitrile, 50% water); and elution buffer (0.2% formic, 75% acetonitrile, 25% water). If the plate is to be regenerated and reused, prepare regeneration buffer (0.2% formic acid, 95% MeOH, 5% water).

Resuspend each lyophilized sample in a 200 µL equilibrium buffer. Keep samples on ice.

1. Place the SPE plate on top of the waste tray.
2. Add 200 µL activation buffer to each SPE well.
3. Centrifuge on 500 rcf for 1 min.
4. Empty waste tray
5. Proceed with steps 1-4 for 4 times.

Activation

6. Place the SPE plate on top of the waste tray.
7. Add 200 µL equilibrium buffer to each SPE well.
8. Centrifuge on 1000 rcf for 1 min.
9. Empty waste tray
10. Proceed with steps 6-9 for 4 times.

Equilibrium

11. Place the SPE plate on top of the waste tray.
12. Load each sample in each well of the SPE plate.
13. Centrifuge on 1000 rcf for 1 min.
14. Empty waste tray
15. Proceed with steps 6-9 for 5 times.

Loading

16. Place SPE plate on top of HPLC sampler plate.
17. Add 20 µL elution buffer to each SPE well.
18. Centrifuge on 500 rcf for 1 min.
19. Proceed with steps 17-18 for 5 times with the same collection plate.

Elution

20. Evaporate the solvent from the sampler plate with a swing bucket centrifuge connected to lyophilizer.
21. Seal lyophilized plate and store at -20 ºC for LC-MS/MS analysis
22. Place the SPE plate on top of the waste tray.
23. Add 200 µL regeneration buffer to each SPE well.
24. Centrifuge on 500 rcf for 1 min.
25. Empty waste tray
26. Proceed with steps 21-24 for 4 times.

Regeneration (Optional)

Chapter XI Appendix V Other contributions

I have made other important contributions to Ph.D. projects in the lab. They are listed below.

- *Vera-Chang, M. N., A. D. St-Jacques, R. Gagné, C. J. Martyniuk, C. L. Yauk, T. W. Moon and V. L. Trudeau (2018). "Transgenerational hypocortisolism and behavioral disruption are induced by the antidepressant fluoxetine in male zebrafish Danio rerio." Proceedings of the National Academy of Sciences 115(52): E12435.*
  I confirmed standard solutions of fluoxetine using MS. I was not included as a co-author because this was a late addition to the manuscript in response to a review comment. I am, however, acknowledged for this contribution.

- *Vera-Chang, M. N., A. D. St-Jacques, **C. Lu**, T. W. Moon and V. L. Trudeau (2019). "Fluoxetine Exposure During Sexual Development Disrupts the Stress Axis and Results in Sex- and Time- Dependent Effects on the Exploratory Behavior in Adult Zebrafish Danio rerio." Frontiers in Neuroscience 13: 1015.*

  I confirmed standard solutions of fluoxetine using LC-MS/MS.

- *Mitchell, K., M. Mikwar, D. Da Fonte, **C. Lu**, B. Tao, D. Peng, W. Erandani, W. Hu and V. L. Trudeau (2020). "Secretoneurin is a secretogranin-2 derived hormonal peptide in vertebrate neuroendocrine systems." Gen Comp Endocrinol 299: 113588.*

  This is a review paper from our laboratory on secretoneurin.

- *Mitchell, K., W. S. Zhang, **C. Lu**, B. Tao, L. Chen, W. Hu and V. L. Trudeau (2020). "Targeted mutation of secretogranin-2 disrupts sexual behavior and reproduction in zebrafish." Proceedings of the National Academy of Sciences 117(23): 12772.*

  This is where I first synthesized SN that was used for in vivo bioactivity studies.

- *Nozari, A., R. Gagné, **C. Lu**, C. Yauk and V. L. Trudeau (2022). "Brief Developmental Exposure to Fluoxetine Causes Life-Long Alteration of the Brain Transcriptome in Zebrafish." Frontiers in Endocrinology 13; DOI=10.3389/fendo.2022.847322.*

  I confirmed standard solutions of fluoxetine using LC-MS/MS.

References

1. Fischer-Colbrie, R., A. Laslop, and R. Kirchmair, *Secretogranin II: molecular properties, regulation of biosynthesis and processing to the neuropeptide secretoneurin.* Prog Neurobiol, 1995. **46**(1): p. 49-70.
2. Zhao, E., A. Basak, and V.L. Trudeau, *Secretoneurin stimulates goldfish pituitary luteinizing hormone production.* Neuropeptides, 2006. **40**(4): p. 275-82.
3. Zhao, E., et al., *The secretogranin II-derived peptide secretoneurin stimulates luteinizing hormone secretion from gonadotrophs.* Endocrinology, 2009. **150**(5): p. 2273-82.
4. Zhao, E., et al., *Secretoneurin stimulates the production and release of luteinizing hormone in mouse L{beta}T2 gonadotropin cells.* Am J Physiol Endocrinol Metab, 2011. **301**(2): p. E288-97.
5. Marksteiner, J., et al., *Distribution of secretoneurin, a peptide derived from secretogranin II, in rat brain: an immunocytochemical and radioimmunological study.* Neuroscience, 1993. **54**(4): p. 923-44.
6. Fischer-Colbrie, R., et al., *Secretoneurin: a new player in angiogenesis and chemotaxis linking nerves, blood vessels and the immune system.* Curr Protein Pept Sci, 2005. **6**(4): p. 373-85.
7. Gasser, M.C., et al., *Secretoneurin promotes pertussis toxin-sensitive neurite outgrowth in cerebellar granule cells.* J Neurochem, 2003. **85**(3): p. 662-9.
8. Mitchell, K., et al., *Secretoneurin is a secretogranin-2 derived hormonal peptide in vertebrate neuroendocrine systems.* Gen Comp Endocrinol, 2020. **299**: p. 113588.
9. Mitchell, K., et al., *Targeted mutation of secretogranin-2 disrupts sexual behavior and reproduction in zebrafish.* Proceedings of the National Academy of Sciences, 2020. **117**(23): p. 12772.
10. Kirchmair, R., et al., *Secretoneurin--a neuropeptide generated in brain, adrenal medulla and other endocrine tissues by proteolytic processing of secretogranin II (chromogranin C).* Neuroscience, 1993. **53**(2): p. 359-65.
11. DeAtley, K.L., et al., *Neuropeptidome of the Hypothalamus and Pituitary Gland of Indicine × Taurine Heifers: Evidence of Differential Neuropeptide Processing in the Pituitary Gland before and after Puberty.* Journal of Proteome Research, 2018. **17**(5): p. 1852-1865.
12. Che, F.Y., et al., *Peptidomics of Cpe fat/fat mouse hypothalamus: effect of food deprivation and exercise on peptide levels.* J Biol Chem, 2005. **280**(6): p. 4451-61.
13. Trudeau, V.L., et al., *Is secretoneurin a new hormone?* Gen Comp Endocrinol, 2012. **175**(1): p. 10-8.
14. Van Camp, K.A., et al., *Peptidomics of the zebrafish Danio rerio: In search for neuropeptides.* Journal of Proteomics, 2017. **150**: p. 290-296.
15. Sion, B., et al., *Peptides co-released with luteinizing hormone by perifused pituitary cell aggregates.* Mol Cell Endocrinol, 1988. **60**(2-3): p. 151-61.
16. Chiu, I.M., C.A. von Hehn, and C.J. Woolf, *Neurogenic Inflammation – The Peripheral Nervous System's Role in Host Defense and Immunopathology.* Nature neuroscience, 2012. **15**(8): p. 1063-1067.
17. Shi, C. and E.G. Pamer, *Monocyte recruitment during infection and inflammation.* Nat Rev Immunol, 2011. **11**(11): p. 762-774.

18. Reinisch, N., et al., *Attraction of human monocytes by the neuropeptide secretoneurin.* FEBS Letters, 1993. **334**(1): p. 41-44.
19. Kahler, C.M., et al., *The neuropeptide secretoneurin stimulates adhesion of human monocytes to arterial and venous endothelial cells in vitro.* Regul Pept, 2002. **110**(1): p. 65-73.
20. Brynildsen, J., et al., *Circulating secretoneurin concentrations in patients with moderate to severe aortic stenosis.* Clin Biochem, 2019. **71**: p. 17-23.
21. Røsjø, H., et al., *Prognostic Value of Secretoneurin in Patients With Severe Sepsis and Septic Shock: Data From the Albumin Italian Outcome Sepsis Study.* Crit Care Med, 2018. **46**(5): p. e404-e410.
22. Xu, R., et al., *Secretoneurin Induces Airway Mucus Hypersecretion by Enhancing the Binding of EGF to NRP1.* Cellular Physiology and Biochemistry, 2014. **33**(2): p. 446-456.
23. Hasslacher, J., et al., *Secretoneurin as a marker for hypoxic brain injury after cardiopulmonary resuscitation.* Intensive Care Med, 2014. **40**(10): p. 1518-27.
24. Blanchard, T.L., et al., *Chapter 2 - Reproductive Physiology of the Nonpregnant Mare*, in *Manual of Equine Reproduction (Second Edition)*, T.L. Blanchard, et al., Editors. 2003, Mosby: Saint Louis. p. 9-15.
25. Vadakkadath Meethal, S. and C.S. Atwood, *The role of hypothalamic-pituitary-gonadal hormones in the normal structure and functioning of the brain.* Cell Mol Life Sci, 2005. **62**(3): p. 257-70.
26. Trudeau, V.L., *Neuroendocrine Control of Reproduction in Teleost Fish: Concepts and Controversies.* Annual Review of Animal Biosciences, 2022. **10**(1): p. null.
27. Wun, W.S. and I.H. Thorneycroft, *Estradiol positive feedback on the rat anterior pituitary gland in vitro.* Mol Cell Endocrinol, 1987. **54**(2-3): p. 165-9.
28. Caligioni, C.S., *Assessing reproductive status/stages in mice.* Curr Protoc Neurosci, 2009. **Appendix 4**: p. Appendix 4I.
29. Mikhael, S., A. Punjala-Patel, and L. Gavrilova-Jordan, *Hypothalamic-Pituitary-Ovarian Axis Disorders Impacting Female Fertility.* Biomedicines, 2019. **7**(1).
30. Thompson, I.R. and U.B. Kaiser, *GnRH pulse frequency-dependent differential regulation of LH and FSH gene expression.* Mol Cell Endocrinol, 2014. **385**(1-2): p. 28-35.
31. BUTCHER, R.L., W.E. COLLINS, and N.W. FUGO, *Plasma Concentration of LH, FSH, Prolactin, Progesterone and Estradiol-17β Throughout the 4-Day Estrous Cycle of the Rat.* Endocrinology, 1974. **94**(6): p. 1704-1708.
32. McQuillan, H.J., et al., *GnRH Pulse Generator Activity Across the Estrous Cycle of Female Mice.* Endocrinology, 2019. **160**(6): p. 1480-1491.
33. Czieselsky, K., et al., *Pulse and Surge Profiles of Luteinizing Hormone Secretion in the Mouse.* Endocrinology, 2016. **157**(12): p. 4794-4802.
34. Nielsen, S.E. and A.Y. Herrera, *1.14 - Sex Steroids, Learning and Memory*, in *Hormones, Brain and Behavior (Third Edition)*, D.W. Pfaff and M. Joëls, Editors. 2017, Academic Press: Oxford. p. 399-422.
35. Blazquez, M., et al., *Gamma-aminobutyric acid up-regulates the expression of a novel secretogranin-II messenger ribonucleic acid in the goldfish pituitary.* Endocrinology, 1998. **139**(12): p. 4870-80.
36. Da Fonte, D.F., et al., *Secretoneurin A Directly Regulates the Proteome of Goldfish Radial Glial Cells In Vitro.* Frontiers in Endocrinology, 2018. **9**(68).
37. Da Fonte, D.F., et al., *Secretoneurin A regulates neurogenic and inflammatory transcriptional networks in goldfish (Carassius auratus) radial glia.* Scientific Reports, 2017. **7**(1): p. 14930.

38. Aydin, S., *A short history, principles, and types of ELISA, and our laboratory experience with peptide/protein analyses using ELISA.* Peptides, 2015. **72**: p. 4-15.
39. Konstantinou, G.N., *Enzyme-Linked Immunosorbent Assay (ELISA).* Methods Mol Biol, 2017. **1592**: p. 79-94.
40. Shah, K. and P. Maghsoudlou, *Enzyme-linked immunosorbent assay (ELISA): the basics.* Br J Hosp Med (Lond), 2016. **77**(7): p. C98-101.
41. Stoob, K., et al., *Fully automated online solid phase extraction coupled directly to liquid chromatography–tandem mass spectrometry: Quantification of sulfonamide antibiotics, neutral and acidic pesticides at low concentrations in surface waters.* Journal of Chromatography A, 2005. **1097**(1): p. 138-147.
42. Koal, T., et al., *Standardized LC-MS/MS based steroid hormone profile-analysis.* J Steroid Biochem Mol Biol, 2012. **129**(3-5): p. 129-38.
43. Che, F.Y., et al., *Optimization of neuropeptide extraction from the mouse hypothalamus.* J Proteome Res, 2007. **6**(12): p. 4667-76.
44. Agneter, E., et al., *Sustained dopamine release induced by secretoneurin in the striatum of the rat: a microdialysis study.* J Neurochem, 1995. **65**(2): p. 622-5.
45. Chen, W., et al., *Optimization of a peptide extraction and LC-MS protocol for quantitative analysis of antimicrobial peptides.* Future science OA, 2018. **5**(1): p. FSO348-FSO348.
46. Taves, M.D., et al., *Steroid concentrations in plasma, whole blood and brain: effects of saline perfusion to remove blood contamination from brain.* PLoS One, 2010. **5**(12): p. e15727.
47. Taves, M.D., et al., *Measurement of steroid concentrations in brain tissue: methodological considerations.* Front Endocrinol (Lausanne), 2011. **2**: p. 39.
48. Makin, H.L.J., et al., *General Methods for the Extraction, Purification, and Measurement of Steroids by Chromatography and Mass Spectrometry*, in *Steroid Analysis*, H.L.J. Makin and D.B. Gower, Editors. 2010, Springer Netherlands: Dordrecht. p. 163-282.
49. Andrade-Eiroa, A., et al., *Solid-phase extraction of organic compounds: A critical review (Part I).* TrAC Trends in Analytical Chemistry, 2016. **80**: p. 641-654.
50. Poole, C.F., *New trends in solid-phase extraction.* TrAC Trends in Analytical Chemistry, 2003. **22**(6): p. 362-373.
51. Hennion, M.C., *Solid-phase extraction: method development, sorbents, and coupling with liquid chromatography.* J Chromatogr A, 1999. **856**(1-2): p. 3-54.
52. Taylor, D.R., et al., *A 13-Steroid Serum Panel Based on LC-MS/MS: Use in Detection of Adrenocortical Carcinoma.* Clin Chem, 2017. **63**(12): p. 1836-1846.
53. Thomas, A., et al., *Mass spectrometric determination of gonadotrophin-releasing hormone (GnRH) in human urine for doping control purposes by means of LC-ESI-MS/MS.* J Mass Spectrom, 2008. **43**(7): p. 908-15.
54. Starvin, A.M. *OFFLINE AND ONLINE SOLID PHASE EXTRACTION/PRECONCENTRATION OF INORGANICS*. 2005.
55. Archana, G., R. Dhodapkar, and A. Kumar, *Offline solid-phase extraction for preconcentration of pharmaceuticals and personal care products in environmental water and their simultaneous determination using the reversed phase high-performance liquid chromatography method.* Environ Monit Assess, 2016. **188**(9): p. 512.
56. Vocat, C., et al., *Quantification of Neuropeptide Y and Four of Its Metabolites in Human Plasma by Micro-UHPLC-MS/MS.* Anal Chem, 2020. **92**(1): p. 859-866.

57. Hiller-Sturmhöfel, S. and A. Bartke, *The endocrine system: an overview.* Alcohol Health Res World, 1998. **22**(3): p. 153-64.
58. Hoar, W.S., *COMPARATIVE PHYSIOLOGY: HORMONES AND REPRODUCTION IN FISHES.* Annu Rev Physiol, 1965. **27**: p. 51-70.
59. Denver, N., et al., *Current strategies for quantification of estrogens in clinical research.* The Journal of steroid biochemistry and molecular biology, 2019. **192**: p. 105373-105373.
60. Taylor, A.E., B. Keevil, and I.T. Huhtaniemi, *Mass spectrometry and immunoassay: how to measure steroid hormones today and tomorrow.* Eur J Endocrinol, 2015. **173**(2): p. D1-12.
61. Nouri, M.-Z., et al., *Quantification of steroid hormones in low volume plasma and tissue homogenates of fish using LC-MS/MS.* General and Comparative Endocrinology, 2020. **296**: p. 113543.
62. Searle, B.C., et al., *Chromatogram libraries improve peptide detection and quantification by data independent acquisition mass spectrometry.* Nature Communications, 2018. **9**(1): p. 5128.
63. Song, E., S. Pyreddy, and Y. Mechref, *Quantification of glycopeptides by multiple reaction monitoring liquid chromatography/tandem mass spectrometry.* Rapid communications in mass spectrometry : RCM, 2012. **26**(17): p. 1941-1954.
64. Anderson, M.E., *Will Secretoneurin Be the Next Big Thing?⁎.* Journal of the American College of Cardiology, 2015. **65**(4): p. 352-354.
65. Clevett, K.J., *High-performance liquid chromatography.* Bioprocess Technol, 1990. **6**: p. 47-73.
66. Sahu, P.K., et al., *An overview of experimental designs in HPLC method development and validation.* J Pharm Biomed Anal, 2018. **147**: p. 590-611.
67. Karger, B.L., *HPLC: Early and Recent Perspectives.* Journal of Chemical Education, 1997. **74**(1): p. 45.
68. *A Review of: HPLC Columns, Theory, Technology, and Practice.* Journal of Liquid Chromatography & Related Technologies, 1998. **21**(6): p. 910-912.
69. Baeza-Baeza, J.J. and M.C. García-Álvarez-Coque, *A theoretical plate model accounting for slow kinetics in chromatographic elution.* J Chromatogr A, 2011. **1218**(31): p. 5166-74.
70. *Chapter 11 - Process Design*, in *Lees' Loss Prevention in the Process Industries (Fourth Edition)*, S. Mannan, Editor. 2012, Butterworth-Heinemann: Oxford. p. 443-508.
71. Towler, G. and R. Sinnott, *Chemical Engineering Design: Principles, Practice and Economics of Plant and Process Design*. 2007: Elsevier Science.
72. Don, W.G. and H.P. Robert, *Perry's Chemical Engineers' Handbook, Eighth Edition*. 8th / ed. 2008, New York: McGraw-Hill Education.
73. Martin, A.J. and R.L. Synge, *A new form of chromatogram employing two liquid phases: A theory of chromatography. 2. Application to the micro-determination of the higher monoamino-acids in proteins.* The Biochemical journal, 1941. **35**(12): p. 1358-1368.
74. Wilson, S.R., et al., *Nano-LC in proteomics: recent advances and approaches.* Bioanalysis, 2015. **7**(14): p. 1799-815.
75. Gargano, A.F.G., et al., *Reducing Dilution and Analysis Time in Online Comprehensive Two-Dimensional Liquid Chromatography by Active Modulation.* Analytical Chemistry, 2016. **88**(3): p. 1785-1793.
76. Pedro, R.C., *Principles of Nanoflow Liquid Chromatography and Applications to Proteomics.* Current Nanoscience, 2005. **1**(1): p. 65-71.
77. Gama, M.R., C.H. Collins, and C.B.G. Bottoli, *Nano-Liquid Chromatography in Pharmaceutical and Biomedical Research.* Journal of Chromatographic Science, 2013. **51**(7): p. 694-703.

78. Szumski, M. and B. Buszewski, *State of the Art in Miniaturized Separation Techniques.* Critical Reviews in Analytical Chemistry, 2002. **32**(1): p. 1-46.
79. Wilson, S.R., C. Olsen, and E. Lundanes, *Nano liquid chromatography columns.* Analyst, 2019. **144**(24): p. 7090-7104.
80. Taylor, P., et al., *Automated 2D Peptide Separation on a 1D Nano-LC-MS System.* Journal of Proteome Research, 2009. **8**(3): p. 1610-1616.
81. Gunnarson, C., et al., *Implications of dispersion in connecting capillaries for separation systems involving post-column flow splitting.* J Chromatogr A, 2021. **1639**: p. 461893.
82. Chan, K.C., et al., *Analysis of the human serum proteome.* Clinical Proteomics, 2004. **1**(2): p. 101-225.
83. Nägele, E., et al., *2D-LC/MS techniques for the identification of proteins in highly complex mixtures.* Expert Rev Proteomics, 2004. **1**(1): p. 37-46.
84. Gevaert, K., et al., *Chromatographic Isolation of Methionine-containing Peptides for Gel-free Proteome Analysis: Identification Of More Than 800 Escherichia Coli Proteins * S.* Molecular & Cellular Proteomics, 2002. **1**(11): p. 896-903.
85. Collado-Romero, M., et al., *Quantitative proteomics and bioinformatic analysis provide new insight into the dynamic response of porcine intestine to Salmonella Typhimurium.* Frontiers in Cellular and Infection Microbiology, 2015. **5**: p. 64.
86. Wang, H., et al., *Systematic optimization of long gradient chromatography mass spectrometry for deep analysis of brain proteome.* Journal of proteome research, 2015. **14**(2): p. 829-838.
87. Moruz, L., et al., *Optimized Nonlinear Gradients for Reversed-Phase Liquid Chromatography in Shotgun Proteomics.* Analytical Chemistry, 2013. **85**(16): p. 7777-7785.
88. Eberhard, U., et al., *Determination of the Effective Viscosity of Non-newtonian Fluids Flowing Through Porous Media.* Frontiers in Physics, 2019. **7**: p. 71.
89. Kon, T., et al., *Numerical Simulation of Dripping Behavior of Droplet in Packed Bed Using Particle Method.* ISIJ International, 2012. **52**: p. 1565-1573.
90. Grayson, M.A., *John Bennett Fenn: A Curious Road to the Prize.* Journal of The American Society for Mass Spectrometry, 2011. **22**(8): p. 1301-1308.
91. Griffiths, J., *A Brief History of Mass Spectrometry.* Analytical Chemistry, 2008. **80**(15): p. 5678-5683.
92. Wilm, M. and M. Mann, *Analytical Properties of the Nanoelectrospray Ion Source.* Analytical Chemistry, 1996. **68**(1): p. 1-8.
93. Liu, Q., et al., *Performance Comparisons of Nano-LC Systems, Electrospray Sources and LC–MS-MS Platforms.* Journal of Chromatographic Science, 2014. **52**(2): p. 120-127.
94. G Marshall, A., et al., *Mass resolution and mass accuracy: how much is enough?* Mass spectrometry (Tokyo, Japan), 2013. **2**(Spec Iss): p. S0009-S0009.
95. Todd, J.F.J., *Recommendations for nomenclature and symbolism for mass spectroscopy (including an appendix of terms used in vacuum technology). (Recommendations 1991).* Pure and Applied Chemistry, 1991. **63**(10): p. 1541-1566.
96. Brenton, A.G. and A.R. Godfrey, *Accurate Mass Measurement: Terminology and Treatment of Data.* Journal of the American Society for Mass Spectrometry, 2010. **21**(11): p. 1821-1835.
97. Olsen, J.V., et al., *Parts per Million Mass Accuracy on an Orbitrap Mass Spectrometer via Lock Mass Injection into a C-trap.* Molecular & Cellular Proteomics, 2005. **4**(12): p. 2010-2021.
98. Eng, J.K., et al., *A face in the crowd: recognizing peptides through database search.* Molecular & cellular proteomics : MCP, 2011. **10**(11): p. R111.009522-R111.009522.

99. Chernobrovkin, A.L., et al., *Selection of the peptide mass tolerance value for protein identification with peptide mass fingerprinting.* Russian Journal of Bioorganic Chemistry, 2011. **37**(1): p. 119-122.
100. Kalli, A., et al., *Evaluation and optimization of mass spectrometric settings during data-dependent acquisition mode: focus on LTQ-Orbitrap mass analyzers.* Journal of proteome research, 2013. **12**(7): p. 3071-3086.
101. Johnson, D., et al., *Optimization of data-dependent acquisition parameters for coupling high-speed separations with LC-MS/MS for protein identifications.* Journal of biomolecular techniques : JBT, 2013. **24**(2): p. 62-72.
102. Hashimoto, Y., et al., *Duty Cycle Enhancement of an Orthogonal Acceleration TOF Mass Spectrometer Using an Axially-Resonant Excitation Linear Ion Trap.* Journal of the American Society for Mass Spectrometry, 2006. **17**(12): p. 1669-1674.
103. Trujillo, E.A., et al., *Maximizing Tandem Mass Spectrometry Acquisition Rates for Shotgun Proteomics.* Analytical Chemistry, 2019. **91**(20): p. 12625-12629.
104. Guo, J. and T. Huan, *Comparison of Full-Scan, Data-Dependent, and Data-Independent Acquisition Modes in Liquid Chromatography–Mass Spectrometry Based Untargeted Metabolomics.* Analytical Chemistry, 2020. **92**(12): p. 8072-8080.
105. Gershon, D., *Mass spectrometry goes mainstream.* Nature, 2003. **424**(6948): p. 581-581.
106. Olsen, J.V., et al., *A dual pressure linear ion trap Orbitrap instrument with very high sequencing speed.* (1535-9484 (Electronic)).
107. Köcher, T., K. Swart R Fau - Mechtler, and K. Mechtler, *Ultra-high-pressure RPLC hyphenated to an LTQ-Orbitrap Velos reveals a linear relation between peak capacity and number of identified peptides.* (1520-6882 (Electronic)).
108. Merrifield, R.B., *Solid Phase Peptide Synthesis. I. The Synthesis of a Tetrapeptide.* Journal of the American Chemical Society, 1963. **85**(14): p. 2149-2154.
109. Merrifield, R.B., *Solid Phase Peptide Synthesis. II. The Synthesis of Bradykinin.* Journal of the American Chemical Society, 1964. **86**(2): p. 304-305.
110. Merrifield, R.B., *Solid-Phase Peptide Synthesis. III. An Improved Synthesis of Bradykinin*.* Biochemistry, 1964. **3**(9): p. 1385-1390.
111. Chan, W. and P. White, *Fmoc Solid Phase Peptide Synthesis: A Practical Approach*. Practical Approach Series. 2000: OUP Oxford.
112. Merrifield, B., *Solid phase synthesis.* Science, 1986. **232**(4748): p. 341-7.
113. Carpino, L.A. and G.Y. Han, *9-Fluorenylmethoxycarbonyl function, a new base-sensitive amino-protecting group.* Journal of the American Chemical Society, 1970. **92**(19): p. 5748-5749.
114. Carpino, L.A. and G.Y. Han, *9-Fluorenylmethoxycarbonyl amino-protecting group.* The Journal of Organic Chemistry, 1972. **37**(22): p. 3404-3409.
115. Albericio, F. and A. El-Faham, *Choosing the Right Coupling Reagent for Peptides: A Twenty-Five-Year Journey.* Organic Process Research & Development, 2018. **22**(7): p. 760-772.
116. Kent, S.B.H., *CHEMICAL SYNTHESIS OF PEPTIDES AND PROTEINS.* Annual Review of Biochemistry, 1988. **57**(1): p. 957-989.
117. Hudson, D., *Matrix Assisted Synthetic Transformations: A Mosaic of Diverse Contributions. I. The Pattern Emerges.* Journal of Combinatorial Chemistry, 1999. **1**(5): p. 333-360.
118. Bernatowicz, M.S., S.B. Daniels, and H. Köster, *A comparison of acid labile linkage agents for the synthesis of peptide C-terminal amides.* Tetrahedron Letters, 1989. **30**(35): p. 4645-4648.

119. Hauske, J.R. and P. Dorff, *A solid phase CBZ chloride equivalent — a new matrix specific linker.* Tetrahedron Letters, 1995. **36**(10): p. 1589-1592.
120. Athanassopoulos, P., et al., *Application of 2-chlorotrityl chloride in convergent peptide synthesis.* Tetrahedron Letters, 1995. **36**(31): p. 5645-5648.
121. Tam, J.P., et al., *Disulfide bond formation in peptides by dimethyl sulfoxide. Scope and applications.* Journal of the American Chemical Society, 1991. **113**(17): p. 6657-6662.
122. Calce, E., et al., *Air oxidation method employed for the disulfide bond formation of natural and synthetic peptides.* Amino Acids, 2015. **47**(8): p. 1507-15.
123. Sun, P.C., et al., *Improved Fmoc Solid-Phase Peptide Synthesis of Oxytocin with High Bioactivity.* Synlett, 2017. **28**(14): p. 1780-1784.
124. Kay, R.G., et al., *Peptidomic analysis of endogenous plasma peptides from patients with pancreatic neuroendocrine tumours.* Rapid Commun Mass Spectrom, 2018. **32**(16): p. 1414-1424.
125. Dallas, D.C., et al., *Current peptidomics: applications, purification, identification, quantification, and functional analysis.* Proteomics, 2015. **15**(5-6): p. 1026-1038.
126. Romanova, E.V. and J.V. Sweedler, *Peptidomics for the discovery and characterization of neuropeptides and hormones.* Trends in pharmacological sciences, 2015. **36**(9): p. 579-586.
127. Ottesen, A.H., et al., *Secretoneurin Is a Novel Prognostic Cardiovascular Biomarker Associated With Cardiomyocyte Calcium Handling.* Journal of the American College of Cardiology, 2015. **65**(4): p. 339-351.
128. Troger, J., et al., *Granin-derived peptides.* Prog Neurobiol, 2017. **154**: p. 37-61.
129. Fang, Y., D.P. Robinson, and L.J. Foster, *Quantitative Analysis of Proteome Coverage and Recovery Rates for Upstream Fractionation Methods in Proteomics.* Journal of Proteome Research, 2010. **9**(4): p. 1902-1912.
130. Mitulović, G., et al., *An improved method for tracking and reducing the void volume in nano HPLC-MS with micro trapping columns.* Analytical and bioanalytical chemistry, 2003. **376**: p. 946-51.
131. D'Orazio, G. and S. Fanali, *Pressurized nano-liquid–junction interface for coupling capillary electrochromatography and nano-liquid chromatography with mass spectrometry.* Journal of Chromatography A, 2013. **1317**: p. 67-76.
132. Franke, A.A., et al., *Oxytocin analysis from human serum, urine, and saliva by orbitrap liquid chromatography-mass spectrometry.* Drug Test Anal, 2019. **11**(1): p. 119-128.
133. Picotti, P., et al., *Full Dynamic Range Proteome Analysis of S. cerevisiae by Targeted Proteomics.* Cell, 2009. **138**(4): p. 795-806.
134. Raschke, T.M., J. Tsai, and M. Levitt, *Quantification of the hydrophobic interaction by simulations of the aggregation of small hydrophobic solutes in water.* Proceedings of the National Academy of Sciences of the United States of America, 2001. **98**(11): p. 5965-5969.
135. Wang, L., R.A. Friesner, and B.J. Berne, *Competition of electrostatic and hydrophobic interactions between small hydrophobes and model enclosures.* The journal of physical chemistry. B, 2010. **114**(21): p. 7294-7301.
136. Díez, A., A. Ortega, and J. Garcia de la Tore, *Brownian dynamics simulation of analytical ultracentrifugation experiments.* BMC biophysics, 2011. **4**: p. 6-6.
137. Erikson, D.W., et al., *LC-MS/MS measurement of endogenous oxytocin in the posterior pituitary and CSF of macaques: A pilot study.* Peptides, 2021. **140**: p. 170544.
138. Li, Y., et al., *UPLC-TOF-MS Method for Simultaneous Quantification of Steroid Hormones in Tissue Homogenates of Zebrafish with Solid-Phase Extraction.* Molecules, 2021. **26**(20).

139. Kimmerlin, T. and D. Seebach, *'100 years of peptide synthesis': ligation methods for peptide and protein synthesis with applications to beta-peptide assemblies.* J Pept Res, 2005. **65**(2): p. 229-60.
140. Hackenberger, C.P. and D. Schwarzer, *Chemoselective ligation and modification strategies for peptides and proteins.* Angew Chem Int Ed Engl, 2008. **47**(52): p. 10030-74.
141. Wilkins, M.R., et al., *Detailed peptide characterization using PEPTIDEMASS--a World-Wide-Web-accessible tool.* Electrophoresis, 1997. **18**(3-4): p. 403-8.
142. Fiametti, L.O., C.N. Correa, and L.M.d. Castro, *Peptide Profile of Zebrafish Brain in a 6-OHDA-Induced Parkinson Model.* Zebrafish, 2021. **18**(1): p. 55-65.
143. Teixeira, C.M.M., et al., *Characterization of Intracellular Peptides from Zebrafish (Danio rerio) Brain.* Zebrafish, 2019. **16**(3): p. 240-251.
144. Goodman, R.L., et al., *Neuroendocrine control of gonadotropin-releasing hormone: Pulsatile and surge modes of secretion.* J Neuroendocrinol, 2022: p. e13094.
145. Herbison, A.E., *The Gonadotropin-Releasing Hormone Pulse Generator.* Endocrinology, 2018. **159**(11): p. 3723-3736.
146. Muñoz-Cueto, J.A., et al., *The gonadotropin-releasing hormones: Lessons from fish.* Gen Comp Endocrinol, 2020. **291**: p. 113422.
147. Anderson, R.A. and R.P. Millar, *The roles of kisspeptin and neurokinin B in GnRH pulse generation in humans, and their potential clinical application.* J Neuroendocrinol, 2021: p. e13081.
148. Herbison, A.E., *A simple model of estrous cycle negative and positive feedback regulation of GnRH secretion.* Frontiers in Neuroendocrinology, 2020. **57**: p. 100837.
149. de Roux, N., et al., *Hypogonadotropic hypogonadism due to loss of function of the KiSS1-derived peptide receptor GPR54.* Proc Natl Acad Sci U S A, 2003. **100**(19): p. 10972-6.
150. Borrow, A.P. and N.M. Cameron, *The role of oxytocin in mating and pregnancy.* Horm Behav, 2012. **61**(3): p. 266-76.
151. Domínguez-Ordoñez, R., et al., *Oxytocin induces lordosis behavior in female rats through the prostaglandin E2/GnRH signaling system.* Horm Behav, 2021. **136**: p. 105081.
152. Caligioni, C.S., et al., *Presence of oxytocin receptors in the gonadotrophin-releasing hormone (GnRH) neurones in female rats: a possible direct action of oxytocin on GnRH neurones.* J Neuroendocrinol, 2007. **19**(6): p. 439-48.
153. Evans, J.J., *Peptides interact in gonadotrophin regulation.* Arch Physiol Biochem, 2002. **110**(1-2): p. 154-61.
154. Johnston, C.A., et al., *Physiologically important role for central oxytocin in the preovulatory release of luteinizing hormone.* Neurosci Lett, 1990. **120**(2): p. 256-8.
155. Selvage, D. and C.A. Johnston, *Central Stimulatory Influence of Oxytocin on Preovulatory Gonadotropin-Releasing Hormone Requires More than the Median Eminence.* Neuroendocrinology, 2001. **74**(2): p. 129-134.
156. Buijs, R.M., G. Hurtado-Alvarado, and E. Soto-Tinoco, *Vasopressin: An output signal from the suprachiasmatic nucleus to prepare physiology and behaviour for the resting phase.* J Neuroendocrinol, 2021. **33**(7): p. e12998.
157. Palm, I.F., et al., *The stimulatory effect of vasopressin on the luteinizing hormone surge in ovariectomized, estradiol-treated rats is time-dependent.* Brain Res, 2001. **901**(1-2): p. 109-16.
158. Jasoni, C.L., et al., *Expression of mRNAs encoding receptors that mediate stress signals in gonadotropin-releasing hormone neurons of the mouse.* Neuroendocrinology, 2005. **82**(5-6): p. 320-8.

159. Mahata, S.K., et al., *Concomitant changes of messenger ribonucleic acid levels of secretogranin II, VGF, vasopressin and oxytocin in the paraventricular nucleus of rats after adrenalectomy and during lactation.* J Neuroendocrinol, 1993. **5**(3): p. 323-30.
160. Mahata, S.K., et al., *In situ hybridization: mRNA levels of secretogranin II, neuropeptides and carboxypeptidase H in brains of salt-loaded and Brattleboro rats.* Neuroscience, 1992. **48**(3): p. 669-80.
161. Gonzalez, G., *Determining the Stage of the Estrous Cycle in Female Mice by Vaginal Smear.* Cold Spring Harb Protoc, 2016. **2016**(8).
162. Moore, D.S., W.I. Notz, and M.A. Fligner, *The Basic Practice of Statistics* 6th ed. 2013, New York: W.H. Freeman and Co.
163. Brooks, J., et al., *Cloning and sequencing of the sheep pituitary gonadotropin-releasing hormone receptor and changes in expression of its mRNA during the estrous cycle.* Mol Cell Endocrinol, 1993. **94**(2): p. R23-7.
164. Kang, S.K., et al., *Gonadotropin-releasing hormone activates mitogen-activated protein kinase in human ovarian and placental cells.* Mol Cell Endocrinol, 2000. **170**(1-2): p. 143-51.
165. Aiyer, M.S., G. Fink, and F. Greig, *Changes in the sensitivity of the pituitary gland to luteinizing hormone releasing factor during the oestrous cycle of the rat.* J Endocrinol, 1974. **60**(1): p. 47-64.
166. Wood, G.A., et al., *Circulating hormones and estrous stage predict cellular and stromal remodeling in murine uterus.* Reproduction, 2007. **133**(5): p. 1035-1044.
167. Sinchak, K., M.A. Mohr, and P.E. Micevych, *Hypothalamic Astrocyte Development and Physiology for Neuroprogesterone Induction of the Luteinizing Hormone Surge.* Frontiers in Endocrinology, 2020. **11**.
168. Kim, J., I.C. Bagchi, and M.K. Bagchi, *Control of ovulation in mice by progesterone receptor-regulated gene networks.* Molecular human reproduction, 2009. **15**(12): p. 821-828.
169. Naik, S.I., et al., *Evidence for a pituitary site of gonadal steroid stimulation of GnRH receptors in female mice.* Reproduction, 1985. **74**(2): p. 615-624.
170. Thackray, V.G., et al., *Progesterone Inhibits basal and gonadotropin-releasing hormone induction of luteinizing hormone beta-subunit gene expression.* Endocrinology, 2009. **150**(5): p. 2395-403.
171. McCarthy, M.M., *Estradiol and the developing brain.* Physiological reviews, 2008. **88**(1): p. 91-124.
172. *Inverse relationship between ovarian aromatase cytochrome P450 and 5 alpha-reductase enzyme activities and mRNA levels during the estrous cycle in the rat.* Journal of Steroid Biochemistry and Molecular Biology, 1992. **42**(5): p. 439-447.
173. Miller, B.H. and J.S. Takahashi, *Central circadian control of female reproductive function.* Frontiers in endocrinology, 2014. **4**: p. 195-195.
174. Terasawa, E. and B.P. Kenealy, *Neuroestrogen, rapid action of estradiol, and GnRH neurons.* Frontiers in neuroendocrinology, 2012. **33**(4): p. 364-375.
175. Miller, B.H., et al., *Vasopressin regulation of the proestrous luteinizing hormone surge in wild-type and Clock mutant mice.* Biol Reprod, 2006. **75**(5): p. 778-84.
176. Piet, R., et al., *Estrogen Permits Vasopressin Signaling in Preoptic Kisspeptin Neurons in the Female Mouse.* The Journal of Neuroscience, 2015. **35**(17): p. 6881.
177. Lee, J.E., et al., *Endogenous peptide discovery of the rat circadian clock: a focused study of the suprachiasmatic nucleus by ultrahigh performance tandem mass spectrometry.* Mol Cell Proteomics, 2010. **9**(2): p. 285-97.
178. Hannon, P.R., et al., *Ovulatory Induction of SCG2 in Human, Nonhuman Primate, and Rodent Granulosa Cells Stimulates Ovarian Angiogenesis.* Endocrinology, 2018. **159**(6): p. 2447-2458.

179. Shu, H., et al., *Identification and functional characterization of two Secretogranin II genes in orange-spotted grouper (Epinephelus coioides).* Gen Comp Endocrinol, 2018. **261**: p. 115-126.
180. López-Morales, C.A., et al., *Determination of Peptide Profile Consistency and Safety of Collagen Hydrolysates as Quality Attributes.* J Food Sci, 2019. **84**(3): p. 430-439.
181. Cho, S.H., et al., *Monitoring of 35 illegally added steroid compounds in foods and dietary supplements.* Food Addit Contam Part A Chem Anal Control Expo Risk Assess, 2014. **31**(9): p. 1470-5.
182. Ojoghoro, J.O., M.D. Scrimshaw, and J.P. Sumpter, *Steroid hormones in the aquatic environment.* Science of The Total Environment, 2021. **792**: p. 148306.
183. Siegel, P.D., et al., *Measurement of environmental formylmethionyl‐peptides.* Journal of Toxicology and Environmental Health, 1994. **42**(3): p. 275-288.
184. Keller, H.P., et al., *Dynamic slurry-packing technique for liquid chromatography columns.* Analytical Chemistry, 1977. **49**(13): p. 1958-1963.
185. Kovalchuk, S.I., O.N. Jensen, and A. Rogowska-Wrzesinska, *FlashPack: Fast and Simple Preparation of Ultrahigh-performance Capillary Columns for LC-MS.* Mol Cell Proteomics, 2019. **18**(2): p. 383-390.
186. Berg, H.S., et al., *Self-packed core shell nano liquid chromatography columns and silica-based monolithic trap columns for targeted proteomics.* Journal of Chromatography A, 2017. **1498**: p. 111-119.
187. Hsieh, M.Y. and H.H. Hsiao, *Stage-frit: A straightforward sub-2 µm nano-liquid chromatography column fabrication for proteomic analysis.* Anal Chim Acta, 2015. **886**: p. 200-6.
188. Tan, F., et al., *A simple and efficient frit preparation method for one-end tapered-fused silica-packed capillary columns in nano-LC-ESI MS.* Proteomics, 2010. **10**(8): p. 1724-7.
189. Audsley, N., R.E. Down, and R.E. Isaac, *Genomic and peptidomic analyses of the neuropeptides from the emerging pest, Drosophila suzukii.* Peptides, 2015. **68**: p. 33-42.
190. Rahman, M.M., S. Neupert, and R. Predel, *Neuropeptidomics of the Australian sheep blowfly Lucilia cuprina (Wiedemann) and related Diptera.* Peptides, 2013. **41**: p. 31-7.
191. Marciniak, P., et al., *Identification and localisation of selected myotropic neuropeptides in the ventral nerve cord of tenebrionid beetles.* Comp Biochem Physiol A Mol Integr Physiol, 2013. **166**(1): p. 44-51.
192. Maes, K., et al., *Strategies to reduce aspecific adsorption of peptides and proteins in liquid chromatography-mass spectrometry based bioanalyses: an overview.* J Chromatogr A, 2014. **1358**: p. 1-13.
193. Karapinar, I., et al., *LC-MS/MS signal enhancement for estrogenic hormones in water samples using experimental design.* RSC Advances, 2016. **6**(45): p. 39188-39197.
194. Zhou, H., et al., *Simultaneous measurement of total estradiol and testosterone in human serum by isotope dilution liquid chromatography tandem mass spectrometry.* Analytical and bioanalytical chemistry, 2017. **409**(25): p. 5943-5954.
195. Takkis, K., et al., *Signal Enhancement in the HPLC-ESI-MS/MS analysis of spironolactone and its metabolites using HFIP and NH4F as eluent additives.* Analytical and Bioanalytical Chemistry, 2017. **409**(12): p. 3145-3151.
196. Schratzberger, P., et al., *Differential chemotactic activities of sensory neuropeptides for human peripheral blood mononuclear cells.* J Immunol, 1997. **158**(8): p. 3895-901.
197. Aoshima, K., et al., *A simple peak detection and label-free quantitation algorithm for chromatography-mass spectrometry.* BMC Bioinformatics, 2014. **15**(1): p. 376.

198. Panuwet, P., et al., *Biological Matrix Effects in Quantitative Tandem Mass Spectrometry-Based Analytical Methods: Advancing Biomonitoring.* Critical reviews in analytical chemistry, 2016. **46**(2): p. 93-105.
199. Kovalchuk, S.I., et al., *Bovine serum albumin as a universal suppressor of non-specific peptide binding in vials prior to nano-chromatography coupled mass-spectrometry analysis.* (1873-4324 (Electronic)).
200. Kristensen, K., J.R. Henriksen, and T.L. Andresen, *Adsorption of Cationic Peptides to Solid Surfaces of Glass and Plastic.* PLOS ONE, 2015. **10**(5): p. e0122419.
201. Goebel-Stengel, M., et al., *The importance of using the optimal plasticware and glassware in studies involving peptides.* Analytical biochemistry, 2011. **414**(1): p. 38-46.
202. Weikart, C.M., et al., *Enhanced recovery of low concentration protein and peptide solutions on ultra-low binding microplates.* Future science OA, 2019. **5**(2): p. FSO367-FSO367.
203. Schneitler, C., et al., *Specific binding of a 125I-secretoneurin analogue to a human monocytic cell line.* J Neuroimmunol, 1998. **86**(1): p. 87-91.